Calhoun
Institutional Archive of the Naval Postgraduate School

Calhoun: The NPS Institutional Archive

DSpace Repository

Theses and Dissertations | 1. Thesis and Dissertation Collection, all items

1967

Transonic fan for aircraft air-conditioning unit

Pyle, Ronald William.; York, Milton Ward.

Monterey, California. U.S. Naval Postgraduate School

https://hdl.handle.net/10945/13317

Downloaded from NPS Archive: Calhoun

http://www.nps.edu/library

Calhoun is the Naval Postgraduate School's public access digital repository for research materials and institutional publications created by the NPS community. Calhoun is named for Professor of Mathematics Guy K. Calhoun, NPS's first appointed -- and published -- scholarly author.

Dudley Knox Library / Naval Postgraduate School
411 Dyer Road / 1 University Circle
Monterey, California USA 93943

NPS ARCHIVE
1967
PYLE, R.

TRANSONIC FAN FOR AIRCRAFT AIR-CONDITIONING UNIT

RONALD WILLIAM PYLE
and
MILTON WARD YORK

LIBRARY
NAVAL POSTGRADUATE SCHOOL
MONTEREY, CALIF. 93940

TRANSONIC FAN FOR AIRCRAFT AIR-CONDITIONING UNIT

by

Ronald William Pyle
Lieutenant Commander, United States Navy
B.M.E., Villanova University, 1958

and

Milton Ward York
Lieutenant, United States Navy
B.S., University of Washington, 1959

Submitted in partial fulfillment of the
requirements for the degree of

MASTER OF SCIENCE IN AERONAUTICAL ENGINEERING

from the

NAVAL POSTGRADUATE SCHOOL
June 1967

NPS ARCHIVE
967
PYLE, R.

ABSTRACT

This study presents the results of the aerodynamic design of a transonic axial-flow fan for an aircraft air-conditioning unit. The design is based on fan design-point specifications and the experimental test results for a model of a proposed fan-inlet.

The fan-inlet model was tested under flow conditions that gave Reynolds number similarity to the design inlet conditions. Three-dimensional pressure probes were used to measure the model discharge flow conditions at eight stations. The flow was found to lack axial symmetry. Therefore, several internal modifications were made. Complete axial symmetry was not achieved for a reasonable loss in total pressure. It was necessary to circumferentially average the velocity distribution and mass-average the total-pressure loss in order to provide a basis for the fan design.

Concurrently another design based on uniform flow and model losses was made. The results were nearly identical.

Thesis by: Ronald William Pyle and Milton Ward York entitled Transonic Fan For Aircraft Air-Conditioning Unit.

ERRATA

Page	Line	change	to
32	14/15	ne-glected	neg-lected
33	4/5	equilib-rium	equili-brium
107	item 2	Karmon	Karman

TABLE OF CONTENTS

LIST OF ILLUSTRATIONS

1. Introduction

An axial-flow fan may be distinguished from an axial-flow compressor in that a fan is generally classified as a high capacity, low head, single-stage unit which operates at a high, constant speed. Although used for different purposes than a compressor, an axial-flow fan may be designed or analyzed with the available theoretical and experimental methods for axial-flow compressors.

One of the principal assumptions made in the aerodynamic design of axial-flow compressors is that of axially symmetric flow. This condition is primarily assumed to reduce the general flow equations from a complex three-dimensional to a simplified two-dimensional system. At a given radial location the physical requirement of this assumption is for circumferentially constant flow conditions ahead of any blade row.

The single-stage transonic fan, with its relatively higher flow capacity and pressure ratio over conventional subsonic fans, has been successfully used in modern aircraft systems. However, for compact systems the transonic turbomachine becomes more demanding of inlet flow uniformity. Thus, proper matching of an inlet-scroll to a fan stage becomes more critical for a given set of dimensional restrictions.

The purpose of this paper was the aerodynamic design of a single-stage transonic fan for an aircraft air-conditioning unit. The design was to be based on a list of design-point specifications and also on a proposed fan inlet that complied with the geometrical design envelope.

A double-scale model of the proposed fan inlet was tested. Internal modifications were made in an attempt to attain uniform, axially symmetric flow at a location just ahead of the required rotor position. Final model test results were used to predict the losses through the fan inlet and the flow conditions ahead of the fan rotor. The aerodynamic fan design was based on these conditions.

A similar fan design was made which was based on assumed uniform, axially symmetric flow ahead of the rotor. Thus, a comparison could be made between the two designs, and also with the design specifications.

The authors wish to express their appreciation for the guidance and assistance given them by Professor M. H. Vavra of the Department of Aeronautics of the Naval Postgraduate School.

2. List of Symbols

A	area, in^2
B	number of blades
b	blade height, in
c_p	specific heat, $BTU/lb_m\ ^oR$
c	blade chord, in
D	diffusion factor
DP	driving power
f_r	Reynolds number factor
f_t	area multiplier
g	gravitational constant, 32.2 ft/sec^2
H	total enthalpy, BTU/lb_m
i	incidence angle, degrees
i_o	incidence angle of uncambered blade section, degrees
J	conversion factor, 778.2 ft lb/BTU
K_{bk}	weight flow blockage factor
K_i	correction factor in incidence-angle relation
K_s	correction factor in deviation-angle relation
l	characteristic length, in
M	Mach number
m	factor in deviation-angle relation at $\sigma = 1$
N	revolutions per minute, RPM
N_{Re}	Reynolds number
n	slope factor in incidence-angle relation

n_p	polytropic exponent
P	total pressure
p	static pressure
q	dynamic pressure
q_{av}	theoretical average dynamic pressure
R	gas constant, 53.34 ft lb/lb_m ^oR
r	radius, in
r_i, r_o	radius, inner and outer, in
S	entropy, BTU/lb_m ^oR
s	blade spacing, in
T	total temperature, ^oR
t	static temperature, ^oR
t/c	blade maximum-thickness-to-chord ratio
U	peripheral speed, ft/sec
V	velocity, ft/sec
$\dot{w}$	flow rate, lb_m/sec
w^*	equivalent flow rate, in^2
X	pressure ratio parameter
x	distance from annulus outer wall, in
z	coordinate along axis, in
α	discharge coefficient
β	air angle, angle between air velocity and axial direction, degrees
γ	ratio of specific heats
δ°	deviation angle, degrees
ϵ	density coefficient
ζ	inlet total-pressure-loss coefficient

η_p	polytropic loss coefficient
η_{ad}	adiabatic efficiency
Θ	pitch angle in model discharge annulus, degrees
μ	viscosity, lb_m/sec ft
ρ	density, slugs/ft^3
σ	solidity, ratio of chord to spacing
Φ	dimensionless flow function
φ	blade camber angle, degrees
ψ	yaw angle in model discharge annulus, degrees
ω	angular velocity, radians/sec
$\bar{\omega}$	fan total-pressure-loss coefficient

Subscripts:

0	station ahead of inlet
1	station at rotor inlet
2	station at stator inlet
2-D	low speed two-dimensional cascade
3	station at stator exit
10	blade maximum-thickness-to-chord ratio of 10 percent
ad	adiabatic
av	average
ax	axial
c	compressor
D	design
d	model discharge

H	horizontal
h	hub
I	model entrance
j	summation index
M	model
m	mean
ma	mass averaged
mer	meridional
min	minimum
n	nozzle
P	plenum
r	radial direction
ST	stage
t	tip
u	upstream of nozzle
V	vertical
z	axial direction
θ	tangential direction

Superscripts:

′	relative to rotor
b	exponent in deviation-angle relation

3. Design Specifications

The fan is to deliver air at γ = 1.3947 and R = 53.34 ft lb/lbm $^{\circ}$R. Design point conditions are as follows:

a) Speed = 85,000 RPM

b) Flow rate = 83.5 lbm/min

c) Driving power = 23.916 HP

d) Conditions ahead of fan inlet-scroll-housing are:

1) uniform flow

2) $T_o = 714^{\circ}R$

3) P_o = 13.656 psia

e) Required total pressure ratio between stator discharge and the entrance plane of the scroll-housing is P_3/P_o = 1.178

The inlet-scroll-housing has a rectangular entrance (5.65 in. by 7.82 in.) and a flange 3.125 in. from the center line of the fan. The distance of the center plane of the rotor from the back plate cannot exceed 2.1 in. because of the critical speed of the shaft. The hub diameter on the upstream side of the rotor cannot be less than 1.82 in. to accommodate the bearings. The discharge pipe of the fan has an ID of 3.75 inches. For manufacturing reasons, and to facilitate assembly, the outer diameters of the blading should be constant. The fan is to be single-stage and without inlet guide vanes.

4. Equipment and Instrumentation

Air supply for the test facility is from a Carrier centrifugal compressor driven by a 300 HP electric motor. The compressor has a rated output of 4 lb/sec at a pressure ratio of 2.

A general schematic of the test installation is shown in Figure 1. The major portion of the test equipment is shown in Figure 2.

The duct from the plenum to the model is 4 ft. long and has 11.3 in. by 15.64 in. inside dimensions. It has two 3 in. long pieces of honeycomb material to provide uniform flow at the entrance to the model.

Flow rate through the model is controlled with the by-pass valves. The primary by-pass provides coarse adjustment of flow rate. The secondary by-pass, located in the test room, is used for fine flow rate adjustments.

Flow rate is measured by a VDI standard flow nozzle, in the 4 in. inlet pipe, upstream of the plenum. The static pressure drop across the nozzle is measured on a 20 in. mercury micromanometer. Static pressure upstream of the nozzle is measured on a 92 in. water manometer.

The plenum temperature and the temperature upstream of the nozzle are measured with iron-constantan thermocouples.

Total pressure at the model entrance is measured by two Kiel probes mounted horizontally and vertically, and read on a 250 cm. water manometer.

Measurements in the model discharge annulus are made with a United Sensor three-dimensional five hole pressure probe. Pressure measurements are read on a 120 cm. water manometer. Yaw angle, ψ , is read from an angle scale on the probe support.

5. Inlet Analysis

Velocity distribution ahead of the rotor and pressure loss through the inlet must be known in order to start the fan design. This determination was made by testing a double-scale model of a proposed inlet design. The model casing is shown in Figures 3 and 4. The bellmouth for the model is shown in Figure 5. The bellmouth hub is shown in Figures 6 and 7.

In order to generalize the test results, all flow rates were reduced to an equivalent flow rate

$$w^* = \frac{\dot{w}\sqrt{T}}{p}\sqrt{\frac{R}{g}}$$

where p and T are the conditions at any point.

Similarity Conditions

The ability to apply data from the testing of one size machine to another is based on the concept of geometric and flow similarity. Geometric similarity was achieved by changing all dimensions by the same ratio. Flow similarity is defined by the similarity parameters of Mach number and Reynolds number. The matching of these two parameters assures similar flow.

Using the definitions of Mach number and the speed of sound, the Mach number, in terms of equivalent flow rate, becomes

$$M = \frac{w^*}{A\sqrt{\gamma}}$$

Noting that the area of the model is four times the area of the design and that γ is the same, the equivalent flow rate of the model, for equal Mach numbers, is

$$w^*(\text{Model}) = 4w^*(\text{Design})$$

The Reynolds number is defined by

$$N_{Re} = \frac{\rho V l}{\mu}$$

and in terms of w^* it becomes

$$N_{Re} = \frac{w^* p}{\mu \sqrt{gRT}} \frac{1}{A}$$

Noting that the area of the model is four times the area of the design and that the characteristic length, l, of the model is twice that of the design, the equivalent flow rate of the model, for equal Reynolds numbers, is

$$w^*(\text{Model}) = 2 \frac{\mu_M}{\mu_D} \frac{p_D}{p_M} \sqrt{\frac{t_M}{t_D}} w^*(\text{Design})$$

Using the specification conditions for the design, and average conditions for the model of

$$p_M = 14.7 \text{ psia}$$
$$t_M = 550^\circ \text{ R}$$

the equivalent flow rate of the model, for equal Reynolds numbers, becomes

$$w^*(\text{Model}) = 1.344\ w^*(\text{Design})$$

The equivalent flow rate for the design, calculated from the specifications, is 3.505 in.^{2}. For Mach number simi-

larity this requires a flow rate of 6.8 lb/sec in the model. For Reynolds number similarity a model flow rate of 2.29 lb/sec is required.

Since the flow through the inlet is in the low subsonic range, the effects of Mach number are small and were neglected. The model testing was done at a flow rate which gave the Reynolds number similarity condition.

Test Procedure

The flow rate was set and held constant by maintaining a constant static pressure upstream of the flow measuring nozzle. Readings were taken at intervals during each traverse to determine the average flow rate and total pressure at the model entrance.

The five hole pressure probe was traversed across the annulus height at the model discharge. Measurements were taken at each 10% point of the annulus height from the outer radius. Additional measurements were taken at 3, 6, 94, and 97 percent of the annulus height to get an indication of the boundary layer formation. Data was obtained to determine total and static pressure, and yaw and pitch angle. Traverses were taken at eight stations, spaced every 45 degrees around the annulus, as shown in Figure 8.

Data Reduction

The reduced data for a typical model test is given in Appendix A. Due to the volume of data obtained only that for Modification 7 (Mod. 7) is given.

Equivalent flow rate at the nozzle was determined by the method presented by Kelly [1]. The relevant equation from [1] is

$$w_n^* = \alpha \varepsilon f_t f_r A_n \sqrt{2} \sqrt{\frac{\Delta p}{p_u}} \qquad (5.1)$$

Equivalent flow rate at the model discharge is related to the equivalent flow rate at the nozzle by

$$w_d^* = w_n^* \frac{p_u}{p_{av}} \sqrt{\frac{t_d}{t_u}} \qquad (5.2)$$

where p_{av} is the average static pressure at the discharge. Since the discharge velocities were small, the discharge static temperature was assumed equal to the total temperature, which in turn was considered to be the measured plenum temperature.

The average static pressures at each of the eight stations were determined from the pressure probe data. The data from the probe traverses was used in conjunction with the probe calibration chart (Fig. 9) to determine the following local flow conditions: the total and static pressures, yaw and pitch angles, and the local total-pressure-loss coefficient. The parameter used to enter Figure 9 is $\frac{P_4-P_5}{P_1-P_2}$. The further procedures are indicated in Appendix A.

The yaw angle ψ was measured directly from a vernier scale protractor mounted on the probe support. Positive yaw was defined as that producing clockwise whirl if looking

upstream into the discharge annulus. The pitch angle was determined from Figure 9 and defined as positive for radial velocity component pointing outward from the discharge centerline.

In order to give an indication of loss characteristics for various points, stations, and model modifications, the local total-pressure-loss coefficient was defined as

$$\zeta = \frac{P_I - P}{P - p} \tag{5.3}$$

where P_I is the average total pressure at the entrance to the model.

In order to compare flow distributions at the various stations, and for different modifications, the dynamic pressure ratio q/q_{av} was determined at each data point, where q_{av} is defined as the theoretical dynamic pressure that should occur at the discharge annulus for uniform flow and a given discharge equivalent flow rate. That is,

$$q = P - p \tag{5.4}$$

and

$$q_{av} = \left(\frac{w_d^*}{A_d} \right)^2 \frac{p_{av}}{2} \tag{5.5}$$

Derivation of equation (5.5) was based on the following relations:

continuity equation: $$\dot{w} = \rho_{av} g A_d V_{av} \tag{5.6}$$

equation of state: $$\rho_{av} = \frac{p_{av}}{g R t_{av}} \tag{5.7}$$

discharge equivalent flow rate:

$$w_d^* = \frac{\dot{w}\sqrt{t_{av}}}{p_{av}}\sqrt{\frac{R}{g}} \tag{5.8}$$

definition of dynamic pressure: (for incompressible flow)

$$q_{av} = \frac{\rho_{av}}{2} V_{av}^2 \tag{5.9}$$

Substitution of V_{av} from equation (5.6) into equation (5.9) gives

$$q_{av} = \frac{\rho_{av}}{2} \frac{\dot{w}^2}{\rho_{av}^2 g^2 A_d^2} = \frac{\dot{w}^2}{2 \rho_{av} g^2 A_d^2}$$

or, from equation (5.7)

$$q_{av} = \frac{\dot{w}^2}{2 g A_d^2} \frac{R t_{av}}{p_{av}}$$

Substituting $\dot{w}$ from equation (5.8) gives

$$q_{av} = (w_d^*)^2 \frac{p_{av}^2}{t_{av}} \frac{g}{R} \frac{R t_{av}}{2 g A_d^2 p_{av}}$$

therefore

$$q_{av} = \left(\frac{w_d^*}{A_d}\right)^2 \frac{p_{av}}{2}$$

The dynamic pressure ratio then becomes

$$\frac{q}{q_{av}} = \frac{P - p}{\left(\frac{w_d^*}{A_d}\right)^2 \frac{p_{av}}{2}} \tag{5.10}$$

The local velocity parameter V_{ax}/V_{av} was considered useful for noting the effectiveness of the various modifications made to the model in an attempt to attain axisymmetric flow.

For a local velocity V with components in the radial, axial, and tangential directions the axial velocity is $V_{ax} = V \cos \Theta \cos \Psi$. Therefore, for constant density

$$\frac{V_{ax}}{V_{av}} = \sqrt{\frac{q}{q_{av}}} \cos \Theta \cos \Psi \qquad (5.11)$$

Modifications

Several modifications were made to the model in an attempt to attain the same flow conditions at each of the eight stations shown in Figure 8. Initial testing indicated that deficient flow existed at stations 1, 2, and 8. Stations 4, 5, and 6 had excessive flow, while stations 3 and 7 were receiving the desired amount of flow. Yaw angles were excessive at stations 2, 3, 7, and 8 (about 15°-20°). Pitch angles were highest at stations 4, 5, and 6 (about 8°-10°).

In an attempt to correct the flow pattern and achieve axisymmetric flow in the model discharge, seven internal modifications were made to the model. These modifications were tested individually except as noted below. The following is a description of each modification with a discussion of the reason for the change and a summary of the results obtained. For clarity, the pictures of each modification (except Mod. 7) are shown in the relevant figures without the hub and bellmouth assembled.

Mod. 1 - A flow splitter with a 2 in. radius of curvature was placed at the top of the model casing (station 1) as shown in Figure 10. This change was made for two reasons. The original splitter was unavoidably damaged during the process of boring a probe hole for stations 1 and 5. It was also considered appropriate for the splitter to have some curvature so as to provide a smoother change of flow direction at the top of the casing. The flow distribution (Fig. 11) remained unchanged and the local loss distribution (Fig. 12) was almost identical to the preliminary test results. For these reasons and due to the fact that this modification was used in all subsequent testing, the Mod. 1 results were used as a basis for comparison with other modifications.

Mod. 2 - A flow splitter was placed at the bottom of the casing (station 5) as shown in Figure 13. It extended from the front wall of the casing to the beginning of the curvature of the bellmouth. This change was made to provide a smoother change of flow path and to direct more flow to the top of the casing. The only effect seen in this test was an increase in the pressure loss. The flow distribution was not altered. Therefore, these results are not shown.

Mod. 3 - A full width flat guide vane was placed in the model entrance at the end of the flow splitter of Mod. 2. The guide vane alone is shown in Figure 14. It was set at zero angle of attack to the flow. The trailing edge has a circular cutout so that it wraps around a portion of the bellmouth. The maximum chord is 4.25 in. at the wall.

This guide vane was designed and placed so as to block a portion of the flow going to stations 4, 5, and 6 and to force it to the upper stations 1, 2, and 8, where the flow was deficient. It was considered to be a gross over-correction as it was placed very close to the bellmouth lip and extended completely across the model entrance width. That is, an over-correction was made in hopes of later reducing the correction to some optimum.

The results for this modification showed that high pitch angles and high losses existed at station 5. The flow was deficient at this station near the outer radius but actually increased in magnitude near the hub (inner radius). The flow conditions at station 1 were unchanged from those of Mod. 1. Therefore, these results are not shown.

Mod. 4 - Two guide vanes were placed at the model entrance as shown in Figure 15. The vanes are flat and have a 1.5 in. chord. They were set at zero angle to the flow and 2 in. from the plane of symmetry of the casing. This modification was designed to split the flow into three sections. The middle section (between the vanes) would go to the lower stations 4, 5, and 6, and the two outer sections would go to the side and upper stations. The chord length was selected so as not to interfere with the flow close to the bellmouth.

The supports for these vanes were designed such that each vane could be adjusted over a 2 in. slotted-track and set at any angle of attack. For this modification a neutral position was used as a preliminary choice of vane positioning.

The results for this test showed no change in flow distribution or losses from that of Mod. 1 and are therefore not presented.

Mod. 5 - The guide vanes used in Mod. 4 were reset at a 25 degree angle to the flow with the leading edge 0.6 in. from the plane of symmetry as shown in Figure 16. The repositioning of the guide vanes in this manner was considered to be a large correction in a further attempt to reduce the flow going to the lower stations and to direct it to the upper stations.

For the purpose of reducing experimental testing time such that other modifications could be tested, preliminary data for this modification was taken only for five points (10, 30, 50, 70, and 90 percent of the annulus height) at each of stations 1, 3, 5, and 7. If the results for this data indicated significant improvement then a complete annulus traverse would have been carried out.

Comparison to Mod. 1 can be made at the same percentage values of the annulus height. Results for Mod. 5 are shown in Figures 17 and 18 for axial velocity and loss distributions, respectively. The flow at station 1 was increased slightly. The flow at station 5 was more uniform but of about the same amount as before. Changes at station 3 and 7 were small. Figure 18 shows that the local losses increased at station 5 and changed only slightly at stations 1, 3, and 7.

Mod. 6 - Two guide vanes were placed at the model entrance as shown in Figure 19. The vanes are "S" shaped with a 5.35 in. chord. The leading edge was set at zero angle to the flow and was 0.75 in. from the plane of symmetry. From the leading edge they have a radius of curvature of 2 in. for 2.25 in., then a straight portion for 0.8 in., then an opposite radius of curvature of 3.5 in. for 2.55 in. to the trailing edge. The vanes are tangent to the bellmouth at the trailing edge.

This modification was a gross correction to divide the flow into three sections and force sufficient flow to the upper stations. Although considered impractical this change was made and tested in the hope that an optimum and more practical configuration could be established.

The Mod. 6 Velocity Distribution (Fig. 20) shows that in comparison with Mod. 1 the flow was increased at all stations except 4 and 6 which were very deficient. Stations 1, 2, and 8 now had excessive flow, and the flow at station 5 became even more excessive. Several stations had less uniform axial velocity distributions than in Mod. 1. Stations 4 and 6 experienced very high losses as shown in the Mod. 6 Loss Distribution (Figure 21).

Mod. 7 - A groove 1 in. deep and 2.28 in. long was cut in the bellmouth outer wall as shown in Figures 5 and 22. The purpose of this change was to provide more area for flow to the upper stations and to improve the bellmouth shape. The assembled configuration is shown in Figure 23.

Figures 24 and 25 show the axial velocity and loss distributions, respectively. The results in general are very similar to those for Mod. 1. However, the station that changed the most was station 1, and this was as an improved (increased) flow distribution. Stations 2 and 8 showed increased losses near the outer radius. Station 1 experienced somewhat lower and more uniform losses. The other stations indicated little or no change over Mod. 1. The pitch and yaw angles were reduced slightly, but fairly significant yaw angles (15^{o}) still existed at stations 2, 3, 7, and 8.

Predicted Conditions Ahead of Fan Rotor

The final part of the inlet analysis was the prediction of the flow conditions ahead of the rotor for the fan design. This prediction was based on the non-dimensional velocity ratio and the total-pressure-loss coefficient from the model tests, and on the fan-inlet entrance conditions given in the specifications.

Final Model Analysis. - The model test data indicated that the Mod. 1 and Mod. 7 configurations were similar. For better comparison the data for these two configurations was circumferentially averaged for Θ , Ψ , ζ , and V_{ax}/V_{av}. It was decided that Mod. 7 gave slightly better flow distribution between the outer and inner walls, and that the

averaged yaw and pitch angles were somewhat smaller. The loss characteristics of the two configurations were nearly identical. Therefore, the Mod. 7 data was chosen for use in the prediction of rotor entrance conditions.

The circumferentially averaged velocity distribution, as shown in Figure 26, was somewhat in error as the area under this curve was about three percent greater than unity (1.0316), although theoretically this area must equal unity; that is,

$$\int_{\frac{r_i}{r_o}}^{1.0} \frac{V_{ax}}{V_{av}} \, d\left(\frac{r}{r_o}\right) = 1.0 \qquad (5.12)$$

Conditions that were considered likely causes of this discrepancy are: decreased discharge area due to probe blockage, general instrumentation errors, improper estimation of the velocity profile near the walls, increased probe inaccuracies in the boundary layer, and the assumptions made in the calculations (such as $t_d = T_d$, ρ = constant, etc.).

To correct this apparent error the Mod. 7 velocity distribution was normalized such that equation (5.12) was satisfied. This was done by dividing each ordinate value of V_{ax}/V_{av} by the area under the curve. Both distributions, Mod. 7 and corrected Mod. 7, are shown in Figure 26.

The mass-averaged total-pressure-loss coefficient for the model was determined as follows

$$\zeta_{ma} = \frac{P_I - P_{ma}}{P_{ma} - p_{ma}} \qquad (5.13)$$

where P_I is the average total pressure at the model entrance, and P_{ma} and p_{ma} are the mass-averaged total and static discharge pressures, respectively. Thus,

$$P_{ma} = \frac{\int d\dot{w}\, P}{\int d\dot{w}}$$

which may be written as

$$P_{ma} = \frac{\int_0^{2\pi}\int_{r_i}^{r_o} \rho\, g\, r\, \frac{V_{ax}}{V_{av}}\, V_{av}\, dr\, d\phi\, P}{\int_0^{2\pi}\int_{r_i}^{r_o} \rho\, g\, r\, \frac{V_{ax}}{V_{av}}\, V_{av}\, dr\, d\phi}$$

For assumed constant density,

$$P_{ma} = \frac{\int_0^{2\pi}\int_{r_i}^{r_o} r\, \frac{V_{ax}}{V_{av}}\, dr\, d\phi\, P}{\int_0^{2\pi}\int_{r_i}^{r_o} r\, \frac{V_{ax}}{V_{av}}\, dr\, d\phi}$$

The static pressure p at discharge was mass-averaged in the same manner. The integration was carried out radially and then circumferentially. Using equation (5.13) it was determined that $\eta_{ma} = 0.0484$.

Design Prediction. - The conditions ahead of the rotor were determined by the method of Vavra [2] for an adiabatic expansion process with friction and varying cross-section.

The fan-inlet loss coefficient was assumed to be equal to the mass-averaged value for the model.

The dimensionless flow function Φ was determined from the relation in [2]

$$\Phi = \frac{\dot{w}\sqrt{T_o}}{P_o} \frac{1}{A_1}\sqrt{\frac{R}{g}} \qquad (5.14)$$

where $\dot{w}$, T_o, and P_o are given in the design specifications. The area A_1 ahead of the rotor is dependent upon the design choice since dimensional restrictions are given in the specifications. The double-sized model was based on the minimum hub distance and a casing diameter of 3.5 inches. Thus, the value of A_1 was prescribed.

With Φ and η as known parameters, Table C1 of [2] was used to find the pressure ratio P_o/p_1. This procedure was based on the simplifying assumptions that

$$\gamma_D = 1.4$$

and

$$\eta_D = 0.05$$

The following equations from [2] were then used to determine the velocity V_1:

$$X = \left(\frac{p_1}{P_o}\right)^{\frac{\gamma-1}{\gamma}}$$

$$\eta = \frac{X^{1-\eta_p} - X}{1 - X}$$

$$\eta_P = \frac{\gamma}{1 + \eta_P(\gamma - 1)}$$

$$V_1 = \left\{ 2gR \frac{\gamma}{\gamma-1} T_o \left[1 - \left(\frac{p_1}{P_o}\right)^{\frac{\eta_P - 1}{\eta_P}} \right] \right\}^{1/2}$$

where n_p is defined as the polytropic exponent, η_P as the polytropic loss coefficient, and X as a pressure relation used as a simplification of the equations.

The velocity V_1 represents the required average velocity ahead of the rotor for a non-uniform velocity distribution, or the actual velocity for uniform flow that is entirely axial.

Since $T_1 = T_o$ for an adiabatic process, the static temperature was determined by

$$t_1 = T_1 - \frac{V_1^2}{2g\ J\ c_p}$$

The total pressure P_1 was determined by

$$P_1 = \frac{P_1}{p_1} \frac{p_1}{P_o} P_o$$

where

$$\frac{P_1}{p_1} = \left(\frac{T_1}{t_1} \right)^{\frac{\gamma}{\gamma - 1}}$$

The design weight flow was used as a check on these predicted conditions by

$$\dot{w}_D = \frac{p_1}{R\ t_1} A_1\ V_1$$

The absolute Mach number is

$$M_1 = V_1 / (\gamma\ g\ R\ t_1)^{\frac{1}{2}}$$

Given below is a summary of the properties at the rotor inlet:

$P_1 = 13.534$ psia	$T_1 = 714^{\circ}$ R	$V_1 = 627.6$ ft/sec
$p_1 = 11.483$ psia	$t_1 = 681.55^{\circ}$ R	$M_1 = 0.490$

6. Aerodynamic Fan Design

The basic equations that are applicable to the design of an axial-flow compressor or fan are developed in [3]. These are formulated from the laws of conservation of matter, momentum, and energy, along with the thermodynamic equation of state of the working fluid.

The simplifying assumptions that are made in [3] are as follows:

1) The general flow equations are applied only to compute flow distributions between blade-rows where blade forces are nonexistent.
2) The flow is assumed to be steady and axially symmetric.
3) Viscosity effects between blade rows are neglected in the flow equations. However, these effects are considered by use of experimentally determined blade-element performance data. Empirical corrections are also made for wall boundary-layer effects on required flow area.
4) Heat transfer is neglected.

The two principal phases of the aerodynamic fan design are:

1) Determination of blade-row velocity-diagrams for design point operation.
2) Selection of blading to satisfy these velocity-diagrams.

Determination of Velocity-Diagrams

General. - The determination of the various air velocities and flow angles from hub to tip at the inlet and outlet of the rotor and stator was made based on the radial equilibrium equation [3] , which is

$$Jgc_p \frac{\partial T}{\partial r} = Jgt \frac{\partial S}{\partial r} + V_\theta \frac{\partial V_\theta}{\partial r} + \frac{V_\theta^2}{r} + V_z \frac{\partial V_z}{\partial r} - V_z \frac{\partial V_r}{\partial r} \qquad (6.1)$$

This equation results from the preceding simplifying assumptions, and was the theoretical starting point for the fan design.

It was assumed that the meridional velocity $V_{mer} = \sqrt{V_z^2 + V_r^2}$ is given by the axial velocity V_z , and that $\partial V_r/\partial z = 0$. Such a condition has been successfully used in low-aspect-ratio and lightly loaded blade-row designs. Therefore, this assumption was considered appropriate for the fan design.

It was decided that the design should include constant energy addition through the rotor blade-row. That is, the change of total enthalpy through the blade-row is constant along a streamline. If the total enthalpy is assumed constant ahead of the rotor (H_1 = constant), then a constant total enthalpy will exist behind the rotor. This may be expressed as

$$\left(\frac{\partial T}{\partial r}\right)_2 = 0$$

The Euler turbine equation may be written as

$$H_2 - H_1 = \frac{\omega}{Jg} \left[(rV_\theta)_2 - (rV_\theta)_1 \right] \qquad (6.2)$$

Since $V_\theta = 0$ ahead of the rotor, and $H_2 - H_1$ is constant, then $(rV_\theta)_2$ = constant. Thus, the above conditions require that free-vortex flow exists behind the rotor bladerow.

Therefore, neglecting radial velocity components, equation (6.1) becomes

$$V_\theta \frac{\partial V_\theta}{\partial r} + \frac{V_\theta^2}{r} + V_z \frac{\partial V_z}{\partial r} + t \frac{\partial S}{\partial r} = 0 \qquad (6.3)$$

The first two terms in this equation may be written as

$$\frac{V_\theta}{r} \left(r \frac{\partial V_\theta}{\partial r} + V_\theta \right)$$

or

$$\frac{V_\theta}{r} \frac{\partial (r V_\theta)}{\partial r}$$

Since rV_θ = constant, the sum of the first two terms in equation (6.3) equals zero.

The radial equilibrium equation then reduces to

$$V_z \frac{\partial V_z}{\partial r} + t \frac{\partial S}{\partial r} = 0 \qquad (6.4)$$

The simplest solution of equation (6.4) is the "simple-radial-equilibrium solution," based on the further assumption that the derivative of S with respect to r is zero. This condition has been widely used in compressor design, and was considered valid for the single-stage fan for slight change in annular area. This assumption is made only at a fixed value of z.

Therefore, equation (6.4) becomes

$$V_z \frac{\partial V_z}{\partial r} = 0$$

with the solution

$$V_z = \text{constant} \tag{6.5}$$

Using this result as a basis, the velocity diagrams and flow properties were calculated for two assumed rotor inlet conditions; namely,

a) Design A for the circumferentially-averaged axial velocity for the most satisfactory flow determined from the inlet model tests. The mass-averaged total-pressure-loss coefficient for the model was assumed. Total temperature and total pressure were assumed to be constant ahead of the rotor. Pitch and yaw components of velocity were assumed to be zero.

b) Design B for uniform flow with axial velocity components only. The velocity and properties ahead of the rotor were based on the same loss coefficient as Design A.

General calculation procedure. - The calculation method is one of iteration and compromise. Iteration is necessary in order that the continuity equation may be satisfied by proper annular dimensions. Compromise is necessary in order that blade-loading and Mach number limits are not exceeded.

Experimental tests of axial-flow compressors show that a Mach number of 1.2 is the approximate limit for a transonic

design method as used in this paper. Further, the following diffusion-factor limits are appropriate for inlet stages: for the rotor tip, D less than 0.4; for the rotor hub, D less than 0.6; for the stator, D less than 0.6 [3] . Although these criteria are somewhat vague, they remain the best indicators of design limitations that are currently available.

The detailed development of the calculation method is presented in [3] . The iterative procedure is started by selecting the radial stations according to percentages of the passage depth. The computation scheme and results for velocity calculations are shown in Tables I and II, for Design A and Design B, respectively. Only the final results and the final calculation lineups of the iteration procedure are presented.

The velocity leaving the stator was assumed to be entirely axial, thus providing maximum flow rate for a given stage loading.

Design A. - Table I shows the steps taken to determine each parameter. Figure 27 shows a general stage velocity-diagram which is indicative of the fan design.

From the results of the inlet-model analysis, the assumed inlet conditions to the rotor were as follows:

$T_1 = 714^{\circ}$ R

$P_1 = 13.534$ psia

$\frac{V_{z,1}}{V_{av}}$ as shown in Figure 26

V_{av} = 627.6 ft/sec

$r_{1,t}$ = 1.74 in. (for an assumed tip clearance of 0.010 in.)

$r_{1,h}$ = 0.91 in.

The conditions at station 1 are listed as steps 1 through 8 in Table I. The iteration was started by assuming that the hub radius was constant through the rotor (step 9). Most of the steps are clearly indicated under the procedure column in Table I, in which Figure 27 was used. However, several steps had to be related to important design assumptions and will be discussed in detail.

$V_{\theta,2}$ (step 11) was determined by use of the Euler relation, equation (6.2), and the definition of DP, the driving power. That is,

$$DP = \dot{w}(H_2 - H_1)$$

or $$DP = \frac{\dot{w}\omega}{Jg} (rV_\theta)_2$$

Since $\omega = \pi N/30$, the tangential velocity behind the rotor may be found as a function of r_2.

It has been pointed out in [3] that large axial velocity reductions across any blade-element are not conducive to high efficiency. In addition, the available experimental data for transonic rotors shows that the range of $V_{z,2}$ to $V_{z,1}$ ratios across the rotor are as follows: for the tip, 0.85 to 1.05; for the mean radius, 0.90 to 1.15; for the hub, 0.95 to 1.50. Therefore, in step 14 the axial velocity through the rotor at the mean radius was assumed to be constant. This assumption causes the axial velocity changes near the tip and hub regions to be typical of the experimental data.

Steps 24 through 26 involved a compromise in which several important design conditions were considered. These were as follows: the critical blade-chord Reynolds number, frictional losses, shock losses, blade-loading, manufacturing restrictions, and the practicality of rotor diameter measurement.

The critical blade-chord Reynolds number may be defined as the limiting value of Reynolds number below which a large rise in loss occurs. Above this value the losses vary only slightly or not at all. The available experimental data are generally for flow conditions at or above this critical Reynolds number. Therefore, rotor blade design that is based largely on test data should also be for similar flow conditions. Based on the relative inlet velocity to a blade-element, Vavra [4] indicates that this limiting Reynolds number is about 2×10^5.

Too high a solidity is associated with increased frictional losses. Too low a solidity results in higher blade loading, and increased shock losses near the tip. Recommended rotor tip solidity for transonic rotors in regard to shock losses is 1.0 [3].

For manufacturing reasons the minimum blade spacing at the hub is about 0.25 inches.

An even number of rotor blades allows for easier measurement of the tip diameter.

Therefore, in consideration of the above facts, the minimum blade-chord Reynolds number was set at 2×10^5 for the

rotor. The corresponding minimum blade-chord was determined, for the known conditions ahead of the rotor, by

$$N_{Re} = \frac{V_1' \, c \, \rho_1}{\mu_1} \qquad (6.6)$$

where μ_1 was found in [5] for known values of t_1 .

Several combinations of chord distributions and blade numbers were investigated in order to determine a satisfactory solidity range. Pertinent equations used were

$$s = \frac{2 \pi r}{B} \qquad \text{and} \qquad \sigma = \frac{c}{s}$$

It was considered important to have a tip solidity fairly close to 1.0 as recommended in [3] , but also essential to establish a solidity range similar to that for the experimental data for transonic rotors.

As a result, 12 rotor blades with uniformly varying chord were selected such that the Reynolds number was at or above 2×10^5. A summary of this analysis, which was based on no area change through the rotor, is as follows:

Radial position	V_1'	c_{min}	c	s	σ
TIP	1450.1	0.536	0.750	0.911	0.823
10%	1395.5	0.557	0.760	0.868	0.876
50%	1169.1	0.665	0.800	0.694	1.153
90%	960.4	0.809	0.840	0.520	1.615
HUB	914.0	0.850	0.850	0.476	1.786

From this summary the linear chord distribution was expressed as a function of radius for those iterations to follow. Thus,

$$c = c_{1,h} - \frac{c_{1,h} - c_{1,t}}{r_{1,t} - r_{1,h}} (r - r_{1,h}) \qquad (6.7)$$

It should be noted that the above chord-solidity summary refers only to the first iteration. With reduced blade height at the rotor discharge the values of r_1 and r_2 will be slightly different for a given percentage of passage depth. A streamline will follow a curved path through the rotor, depending upon annulus constriction. Therefore, the solidity must be averaged for the values at rotor entrance and exit. This was done in step 27, where σ_1 is referred to the chord and spacing at station 1 for a given percentage passage depth from the casing, and σ_2 to the chord and spacing at station 2 for the same percentage passage depth.

The total-pressure-loss coefficient $\bar{\omega}'$ was determined from the experimental data for a geometrically similar double-circular-arc transonic rotor [6] . This rotor was tested under similar flow conditions. The values of $\bar{\omega}'$ were for minimum-loss incidence angle. This method of determining the loss coefficient was considered appropriate for the simplified theory used in this paper.

The relations used in steps 30 to 32 are developed in [3] .

It was considered probable that the boundary layer in the fan rotor would have significant blockage effects, especially due to the small blade heights. Therefore, in step 34 a blockage factor of 0.96 was assumed. The continuity equation was checked by graphical integration.

The iteration was repeated for a new hub radius at station 2, re-starting at step 9 until continuity was satisfied.

The final rotor outlet conditions were used as stator inlet conditions. A similar process was followed for the stator design. However, the stator blade solidity was determined in a somewhat different manner than for the rotor, as excessive solidities resulted for the criterion that minimum Reynolds number be equal to 2×10^5.

A solidity distribution was sought which would be similar to the available experimental data for the NACA-65(A_{10})- series airfoil. (The specific reasons for choosing this airfoil shape will be given later). The extensive test data for this airfoil includes solidities up to about 1.6, but extrapolated data for blade solidities up to 2.0 are given in [3] .

Several combinations of blade-chord and number of blades were investigated. As a result, the solidity at the 90% position (near the hub) was set at 1.55, and the solidity at the 10% position (near the tip) was set at 1.0. Blade chord was chosen as constant at 0.805 inches, and the number of blades was set at 13.

Step 42 indicates the resulting Reynolds numbers. These values were deemed acceptable for two reasons [3] . First, the relative difference between Reynolds numbers of 1.5×10^5 and 2.0×10^5 is small for the NACA-65(A_{10})- series airfoil under moderate blade loadings. Secondly, lightly loaded blades (such as the fan design of this paper) have only a

gradual increase in loss below the critical Reynolds number, rather than the more typical steep rise in loss for normal blade loadings. The diffusion factor values listed in step 43 indicate that the fan stator is rather lightly loaded as compared to the suggested design limit for stators of D less than 0.6 .

The total-pressure-loss parameter (step 44) was determined from [3] for known diffusion factors.

The continuity equation was checked using an assumed blockage factor of 0.94. Iteration was found to be unnecessary.

The stage total pressure ratios and stage adiabatic efficiencies for the three radial positions were determined. These values were mass averaged as shown in Table I.

Finally, the total pressure ratio over the inlet-fan combination was determined for comparison with the design specification.

Design B. - Table II shows the procedural steps taken to determine each parameter.

From the results of the inlet analysis for uniform flow, the conditions ahead of the rotor were taken as:

$$V_1 = V_{z,1} = V_{av} \text{ of DESIGN A} = 627.6 \text{ ft/sec (uniform)}$$

$$t_1 = 681.5^{\circ} \text{ R}$$

Total properties and rotor radii the same as Design A.

The detailed steps and design assumptions were similar to Design A. Iteration and mass-averaging were likewise similarly done.

Selection of Blading

General. - The blade-sections at each of the three radial positions were selected in order to satisfy the design velocity-diagrams.

Double-circular-arc blading was chosen for the rotor because this relatively simple airfoil shape has been used effectively in transonic compressors.

The NACA-65 (A_{10})-series airfoil was considered to be appropriate for the stator blading. The reasons for this choice were the magnitudes of the design inlet Mach numbers for the stator and the availability of extensive experimental data for this airfoil.

The parameters that describe blade-element flow are total-pressure loss, incidence angle, and deviation angle. The total-pressure-loss coefficient for minimum loss incidence has already been established in the determination of the velocity-diagrams. Therefore, the design incidence angle is for minimum loss.

Camber angle, incidence angle, and deviation angle are used to define the blade camber, air approach, and air leaving directions, respectively. These angles are shown in Fig. 28 for a typical blade-element.

Rotor. - A rotor-blade selection procedure is presented in [3] for the double-circular-arc airfoil. This method is based on a correlation of experimental test results with both annular and rectilinear cascades. Empirical correction

factors are used to modify the basic two-dimensional-cascade predictions for design blade shape. These factors are based largely on the testing of single-stage transonic compressors. Therefore, this method was considered appropriate for the fan design. The following equations from [3] were used to determine the blade-shape parameters:

$$\Delta\beta' = \varphi + i - \delta^\circ \tag{6.8}$$

$$i_c = K_i(i_o)_{10} + n\varphi + (i_c - i_{2\text{-}D}) \tag{6.9}$$

$$\delta_c^\circ = K_\delta(\delta_o^\circ)_{10} + \frac{m}{\sigma^b}\varphi + (i_c - i_{2\text{-}D})\left(\frac{d\delta^\circ}{di}\right)_{2\text{-}D} + (\delta_c^\circ - \delta_{2\text{-}D}^\circ) \tag{6.10}$$

$$\varphi = \frac{\Delta\beta' + (\delta_c^\circ - \delta_{2\text{-}D}^\circ) - (i_c - i_{2\text{-}D})\left[1 - \left(\frac{d\delta^\circ}{di}\right)_{2\text{-}D}\right] - K_i(i_o)_{10} + K_\delta(\delta_o^\circ)_{10}}{1 - \frac{m}{\sigma^b} + n} \tag{6.11}$$

The additional unknown parameters on the right side of these equations were determined from the velocity-diagram properties and an assumed blade thickness distribution as follows: for the rotor tip, t/c equal to 0.050; for the rotor mean radius, t/c equal to 0.075; for the rotor hub, t/c equal to 0.100. The thinning of the blade toward the tip was considered appropriate for the supersonic velocities present there, and the associated shock losses. In addition, this particular distribution matches that for the transonic rotor which was used for the determination of the radial loss distribution [6].

The procedural steps for the determination of camber, incidence, and deviation angles are shown in Tables III and IV for Design A and Design B, respectively.

For both designs the calculated camber angle for the 10% radial position was found to be negative. This occurred due to the very low turning angle required. For this case, a zero-camber blade section was chosen at this location. The corresponding values of incidence angle and deviation angle were determined by equations (6.9) and (6.8), respectively. Only the corrected values are shown in Tables III and IV; namely, those for a zero camber angle.

Stator. - The stator blade-sections were determined from the two-dimensional-cascade performance data for the NACA-65 (A_{10})-series airfoil as presented in [3]. A blade selection method based on a correlation between observed compressor performance and cascade predictions was not followed, as available stator data were considered to be too limited to establish reliable correlations.

The following equations from [3] were used to determine camber, incidence, and deviation angles:

$$\varphi = \frac{\Delta\beta - [(i_o)_{10} - (\delta_o^\circ)_{10}]}{[1 - m + n]} \tag{6.12}$$

$$i_c = i_{1\text{-}D} = (i_o)_{10} + n\varphi \tag{6.13}$$

$$\delta_c^\circ = \delta_{1\text{-}D}^\circ = (\delta_o^\circ)_{10} + \frac{m}{\sigma^b}\varphi \tag{6.14}$$

The additional unknown parameters on the right side of these equations were determined from the velocity-diagram properties and an assumed thickness distribution of t/c equal to 0.10 for the entire blade height. The choice of 10% maximum thickness was considered appropriate for the stator velocity-diagram conditions. This choice also simplified the use of the cascade performance curves in [3].

The procedural steps for the determination of camber, incidence, and deviation angles are shown in Tables III and IV for Design A and Design B, respectively.

7. Results and Discussion

Inlet Model

The primary result of the inlet model testing was the fact that axisymmetric flow could not be achieved for modifications that would be practical and have reasonably low losses.

The various modifications have been discussed in section 5. The axial velocity distributions for Mod. 1, Mod. 5, Mod. 6, and Mod. 7 are shown in Figures 11, 17, 20, and 24, respectively. The loss distributions for Mod. 1, Mod. 5, Mod. 6, and Mod. 7 are shown in Figures 12, 18, 21, and 25, respectively. Results for the other modifications were considered insignificant and are not shown.

Mod. 7 was selected for the fan design because it gave the best flow distribution of the configurations tested. However, the improvement over the original inlet-model was slight. The Mod. 7 results for axial velocity distribution were circumferentially averaged as shown in Figure 26, and corrected for system errors such as probe blockage and instrumentation inaccuracies. This averaging process was necessary so that available fan design procedures could be used. However, Figure 26 could present a misleading impression of the inlet-model test results and should be appraised in conjunction with Figure 24 which shows the Mod. 7 distribution by stations.

Most of the modifications produced only small changes of the flow pattern. Only the large "S" vanes of Mod. 6

produced large variations from the original flow distribution. This modification caused excessive flow to exist at the previously deficient stations 1, 2, and 8. The losses for these stations were also lowest for Mod. 6 as compared to all other configurations. It seems possible that a modification similar to Mod. 6 could produce axisymmetric flow, but only at the expense of high losses. Such a configuration could evolve from a trial and error process of reducing the surface area, curvature, leading-edge spacing between vanes, and/or chord of the "S" vanes.

The reason for the lack of axial symmetry for more practical modifications such as Mod. 7 is largely due to the area constriction forced on the flow as it approaches the top of the model casing (near station 1). The slopes of the casing (13 degrees) as shown in Figure 4 are excessive. Another reason for the lack of axial symmetry might be that the top of the model was not extended far enough from the annulus centerline. This distance was not specified but would necessarily be a design consideration for an aircraft system.

The curvatures of the model bellmouth contours are excessive. This was indicated by the thicker boundary-layers and higher velocities near the outer radius for most of the eight stations. The larger velocities form an adverse gradient ahead of the fan; that is, the relative inlet Mach number at the rotor tip is increased. This condition is especially critical as this Mach number is an important design limit.

The Mod. 7 pitch and yaw angles are shown with the data reduction procedures in Appendix A. Pitch angles were greatest at stations 4, 5, and 6 where they averaged about -9^{o} (radially inward). Yaw angles were highest at stations 2, 3, 7, and 8 where they averaged about 17 degrees.

It should be noted that the algebraic signs of the pitch angles as shown in Appendix A are taken with respect to the pressure probe. Positive pitch angle is for flow that is radially outward. Thus, the signs for $\ominus$ for stations 1, 2, 7, and 8 are correct as indicated; and the signs for stations 3, 4, 5, and 6 must be reversed to comply with the established sign convention. Yaw angles are shown with proper signs. That is, positive yaw angles occur for tangential velocity components producing clockwise flow if looking upstream at the discharge.

Fan Design

The results for Design A and Design B are very similar because the averaged velocity distribution for Design A is nearly uniform (Fig. 26). The performance figures and blade-section values listed below are for both designs.

The velocity-diagram determinations for Design A and Design B are shown in Tables I and II, respectively. The selection of blade-sections are shown in Tables III and IV for the designs in the same order.

The adiabatic stage efficiency (based on total conditions) was 90.5 percent, and the total-pressure ratio was 1.243.

The latter value exceeds the design specification requirement of 1.178 by 5.5 percent.

Twelve double-circular-arc blades were selected for the rotor. The blade chord varied uniformly from 0.85 in. to 0.75 in. from hub to tip, respectively. The maximum thickness distribution varied uniformly from 0.10 to 0.05 from hub to tip, respectively. The blade height at rotor entrance was 0.83 inches. The blade height at rotor discharge was 0.74 inches.

Thirteen NACA-65 (A_{10})-series blades were selected for the stator. A constant blade-chord of 0.805 in. and a constant maximum thickness ratio of 0.10 were used. The height of the stator blades was constant, equal to 0.74 inches.

The rotor blade camber angle was zero degrees near the tip (10% location). This occurred due to the low air turning angle in that region (4^{o} - 5^{o}).

It was necessary to circumferentially average the axial velocity distribution for Design A as the design method is based on the assumption of axial symmetry. The results of this averaging gave nearly uniform flow as shown in Figure 26. However, Figure 24 shows that the actual flow distributions are lacking in axial symmetry. Therefore, the Design A results may be misleading. In addition, the large changes of flow angle for Mod. 7 would cause large variations from the design incidence angle for the rotor blades. This condition is especially undesirable in transonic rotors as low losses occur only over a very narrow range of inlet flow angles at high Mach numbers as pointed out in [3] .

However, Robbins and Glaser [7] have shown that circumferential inlet flow distortion of velocity and flow angle may not have as significant an effect upon compressor performance as might be expected. In [7] the results of considerable circumferential distortion showed that the adiabatic efficiency and pressure ratio were unchanged, and that the equivalent weight flow was slightly reduced. These results pertain to tests on a five-stage transonic compressor. After the first stage most of the flow angle distortion became equalized and the velocity distortion was reduced by about 30 percent.

Therefore, the lack of axial symmetry in the Design A inlet may not be critical. However, the compact size of the fan and the fact that it is only single stage makes comparison with [7] less significant.

Thus, it seems apparent that actual testing would be necessary to determine the effect of the inlet-distortion on the predicted fan performance of Design A. The Design B blading was designed for uniform flow and could be used for a comparison if tested with the Design B assumed rotor entrance conditions (or 'similar' flow conditions).

The design results show that the curvature changes through the rotor blading were small. That is, the three streamlines that were considered (10%, 50%, and 90% locations) experienced relatively small radius changes. Therefore, the design assumption of zero entropy gradient behind the rotor was considered valid.

The simplifying assumptions that V_z equals V_{mer} and $\partial V_r / \partial z = 0$ were also considered appropriate because the design blading had low aspect ratio (about 1.0) and was lightly loaded, having small diffusion factors.

A critical area in the determination of the velocity diagrams was the chord-solidity selection, as the flow through the blade-rows was close to the critical blade-chord-Reynolds number. This condition occurred due to the compactness of the fan.

Operation at higher blade-chord-Reynolds number could be attained by re-design. Since the diffusion factors are relatively low the number of rotor and stator blades could be reduced by one. For the same solidity level the chord could be increased in proportion to the blade spacing increase. Thus the blade-chord-Reynolds number would be higher and the flow would be less likely to experience losses associated with low Reynolds number.

This paper presents a simplified approach for the aerodynamic fan design which is commonly used for the design of axial-flow compressors. The complicated real flow effects such as secondary flow, tip clearance losses, and unsteady flow were ignored, as they were considered to be beyond the scope of this study. Furthermore, it is realized that for an actual design it might be necessary to repeat the design calculations to assure a satisfactory design that is sound both from an aerodynamic and a mechanical point of view.

Table I. Calculation of Velocity-Diagrams for Design A

Step	Parameter	Known Design Condition	Procedure	Radial Position		
				10%	50%	90%
1	r_1	$r_{1,t} = 1.74$ $b_1 = 0.83$	$r_{1,t} - 7.\, b_1$	1.657	1.325	.993
2	$U_1 = V'_{\theta,1}$	$N = 85{,}000$	$r_1\, \omega$	1229.1	982.7	736.6
3	$V_{z,1}/V_{av}$	Fig. 26		1.053	1.009	.982
4	$V_{z,1}$	$V_{av} = 627.6$	$(V_z/V_{av})_1\, V_{av}$	660.9	633.3	616.3
5	β'_1		$\tan^{-1}(V'_{\theta,1}/V_{z,1})$	61.7	57.2	50.1
6	V'_1		$(V_{z,1}^2 + V'^2_{\theta,1})^{1/2}$	1395.5	1169.1	960.4
7	t_1	$T_0 = T_1 = 714°$	$T_1 - V_1'^2/(2gJc_p)$	678.0	681.0	682.7
8	M'_1		$V'_1/(\gamma g R t_1)^{1/2}$	1.095	.915	.751
9	r_2	$r_{2,t} = 1.74$ $b_2 = 0.74$	$r_{2,t} - 7.\, b_2$	1.666	1.370	1.074
10	$(r/r_t)_2$			.957	.787	.617
11	$V_{\theta,2}$	$DP = 23.916$ $\dot{w} = 83.5$ $N = 85{,}000$	$\frac{DP\, g}{\dot{w}\, \omega}\, \frac{1}{r_2}$	246.3	299.5	382.0
12	U_2		$r_2\, \omega$	1235.2	1015.8	796.4

Table I. (Continued)

Step	Parameter	Known Design Condition	Procedure	Radial Position		
				10%	50%	90%
13	$T_2 = T_3$	$T_1 = 714^\circ$	$T_1 + \frac{r_2 \omega V_{\theta,2}}{J g c_p}$	764.1	764.1	764.1
14	$V_{z,2}$	$V_{z,2} = V_{z,1,m}$		633.3	633.3	633.3
15	$V'_{\theta,2}$		$U_2 - V_{\theta,2}$	988.9	716.3	414.4
16	V_2		$(V_{z,2}^2 + V_{\theta,2}^2)^{1/2}$	679.5	700.5	739.6
17	β_2		$\cos^{-1}(V_{z,2}/V_2)$	21.2	25.2	31.0
18	β'_2		$\tan^{-1}(V'_{\theta,2}/V_{z,2})$	57.4	48.5	33.2
19	$\cos\beta'_2$			.53931	.66237	.83677
20	V'_2		$V_{z,2} / \cos\beta'_2$	1174.3	956.1	756.8
21	t_2		$T_2 - V_2^2/(2gJc_p)$	726.1	723.7	719.0
22	M_2		$V_2/(\gamma g R t_2)^{1/2}$	.515	.532	.564
23	M'_2		$V'_2/(\gamma g R t_2)^{1/2}$	.891	.726	.577
24	c_2		$c_{1,h} - \frac{c_{1,h} - c_{1,t}}{r_{1,t} - r_{1,h}}(r - r_{1,h})$	.759	.795	.830
25	s_2	$B = 12$ blades	$\frac{2\pi r_2}{B}$	.872	.717	.562

Table I. (Continued)

Step	Parameter	Known Design Condition	Procedure	Radial Position		
				10%	50%	90%
26	σ_2		c_2 / s_2	.870	1.108	1.477
27	σ_{av}	$\sigma_1 = \sigma_{av}$ For First iteration	$\frac{\sigma_1 + \sigma_2}{2}$	.873	1.130	1.546
28	D'		$1 - \frac{V_2'}{V_1'} + \frac{\Delta V_\theta'}{2 \sigma_{av} V_1'}$	.260	.296	.341
29	$\bar{\omega}'$		[6]	.090	.053	.030
30	$\left(\frac{p}{P'}\right)_2$		$\left[1 + \frac{\gamma - 1}{2} M_2'^2\right]^{\frac{\gamma}{1-\gamma}}$	.59842	.70497	.79872
31	$\frac{P_2}{P_1}$	$P_1 = 13.534$ (assumed)	$\left(\frac{T_2}{T_1}\right)^{\frac{\gamma}{\gamma-1}} \left[1 - \bar{\omega}' \left\{1 - \left(\frac{p}{P'}\right)_2\right\}\right]$	1.225	1.251	1.263
32	$g \rho_2$		$\frac{P_2}{P_1} \frac{P_1}{R T_2} \left[1 - \frac{V_2^2}{2 g J c_p T_2}\right]^{\frac{1}{\gamma-1}}$	.05149	.05214	.05179
33	$(\rho g V_z r)_2$			54.33	45.24	35.23
34	$\dot{w}$	$K_{bK} = 0.96$	$2\pi r_{2,t} K_{bK} \int_{(r_h/r_t)_2}^{1.0} (\rho g V_z r)_2 \, d\left(\frac{r_2}{r_{2,t}}\right)$		83.72	
35	$r_2 = r_3$			1.666	1.370	1.074
36	$\left(\frac{r}{r_t}\right)_3$			.957	.787	.617

Table I. (Continued)

Step	Parameter	Known Design Condition	Procedure	Radial Position		
				10%	50%	90%
37	$V_{z,3}$	$V_{z,3} = V_3$ Assume $V_3 = V_{z,2}$		633.3	633.3	633.3
38	t_3	$T_2 = T_3 = 764.1^\circ$	$T_3 - V_3^2/(2gJc_p)$	731.1	731.1	731.1
39	M_3		$V_3/(\gamma g R t_3)^{1/2}$	.479	.479	.479
40	$\mu_2 \times 10^7$		[5]	154.654	154.318	153.660
41	σ	B = 13 blades c = 0.805	$\frac{c B}{2\pi r_3}$	1.000	1.216	1.550
42	$N_{Re} \times 10^{-5}$		$\left(\frac{\rho V}{\mu}\right)_2 c$	1.518	1.588	1.672
43	D		$1 - \frac{V_3}{V_2} + \frac{\Delta V_\theta}{2\sigma V_2}$	.249	.272	.310
44	$\bar{\omega} \frac{\cos\beta_3}{2\sigma}$		[3]	.0070	.0080	.0088
45	$\bar{\omega}$	$\beta_3 = 0^\circ$	$\left(\frac{\bar{\omega}}{2\sigma}\right) 2\sigma$	.0140	.0195	.0273
46	$\left(\frac{p}{P}\right)_3$		$\left[1 + \frac{\gamma-1}{2} M_3^2\right]^{\frac{\gamma}{1-\gamma}}$	.85536	.85536	.85536
47	$\frac{P_3}{P_2}$		$1 - \bar{\omega}\left\{1 - \left(\frac{p}{P}\right)_3\right\}$	.99798	.99718	.99605

Table I. (Concluded)

Step	Parameter	Known Design Condition	Procedure	Radial Position		
				10%	50%	90%
48	$g\rho_3$	$P_1 = 13.534$	$\frac{P_3}{P_2}\frac{P_2}{P_1}\frac{P_1}{RT_3}\left[1 - \frac{V_3^2}{2gJc_pT_3}\right]^{\frac{1}{\gamma-1}}$	.05227	.05334	.05379
49	$(\rho g V_r)_3$			55.15	46.28	36.59
50	$\dot{w}$	$K_{bk} = 0.94$	$2\pi r_{3,t} K_{bk} \int_{\left(\frac{r_h}{r_t}\right)_3}^{1.0} (\rho g V_r)_3 \, d\left(\frac{r_3}{r_{3,t}}\right)$		83.485	
	$\frac{P_3}{P_1}$	$P_1 = 13.534$		1.22253	1.24747	1.25801
	$\eta_{ad.,ST}$		$\left[\left(\frac{P_3}{P_1}\right)^{\frac{\gamma-1}{\gamma}} - 1\right] \Big/ \left[\frac{T_3}{T_1} - 1\right]$	.8337	.9192	.9563
	$\left(\frac{P_3}{P_1}\right)_{ma}$		$\frac{\sum_j (\Delta r \rho V_r)_j (P_3/P_1)_j}{\sum_j (\Delta r \rho V_r)_j}$		1.243	
	$(\eta_{ad.})_{ma}$		$\left[\left(\frac{P_3}{P_1}\right)_{ma}^{\frac{\gamma-1}{\gamma}} - 1\right] \Big/ \left[\frac{T_3}{T_1} - 1\right]$		.905	
	$\frac{P_3}{P_0}$	$P_0 = 13.656$ $P_1 = 13.534$	$\left(\frac{P_3}{P_1}\right)_{ma} \frac{P_1}{P_0}$		1.232	

Table II. Calculation of Velocity-Diagrams for Design B

Step	Parameter	Known Design Condition	Procedure	Radial Position		
				10%	50%	90%
1	r_1	$r_{1,t} = 1.74$ $b_1 = 0.83$	$r_{1,t} - \tau_0 b_1$	1.657	1.325	.993
2	$U_1 = V_{\theta,1}'$	$N = 85{,}000$	$r_1 \omega$	1229.1	982.7	736.6
3	$V_{z,1}/V_{av}$	Assumed uniform		1.000	1.000	1.000
4	$V_{z,1}$	$V_{av} = 627.6$		627.6	627.6	627.6
5	β_1'		$\tan^{-1}(V_{\theta,1}'/V_{z,1})$	62.95	57.45	49.55
6	V_1'		$(V_{z,1}^2 + V_{\theta,1}'^2)^{1/2}$	1380.1	1166.0	967.7
7	t_1	$T_0 = T_1 = 714°$	$T_1 - V_1'^2/(2gJc_p)$	681.5	681.5	681.5
8	M_1'		$V_1'/(\gamma g R t_1)^{1/2}$	1.080	.913	.757
9	r_2	$r_{2,t} = 1.74$ $b_2 = 0.74$	$r_{2,t} - \tau_0 b_2$	1.666	1.370	1.074
10	$(r/r_t)_2$			.957	.787	.617
11	$V_{\theta,2}$	$DP = 23.916$ $\dot{w} = 83.5$ $N = 85{,}000$	$\frac{DP\ g}{\dot{w}\ \omega}\ \frac{1}{r_2}$	246.3	299.5	382.0
12	U_2		$r_2 \omega$	1235.2	1015.8	796.4

Table II. (Continued)

Step	Parameter	Known Design Condition	Procedure	Radial Position		
				10%	50%	90%
13	$T_2 = T_3$	$T_1 = 714^\circ$	$T_1 + \frac{r_2 \omega V_{\theta,2}}{J g c_p}$	764.1	764.1	764.1
14	$V_{z,2}$	$V_{z,2} = V_{z,1}$		627.6	627.6	627.6
15	$V_{\theta,2}'$		$U_2 - V_{\theta,2}$	988.9	716.3	414.4
16	V_2		$\left(V_{z,2}^2 + V_{\theta,2}^2\right)^{1/2}$	674.2	695.4	734.7
17	β_2		$\cos^{-1}\left(V_{z,2} / V_2\right)$	21.60	25.50	31.30
18	β_2'		$\tan^{-1}\left(V_{\theta,2}' / V_{z,2}\right)$	57.60	48.80	33.45
19	$\cos \beta_2'$			.53583	.65869	.83437
20	V_2'		$V_{z,2} / \cos \beta_2'$	1171.3	952.8	752.2
21	t_2		$T_2 - V_2'^2 / (2 g J c_p)$	726.7	724.3	719.6
22	M_2		$V_2 / (\gamma g R t_2)^{1/2}$	.5110	.5280	.5596
23	M_2'		$V_2' / (\gamma g R t_2)^{1/2}$	.8878	.7234	.5730
24	c_2		$c_{1,h} - \frac{c_{1,h} - c_{1,t}}{r_{1,t} - r_{1,h}}(r - r_{1,h})$	.759	.795	.830
25	s_2	$B = 12$ blades	$\frac{2\pi r_2}{B}$	.872	.717	.562

Table II. (Continued)

Step	Parameter	Known Design Condition	Procedure	Radial Position		
				10%	50%	90%
26	σ_2		c_2 / s_2	.870	1.108	1.477
27	σ_{av}	$\sigma_1 = \sigma_{av}$ for first iteration	$\frac{\sigma_1 + \sigma_2}{2}$	.873	1.130	1.546
28	D'		$1 - \frac{V_2'}{V_1'} + \frac{\Delta V_\theta'}{2 \sigma_{av} V_1'}$	.2535	.2965	.3504
29	$\bar{\omega}'$		[6]	.090	.053	.030
30	$\left(\frac{p}{P'}\right)_2$		$\left[1 + \frac{\gamma - 1}{2} M_2'^2\right]^{\frac{\gamma}{1-\gamma}}$	.6003	.7069	.8012
31	$\frac{P_2}{P_1}$	$P_1 = 13.534$	$\left(\frac{T_2}{T_1}\right)^{\frac{\gamma}{\gamma-1}} \left[1 - \bar{\omega}' \left\{1 - \left(\frac{p}{P'}\right)_2\right\}\right]$	1.2248	1.2508	1.2629
32	$g \rho_2$		$\frac{P_2}{P_1} \frac{P_1}{R T_2} \left[1 - \frac{V_2^2}{2 g J c_p T_2}\right]^{\frac{1}{\gamma-1}}$	.05158	.05222	.05189
33	$(\rho g V_z r)_2$			53.931	44.899	34.976
34	$\dot{w}$	$K_{bK} = 0.96$	$2\pi r_{2,t} K_{bK} \int_{(r_h/r_t)_2}^{1.0} (\rho g V_z r)_2 \, d\left(\frac{r_2}{r_{2,t}}\right)$		83.45	
35	$r_2 = r_3$			1.666	1.370	1.074
36	$\left(\frac{r}{r_t}\right)_3$			.957	.787	.617

Table II. (Continued)

Step	Parameter	Known Design Condition	Procedure	Radial Position		
				10%	50%	90%
37	$V_{z,3}$	$V_{z,3} = V_3$ $V_3 = V_{z,2}$		627.6	627.6	627.6
38	t_3	$T_2 = T_3 = 764.1^\circ$	$T_3 - V_3^2/(2gJc_p)$	731.7	731.7	731.7
39	M_3		$V_3/(\gamma g R t_3)^{1/2}$	.474	.474	.474
40	$\mu_2 \times 10^7$		[5]	154.738	154.402	153.744
41	σ	B = 13 blades c = 0.805	$\frac{c\,B}{2\pi r_3}$	1.000	1.216	1.550
42	$N_{Re} \times 10^{-5}$		$\left(\frac{\rho V}{\mu}\right)_2 c$	1.508	1.578	1.663
43	D		$1 - \frac{V_3}{V_2} + \frac{\Delta V_\theta}{2\sigma V_2}$	.252	.275	.313
44	$\bar{\omega}\frac{\cos\beta_3}{2\sigma}$		[3]	.0071	.0082	.0090
45	$\bar{\omega}$	$\beta_3 = 0^\circ$	$\left(\frac{\bar{\omega}}{2\sigma}\right) 2\sigma$	.0142	.0199	.0279
46	$\left(\frac{p}{P}\right)_3$		$\left[1 + \frac{\gamma-1}{2} M_3^2\right]^{\frac{\gamma}{1-\gamma}}$	.8580	.8580	.8580
47	$\frac{P_3}{P_2}$		$1 - \bar{\omega}\left\{1 - \left(\frac{p}{P}\right)_3\right\}$	.99798	.99717	.99604

Table II. (Concluded)

Step	Parameter	Known Design Condition	Procedure	Radial Position		
				10%	50%	90%
48	$g\rho_3$	$P_1 = 13.534$	$\frac{P_3}{P_2}\frac{P_2}{P_1}\frac{P_1}{RT_3}\left[1 - \frac{V_3^2}{2gJc_pT_3}\right]^{\frac{1}{\gamma-1}}$	.05211	.05317	.05363
49	$(\rho g V_r)_3$			54.49	45.72	36.15
50	$\dot{w}$	$K_{bK} = 0.94$	$2\pi r_{3,t} K_{bK} \int_{\left(\frac{r_h}{r_t}\right)_3}^{1.0} (\rho g V_r)_3 \, d\left(\frac{r_3}{r_{3,t}}\right)$		83.44	
	$\frac{P_3}{P_1}$	$P_1 = 13.534$		1.22233	1.24726	1.25790
	$\eta_{ad,ST}$		$\left[\left(\frac{P_3}{P_1}\right)^{\frac{\gamma-1}{\gamma}} - 1\right] \Big/ \left[\frac{T_3}{T_1} - 1\right]$	.8337	.9192	.9549
	$\left(\frac{P_3}{P_1}\right)_{ma}$		$\frac{\sum_j (\Delta r \rho V_r)_j (P_3/P_1)_j}{\sum_j (\Delta r \rho V_r)_j}$		1.243	
	$(\eta_{ad})_{ma}$		$\left[\left(\frac{P_3}{P_1}\right)_{ma}^{\frac{\gamma-1}{\gamma}} - 1\right] \Big/ \left[\frac{T_3}{T_1} - 1\right]$		.905	
	$\frac{P_3}{P_0}$	$P_0 = 13.656$ $P_1 = 13.534$	$\left(\frac{P_3}{P_1}\right)_{ma} \frac{P_1}{P_0}$		1.232	

Table III. Blade-Sections for Design A

(a.) Rotor

Parameter	Procedure	Radial Position		
		10%	50%	90%
β_1'	Table I	61.7	57.2	50.1
β_2'	Table I	57.4	48.5	33.2
$\Delta\beta'$	$\beta_1' - \beta_2'$	4.3	8.7	16.9
M_1'	Table I	1.095	.915	.751
σ	Table I	.873	1.130	1.546
t/c	Assumed	.055	.075	.095
$\delta_c^\circ - \delta_{2\text{-}D}^\circ$	[3]	- 1.5	- .2	1.16
$i_c - i_{2\text{-}D}$	[3]	4.00	6.20	6.15
$(d\delta^\circ/di)_{2\text{-}D}$	[3]	.148	.070	.025
K_i	[3]	.513	.611	.686
$(i_o)_{10}$	[3]	4.14	4.96	6.08
K_δ	[3]	.330	.485	.662
$(\delta_o^\circ)_{10}$	[3]	1.70	1.80	1.70
m	[3]	.317	.306	.294
n	[3]	- .279	- .201	- .113
b	[3]	.660	.712	.782
φ	eq. (6.11)	0	1.11	13.30
i_c	eq. (6.9)	6.12	9.01	8.82
δ_c°	eq. (6.10)	1.82	1.42	5.22

Table III. (Concluded)

(b.) Stator

Parameter	Procedure	Radial Position		
		10%	50%	90%
$\beta_2=\Delta\beta$	Table I, $\beta_3=0^\circ$	21.2	25.2	31.0
σ	Table I	1.000	1.216	1.550
$(i_o)_{10}-(\delta_o^\circ)_{10}$	[3]	1.34	1.97	3.08
$(1-m+n)$	[3]	.745	.783	.820
$(i_o)_{10}$	[3]	1.70	2.47	3.82
$(\delta_o^\circ)_{10}$	[3]	.35	.48	.73
m	[3]	.180	.184	.191
n	[3]	- .075	- .064	- .050
b	[3]	.918	.905	.886
φ	eq. (6.12)	26.65	29.68	34.04
i_c	eq. (6.13)	- .30	.57	2.11
δ_c°	eq. (6.14)	5.15	5.05	5.15

Table IV. Blade-Sections for Design B

(a.) Rotor

Parameter	Procedure	Radial Position		
		10%	50%	90%
β_1'	Table II	62.95	57.45	49.55
β_2'	Table II	57.60	48.80	33.45
$\Delta\beta'$	$\beta_1' - \beta_2'$	5.35	8.65	16.10
M_1'	Table II	1.080	.913	.757
σ	Table II	.873	1.130	1.546
t/c	Assumed	.055	.075	.095
$\delta_c^\circ - \delta_{2\text{-}D}^\circ$	[3]	- 1.50	- .19	1.18
$i_c - i_{2\text{-}D}$	[3]	3.90	6.15	6.25
$(d\delta^\circ/di)_{2\text{-}D}$	[3]	.150	.070	.025
K_i	[3]	.513	.611	.686
$(i_o)_{10}$	[3]	4.15	4.96	6.00
K_δ	[3]	.330	.485	.662
$(\delta_o^\circ)_{10}$	[3]	1.78	1.80	1.67
m	[3]	.320	.307	.291
n	[3]	- .287	- .202	- .110
b	[3]	.644	.710	.786
φ	eq. (6.11)	0	1.13	11.96
i_c	eq. (6.9)	6.03	8.95	9.05
δ_c°	eq. (6.10)	.68	1.43	4.91

Table IV. (Concluded)

(b.) Stator

Parameter	Procedure	Radial Position		
		10%	50%	90%
$\beta_2=\Delta\beta$	Table II, $\beta_3=0^\circ$	21.6	25.5	31.3
σ	Table II	1.000	1.216	1.550
$(i_o)_{10}-(\delta_o^\circ)_{10}$	[3]	1.36	1.99	3.10
$(1-m+n)$	[3]	.744	.781	.819
$(i_o)_{10}$	[3]	1.72	2.50	3.87
$(\delta_o^\circ)_{10}$	[3]	.36	.49	.74
m	[3]	.181	.185	.192
n	[3]	- .076	- .065	- .051
b	[3]	.916	.903	.885
φ	eq. (6.12)	27.21	30.10	34.42
i_c	eq. (6.13)	- .34	.55	2.10
δ_c°	eq. (6.14)	5.27	5.15	5.22

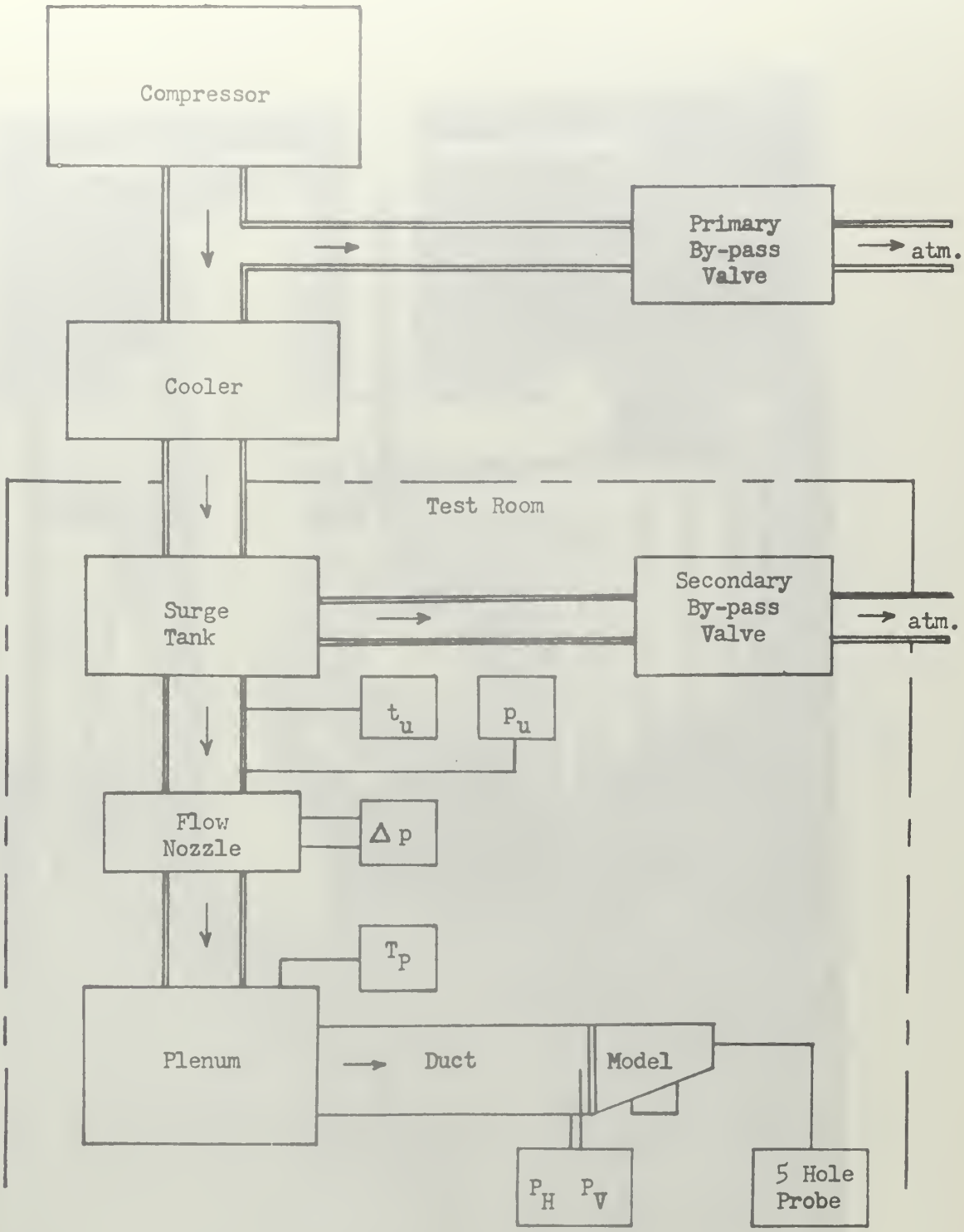

Fig. 1

Test Facility

Fig. 2

Test Equipment

Fig. 3

Inlet Model - Section

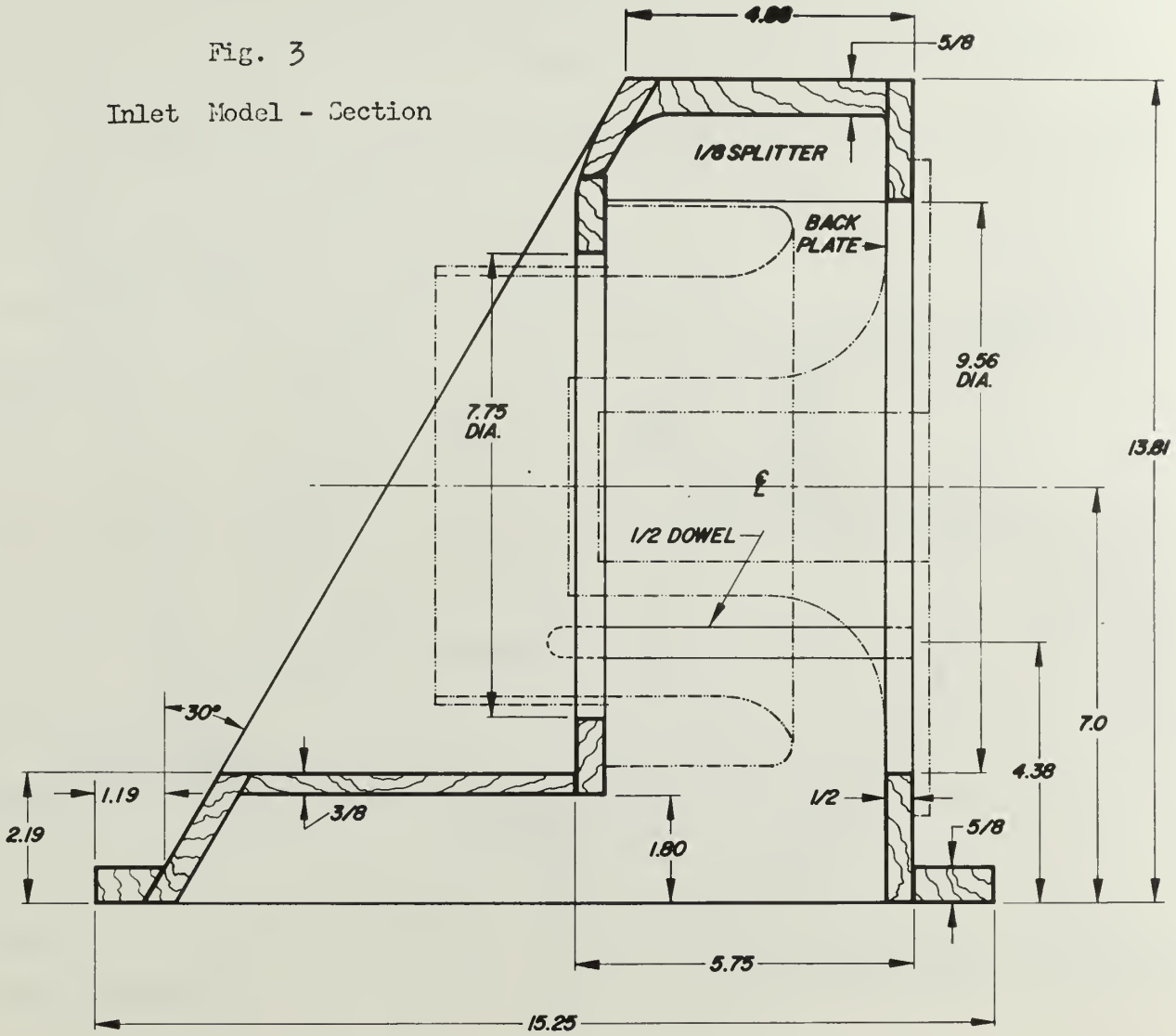

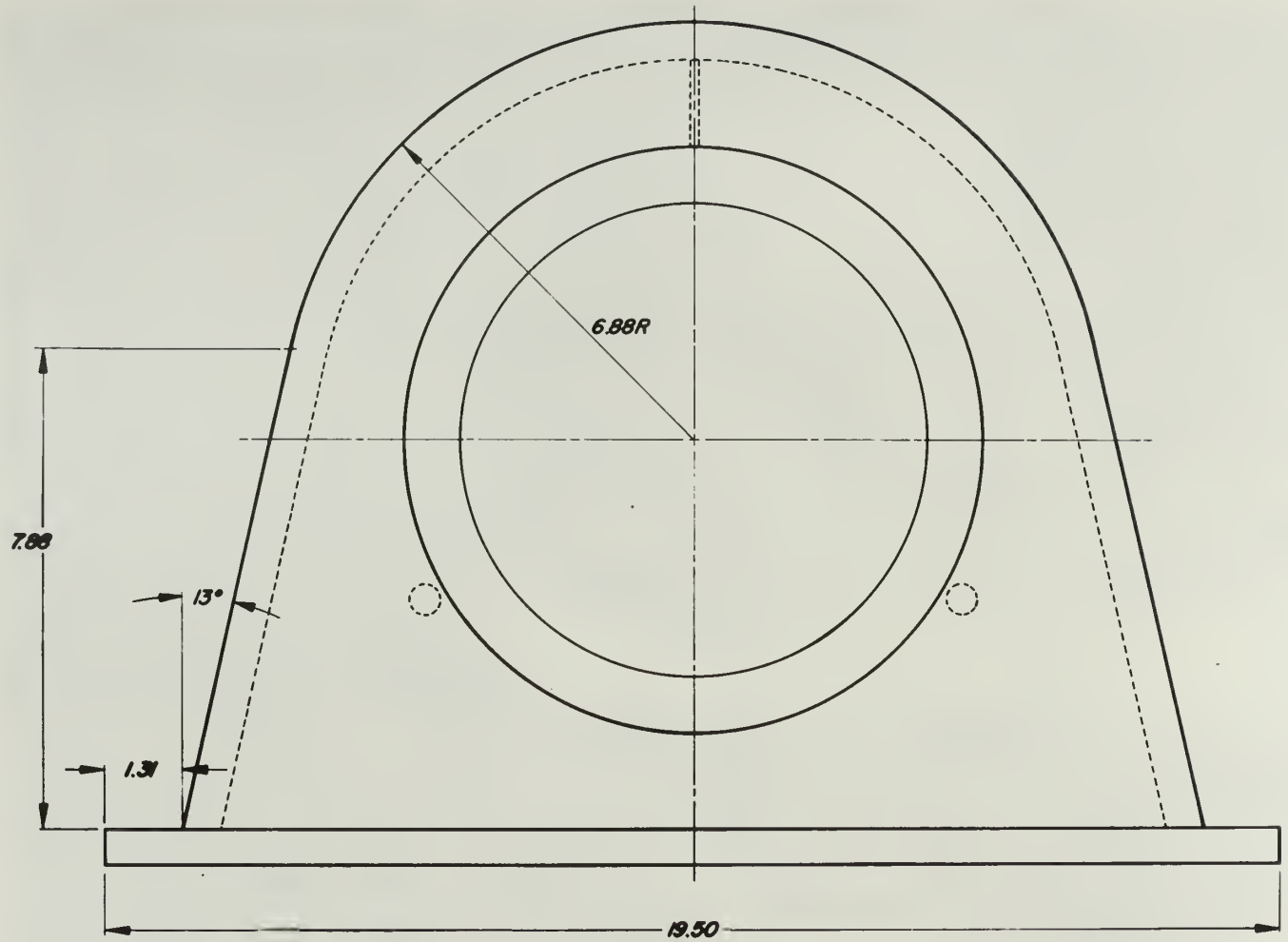

Fig. 4

Inlet Model - Downstream View

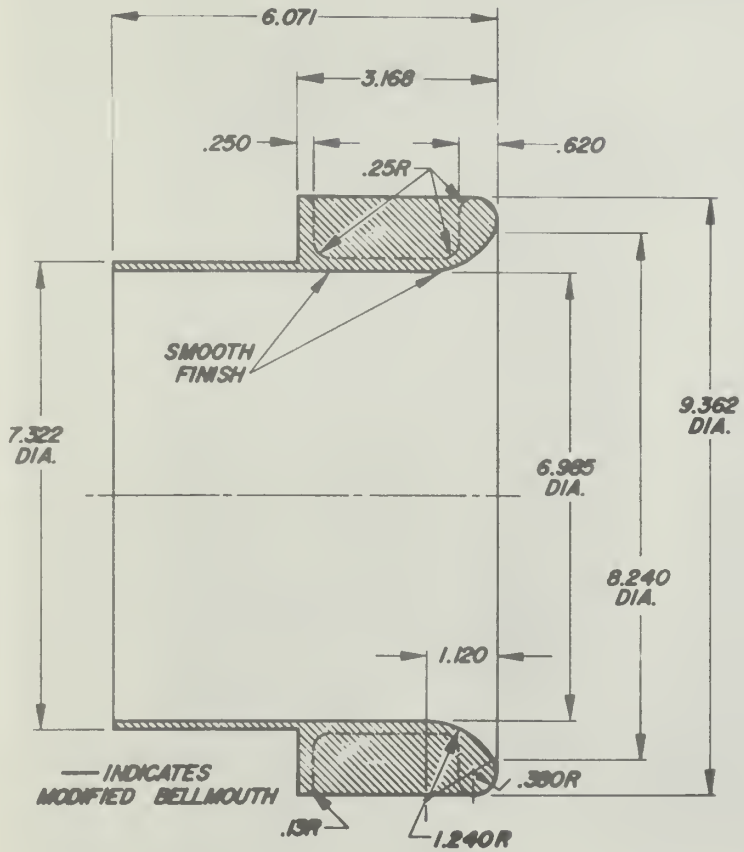

Fig. 5

Inlet Model - Bellmouth

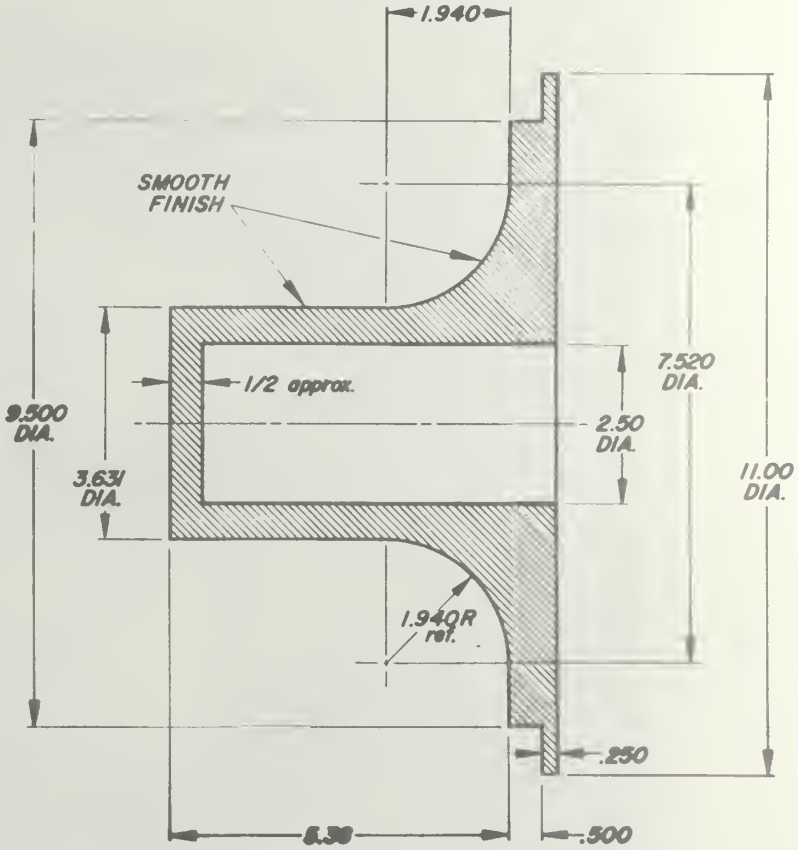

Fig. 6

Inlet Model - Bellmouth Hub Section

Fig. 7

Inlet Model - Bellmouth Hub View

Fig. 8

Probe Traverse Stations

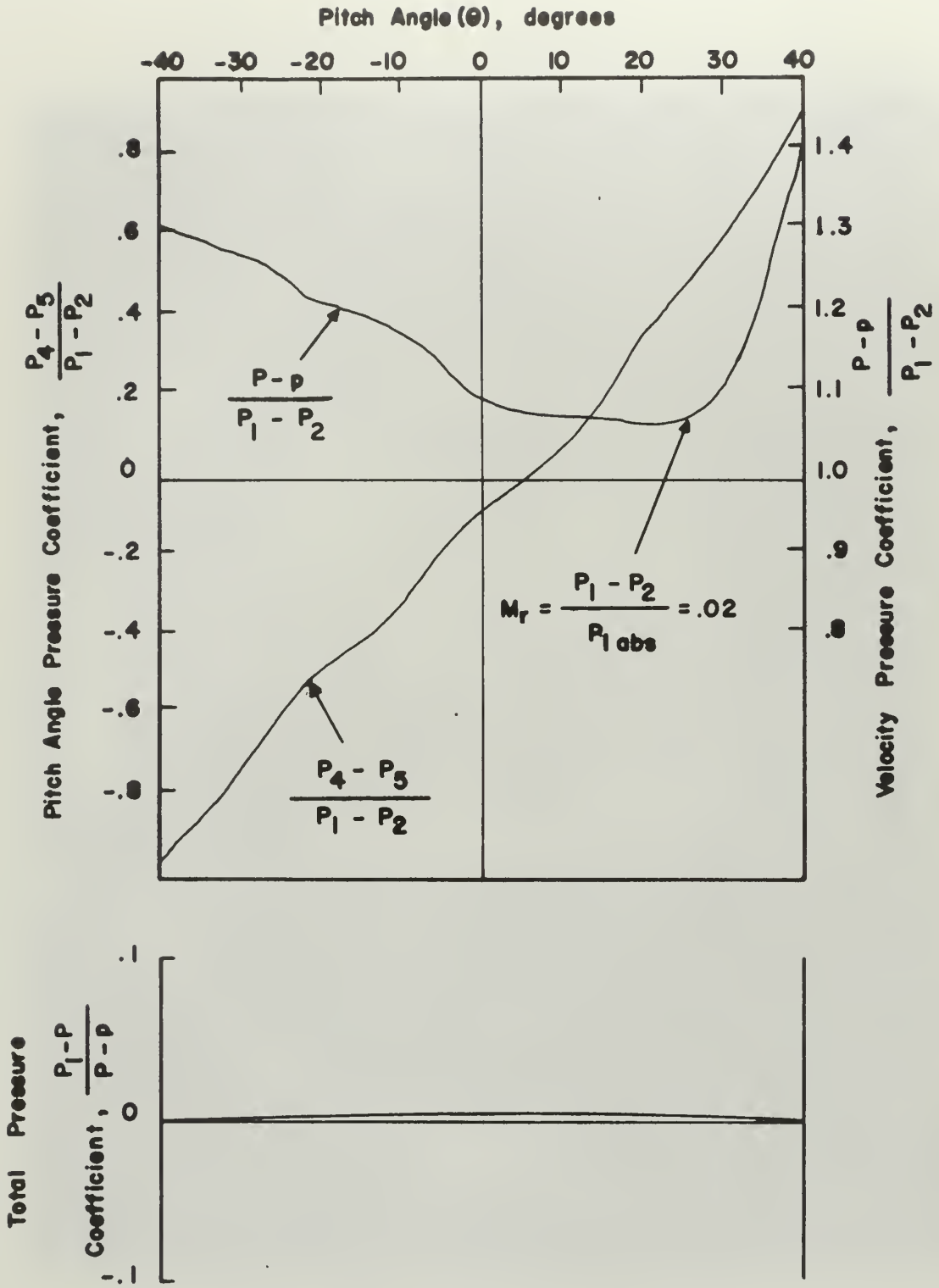

FIG. 9

CALIBRATION OF DA-120 PROBE NO. 535

Fig. 10

Inlet Model - Mod. 1

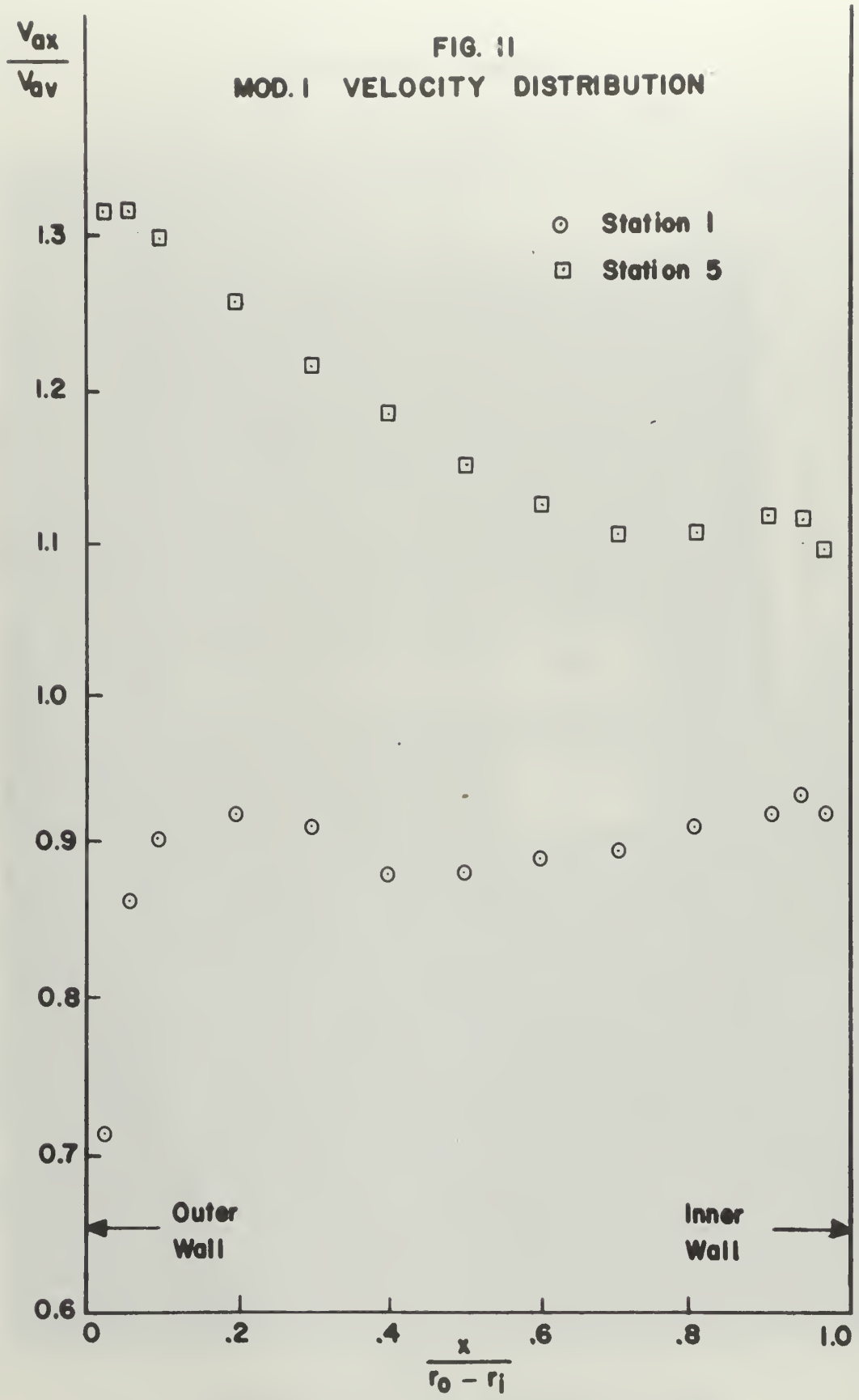
FIG. 11
MOD. 1 VELOCITY DISTRIBUTION
$\frac{V_{ax}}{V_{av}}$
Station 1
Station 5
1.3
1.2
1.1
1.0
0.9
0.8
0.7
0.6
Outer Wall
Inner Wall
0
.2
.4
.6
.8
1.0
$\frac{x}{r_o - r_i}$

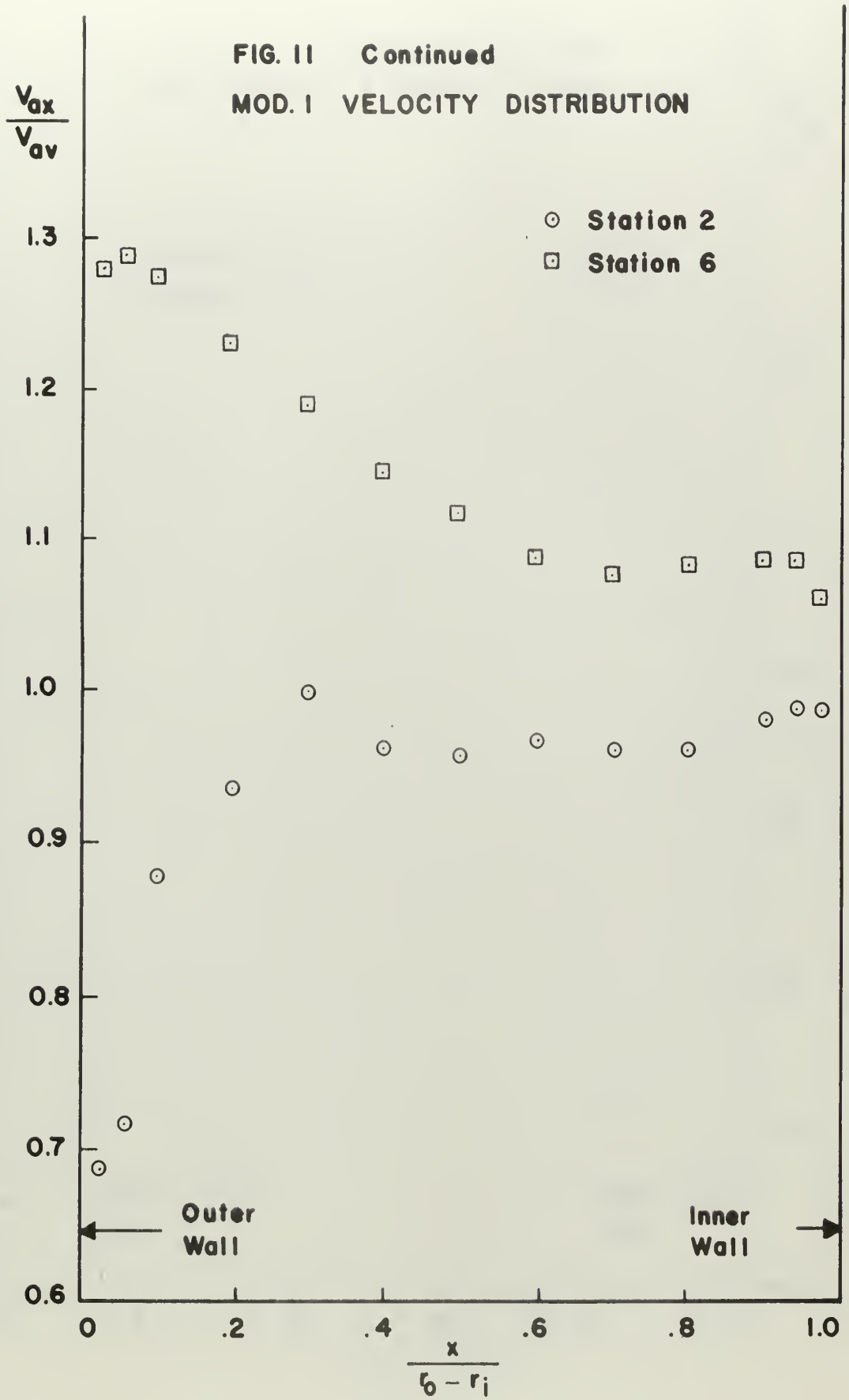
FIG. 11 Continued
MOD. 1 VELOCITY DISTRIBUTION
$\frac{V_{ax}}{V_{av}}$
Station 2
Station 6
1.3
1.2
1.1
1.0
0.9
0.8
0.7
0.6
Outer Wall
Inner Wall
0
.2
.4
.6
.8
1.0
$\frac{x}{r_o - r_i}$

FIG. 11 Continued
MOD. I VELOCITY DISTRIBUTION

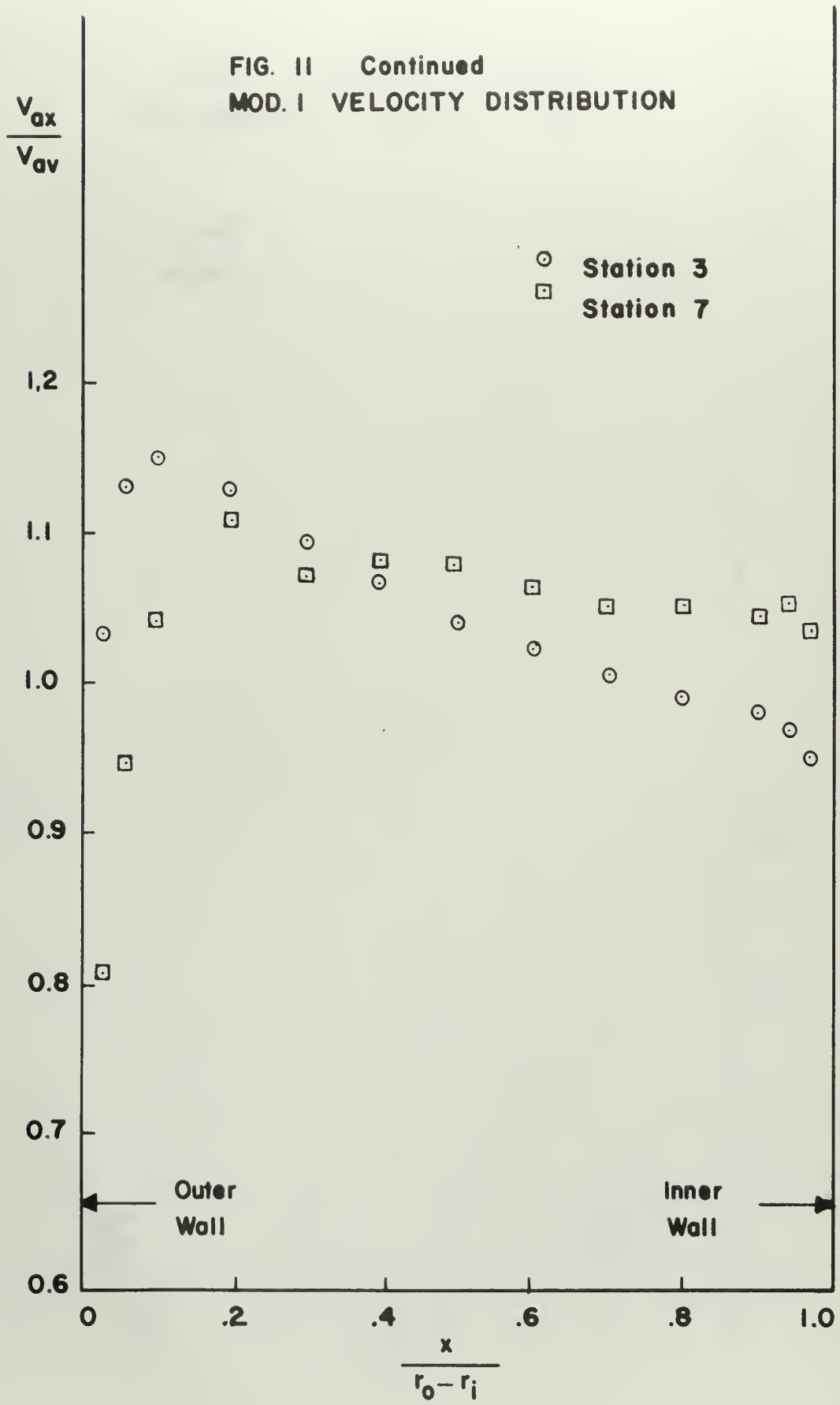

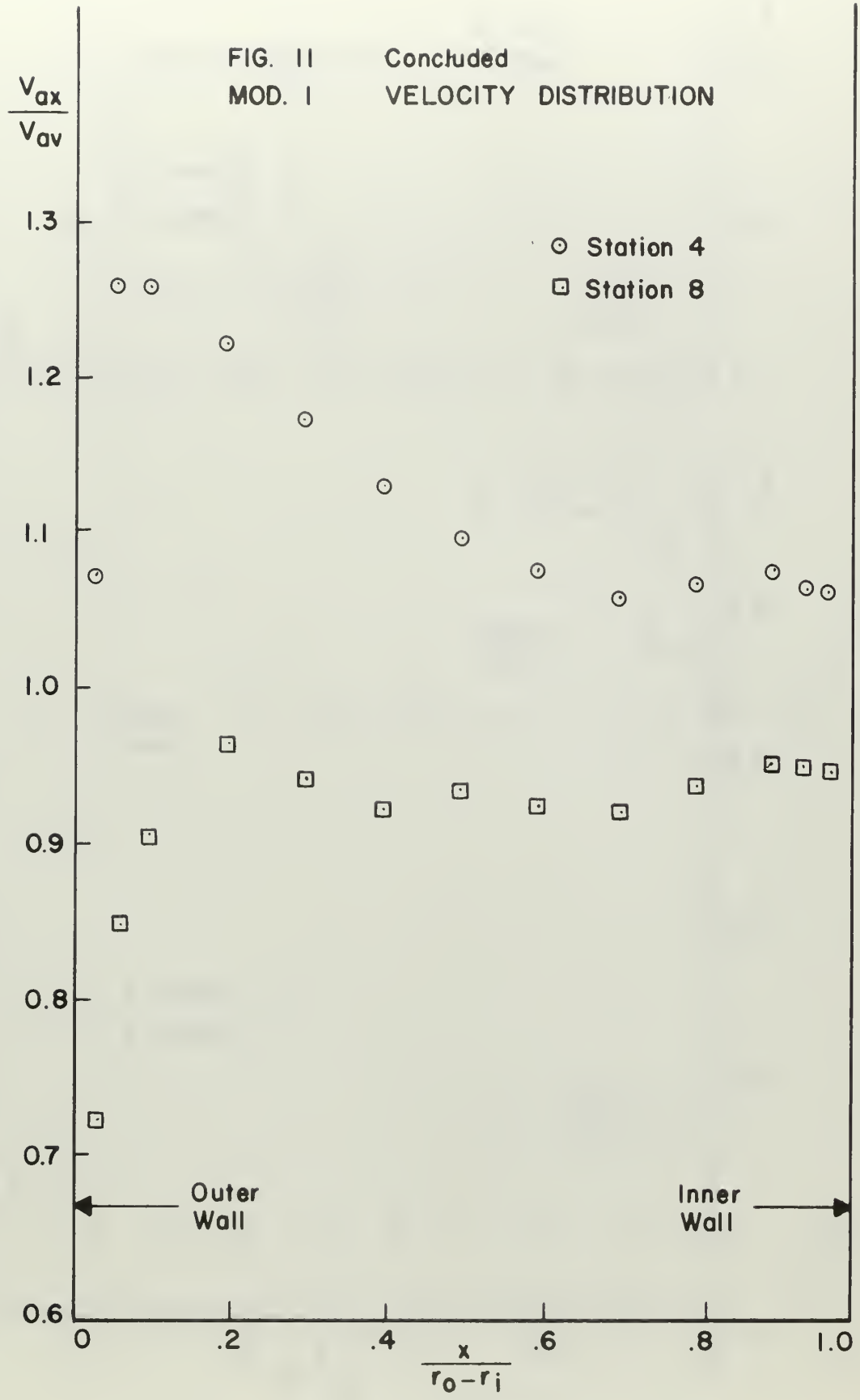
FIG. 11 Concluded
MOD. I VELOCITY DISTRIBUTION
$\frac{V_{ax}}{V_{av}}$
1.3
1.2
1.1
1.0
0.9
0.8
0.7
0.6
Station 4
Station 8
Outer Wall
Inner Wall
0
.2
.4
.6
.8
1.0
$\frac{x}{r_o - r_i}$

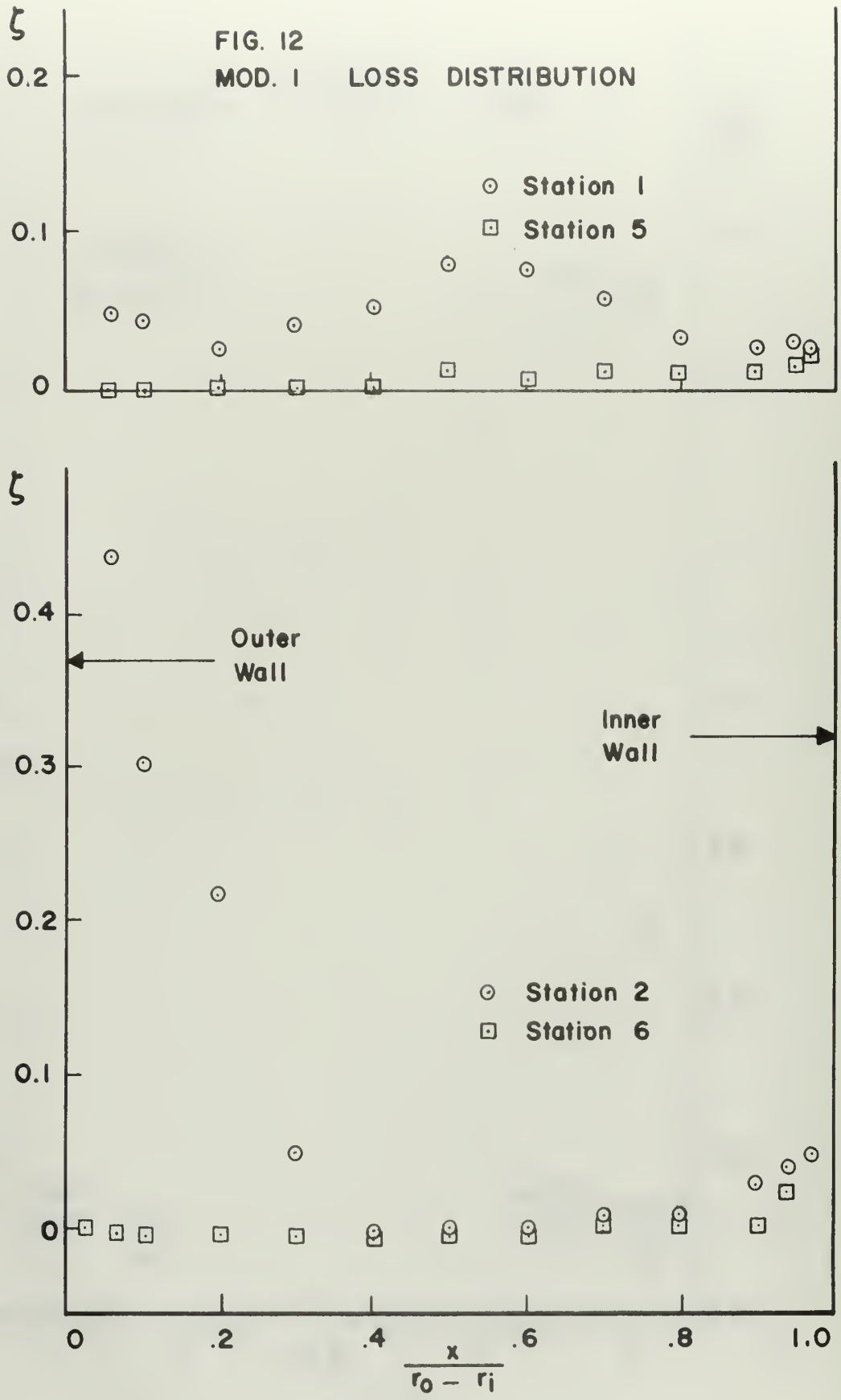
ζ
FIG. 12
MOD. 1 LOSS DISTRIBUTION
0.2
0.1
0
Station 1
Station 5
ζ
0.4
0.3
0.2
0.1
0
Outer Wall
Inner Wall
Station 2
Station 6
0
.2
.4
.6
.8
1.0
x / r0 − ri

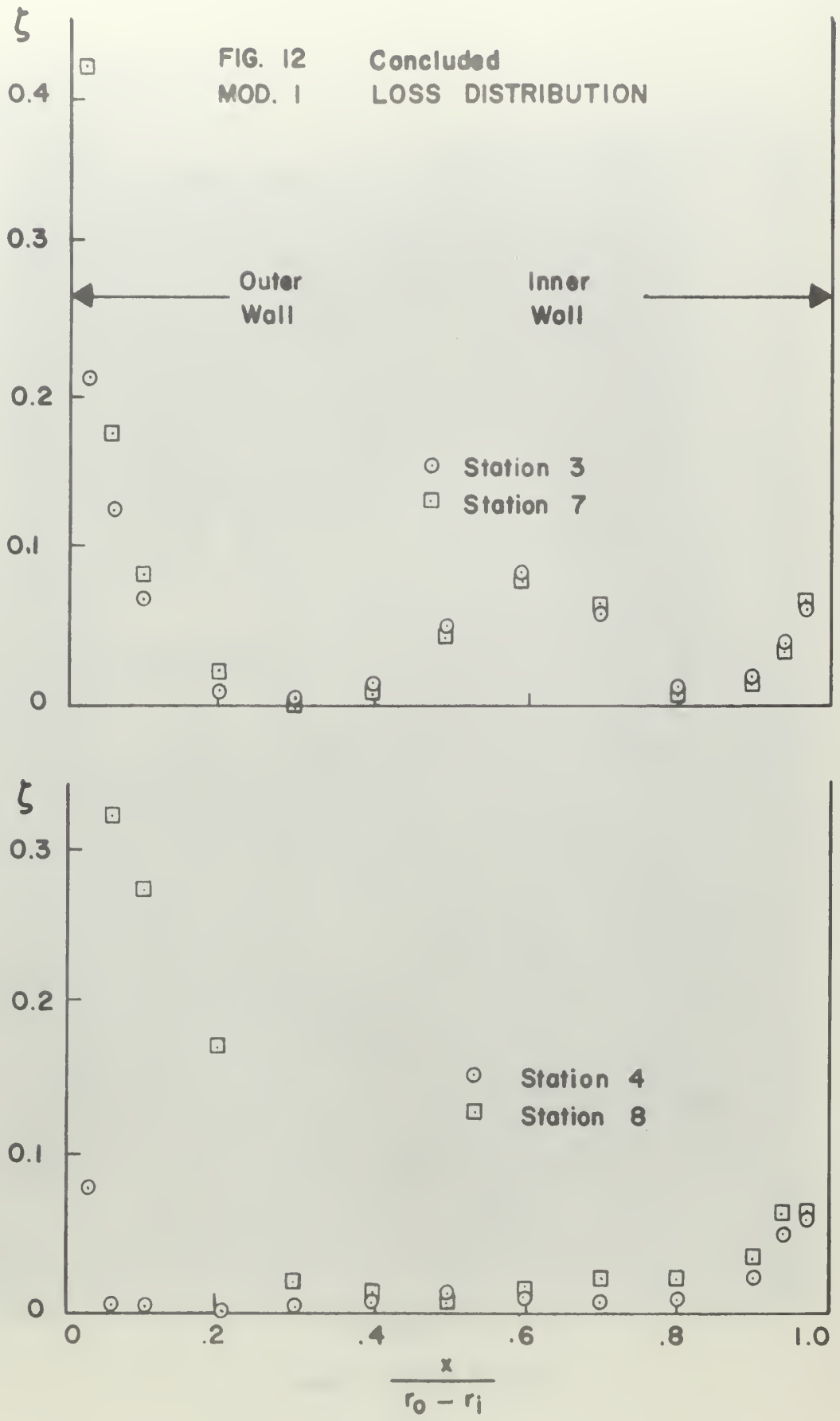

FIG. 12 Concluded
MOD. I LOSS DISTRIBUTION

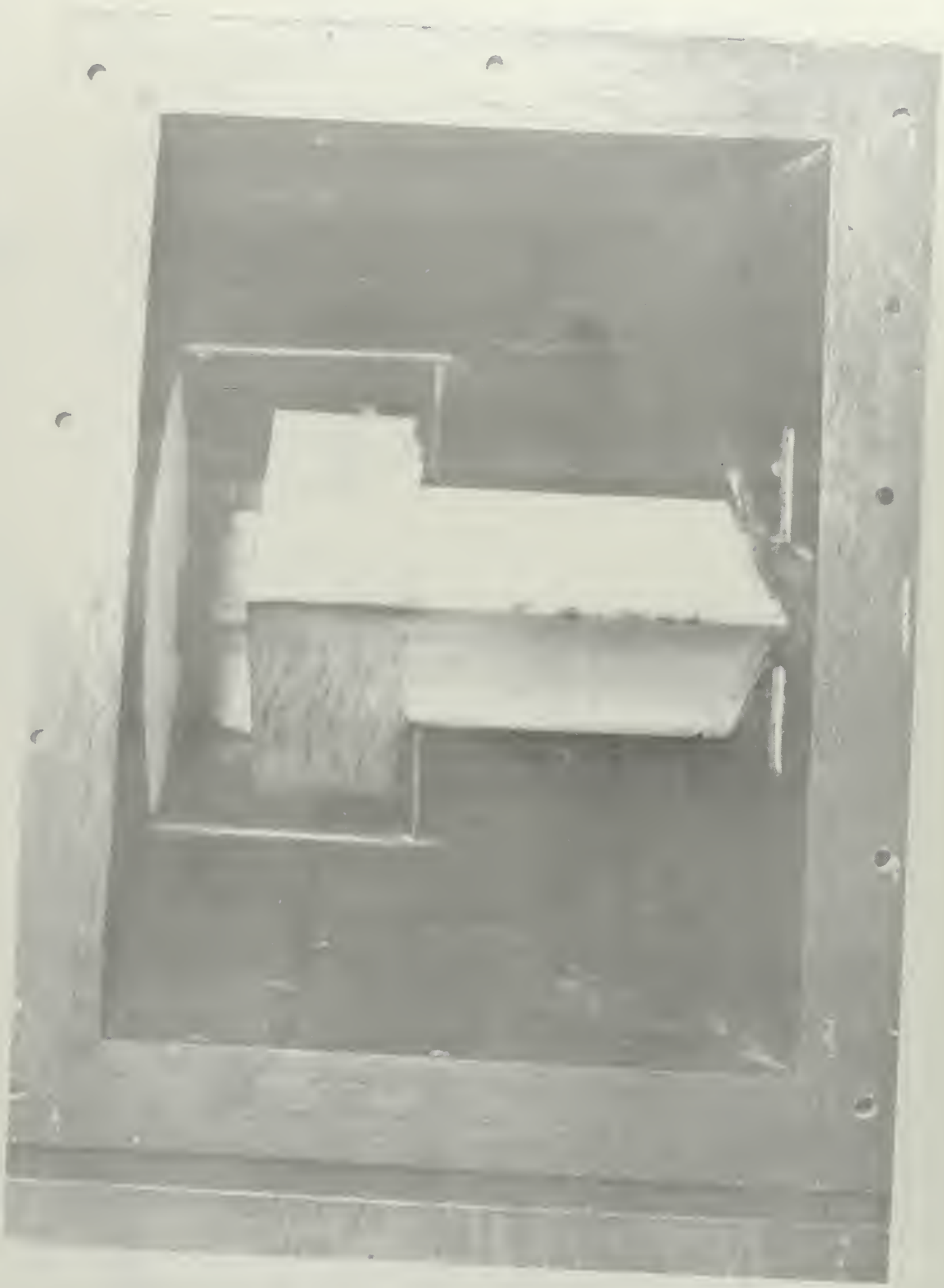

Fig. 13

Inlet Model - Mod. 2

Fig. 14

Inlet Model - Mod. 3

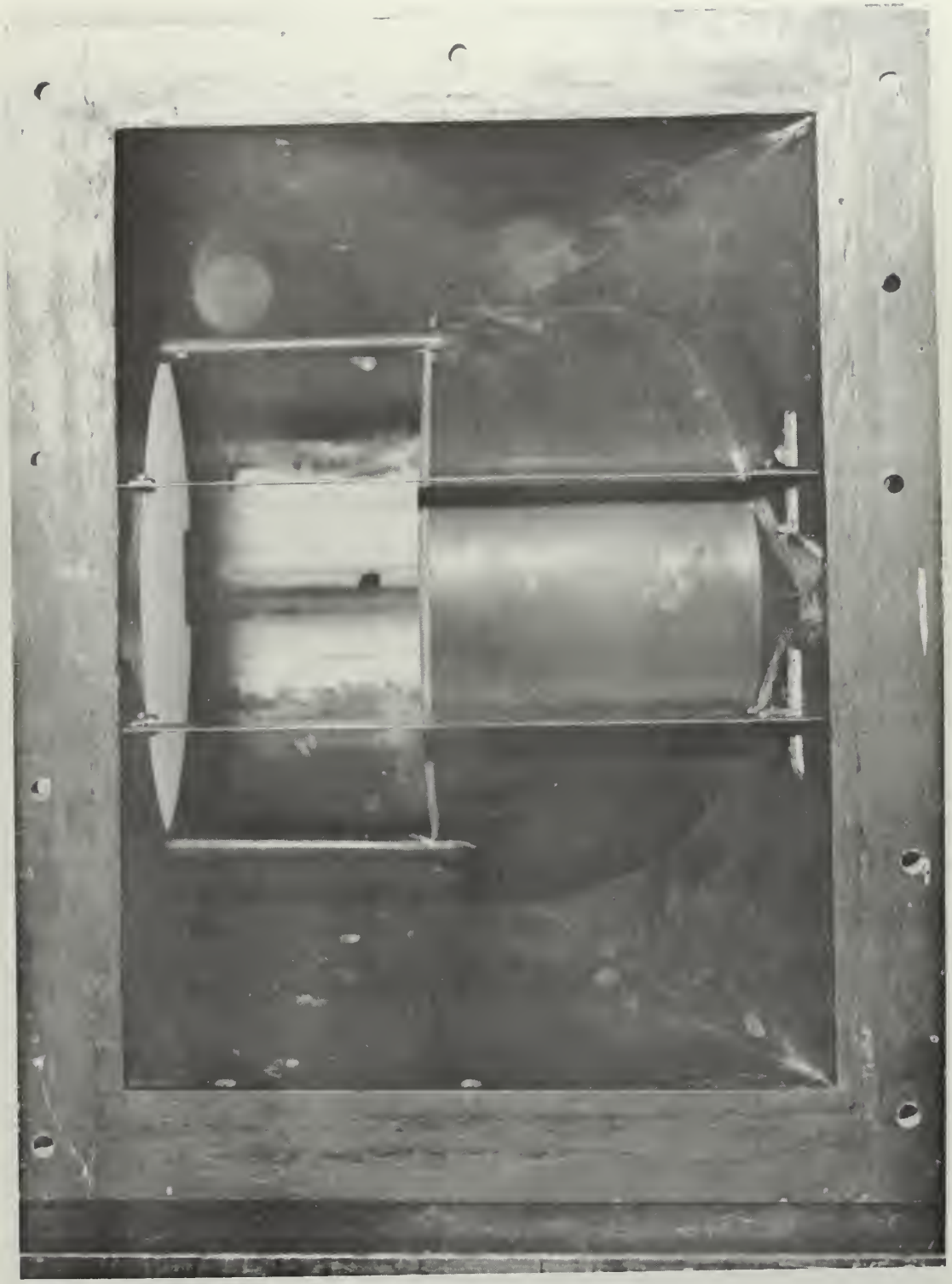

Fig. 15

Inlet Model - Mod. 4

Fig. 16

Inlet Model - Mod. 5

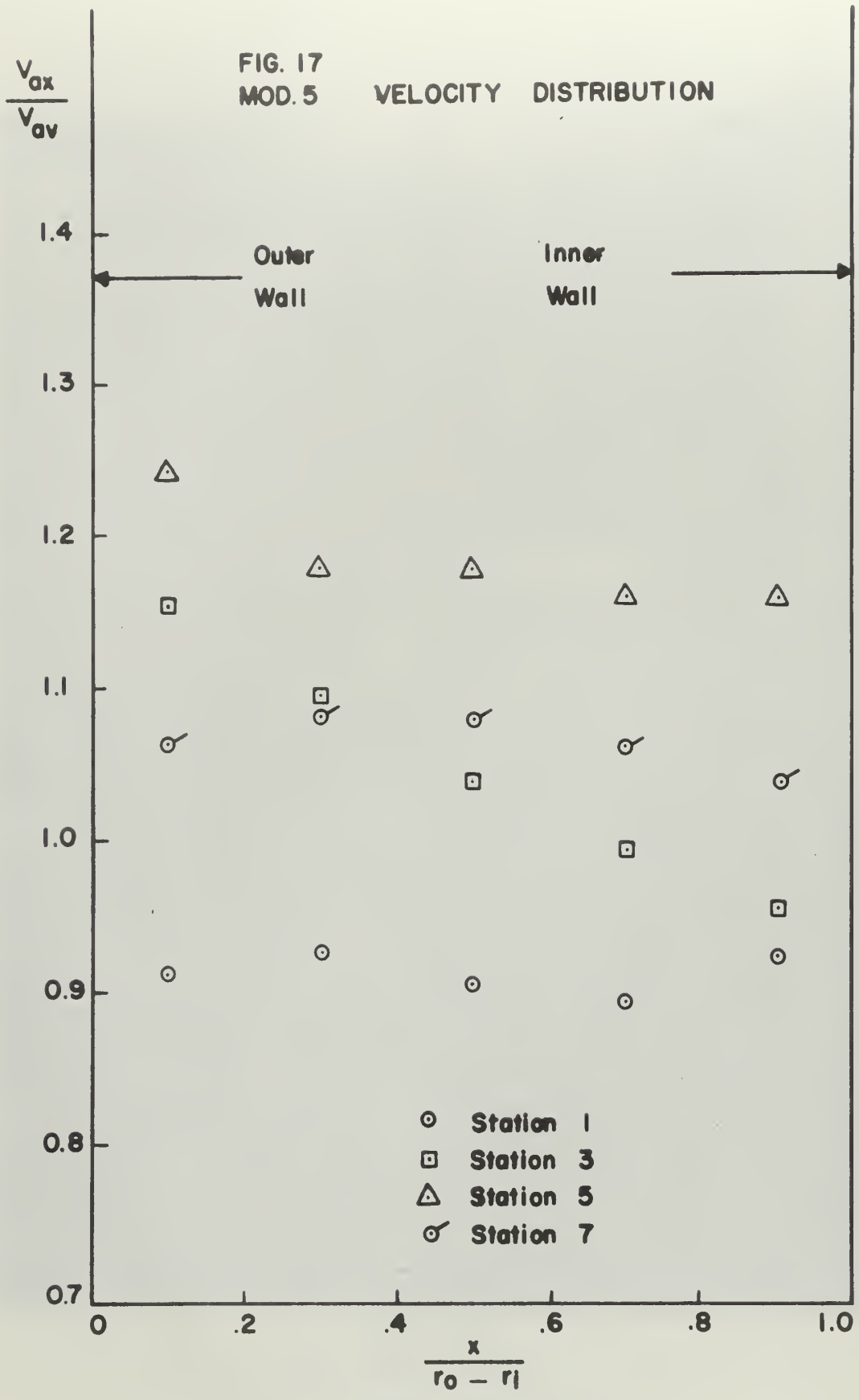
FIG. 17
MOD. 5 VELOCITY DISTRIBUTION
$\frac{V_{ax}}{V_{av}}$
1.4
1.3
1.2
1.1
1.0
0.9
0.8
0.7
Outer Wall
Inner Wall
Station 1
Station 3
Station 5
Station 7
0
.2
.4
.6
.8
1.0
$\frac{x}{r_o - r_i}$

FIG. 18

MOD. 5 LOSS DISTRIBUTION

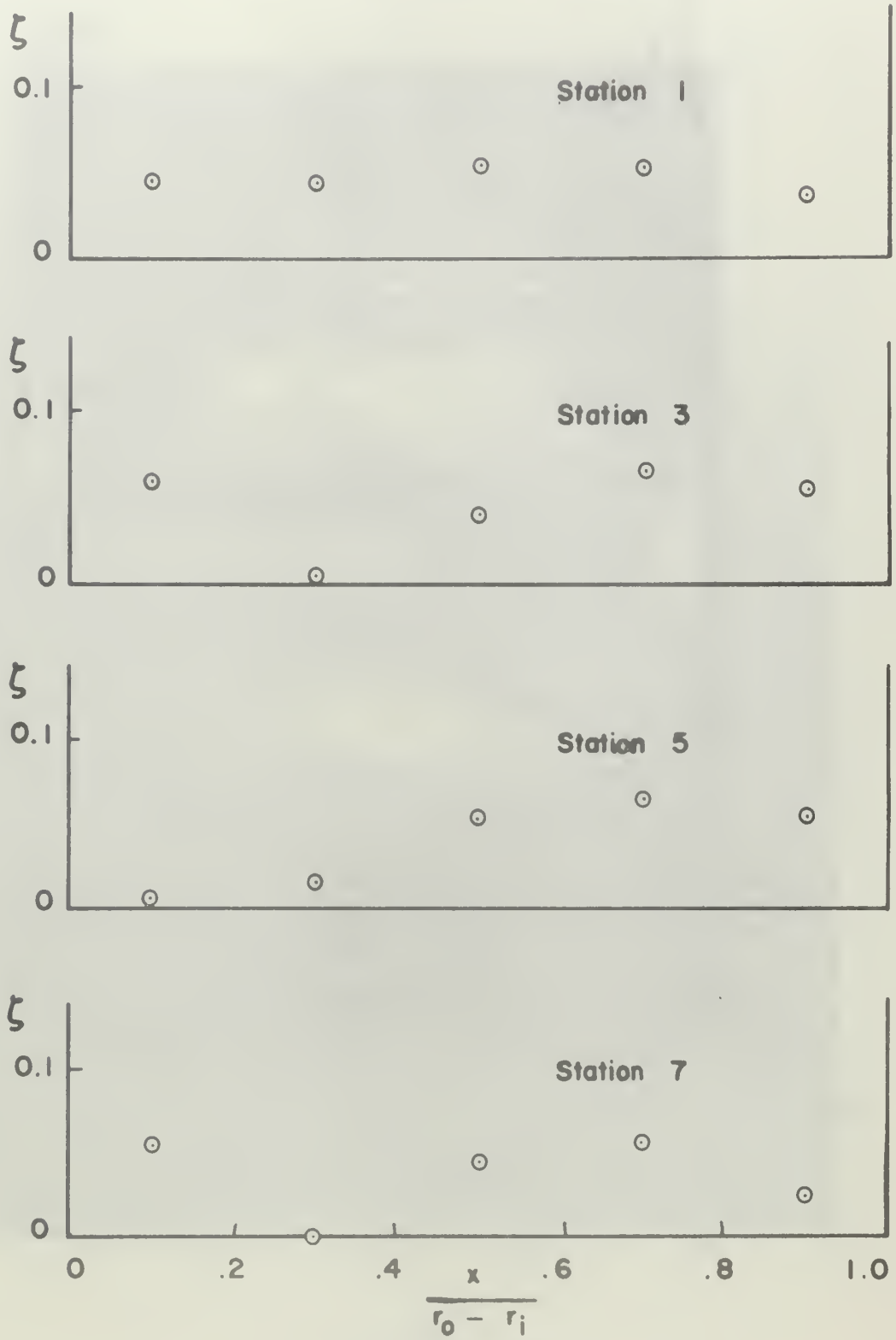

Fig. 19
Inlet Model - Mod. 6

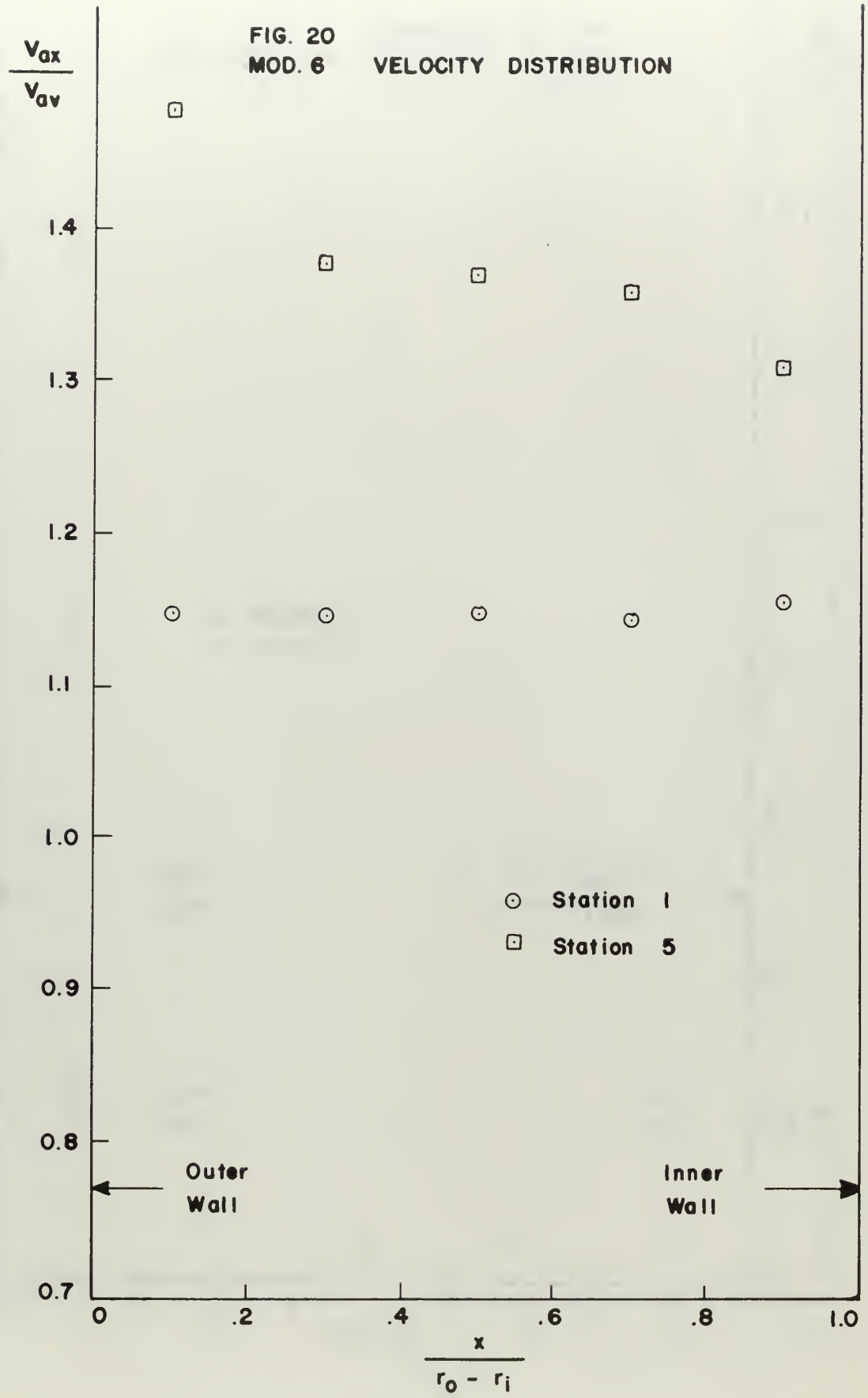
FIG. 20
MOD. 6 VELOCITY DISTRIBUTION
$\frac{V_{ax}}{V_{av}}$
1.4
1.3
1.2
1.1
1.0
0.9
0.8
0.7
Station 1
Station 5
Outer Wall
Inner Wall
0
.2
.4
.6
.8
1.0
$\frac{x}{r_o - r_i}$

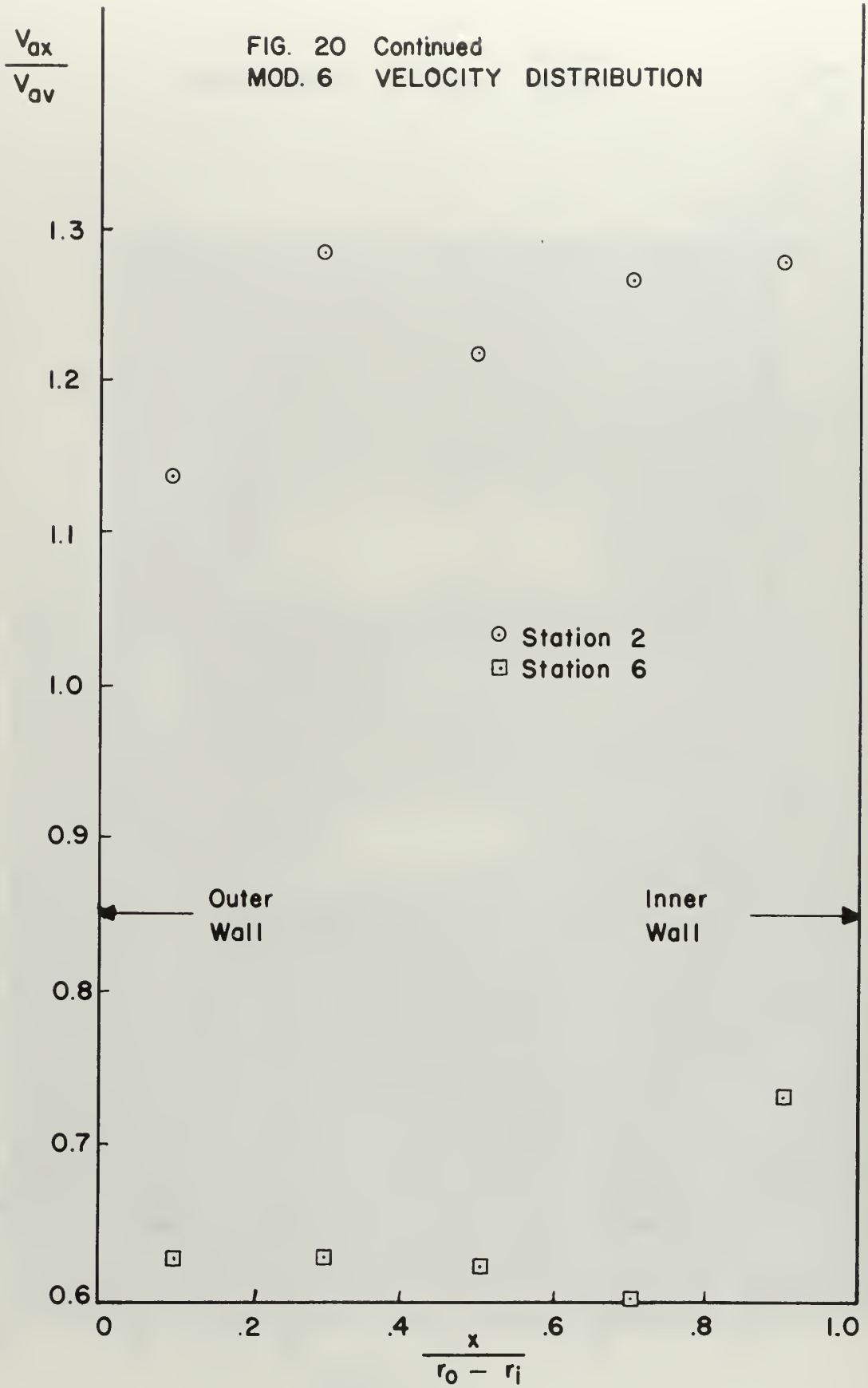
$\frac{V_{ax}}{V_{av}}$
FIG. 20 Continued
MOD. 6 VELOCITY DISTRIBUTION
1.3
1.2
1.1
1.0
0.9
0.8
0.7
0.6
Station 2
Station 6
Outer Wall
Inner Wall
0
.2
.4
.6
.8
1.0
$\frac{x}{r_o - r_i}$

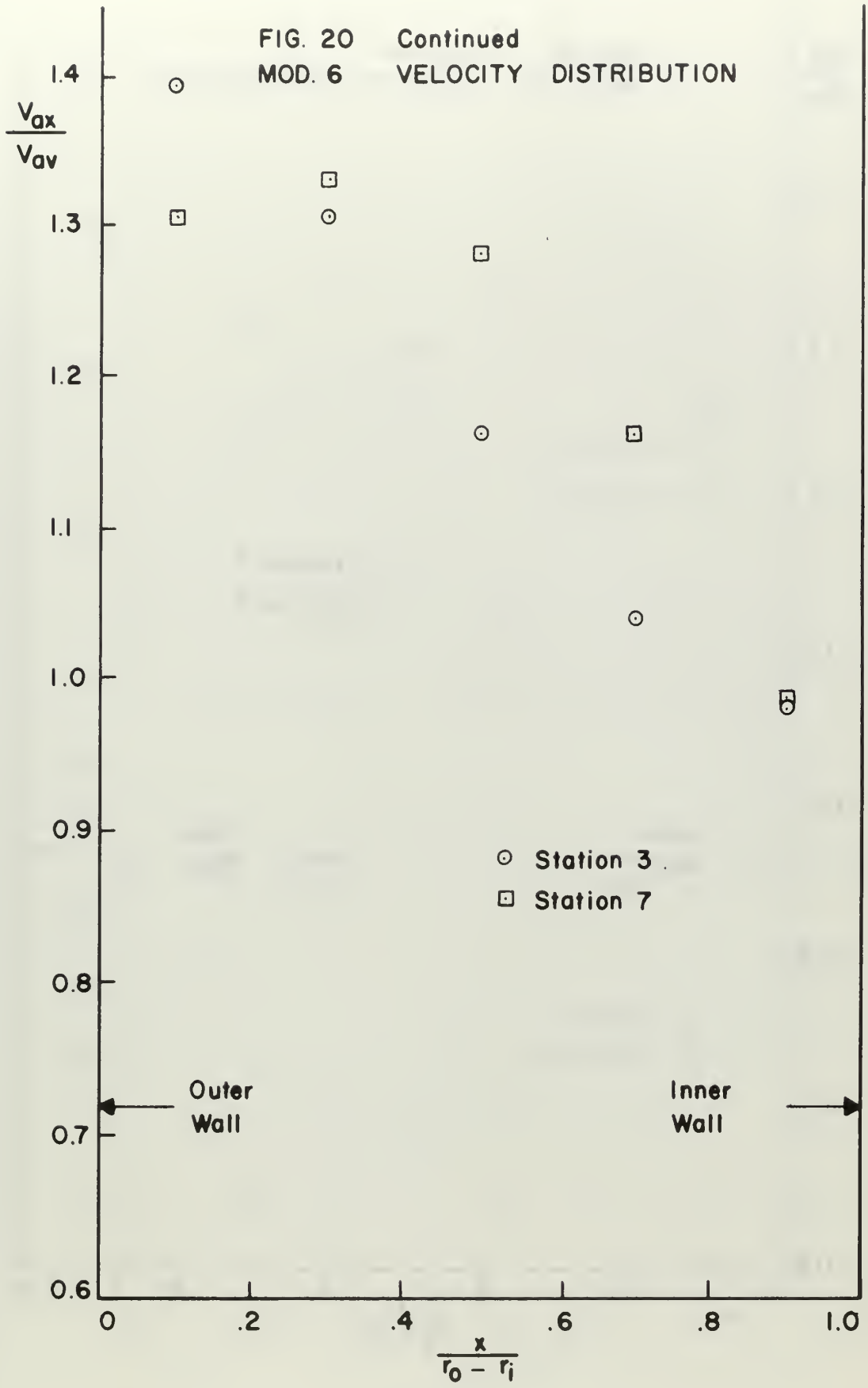
FIG. 20 Continued
MOD. 6 VELOCITY DISTRIBUTION
$\frac{V_{ax}}{V_{av}}$
1.4
1.3
1.2
1.1
1.0
0.9
0.8
0.7
0.6
Station 3
Station 7
Outer Wall
Inner Wall
0
.2
.4
.6
.8
1.0
$\frac{x}{r_o - r_i}$

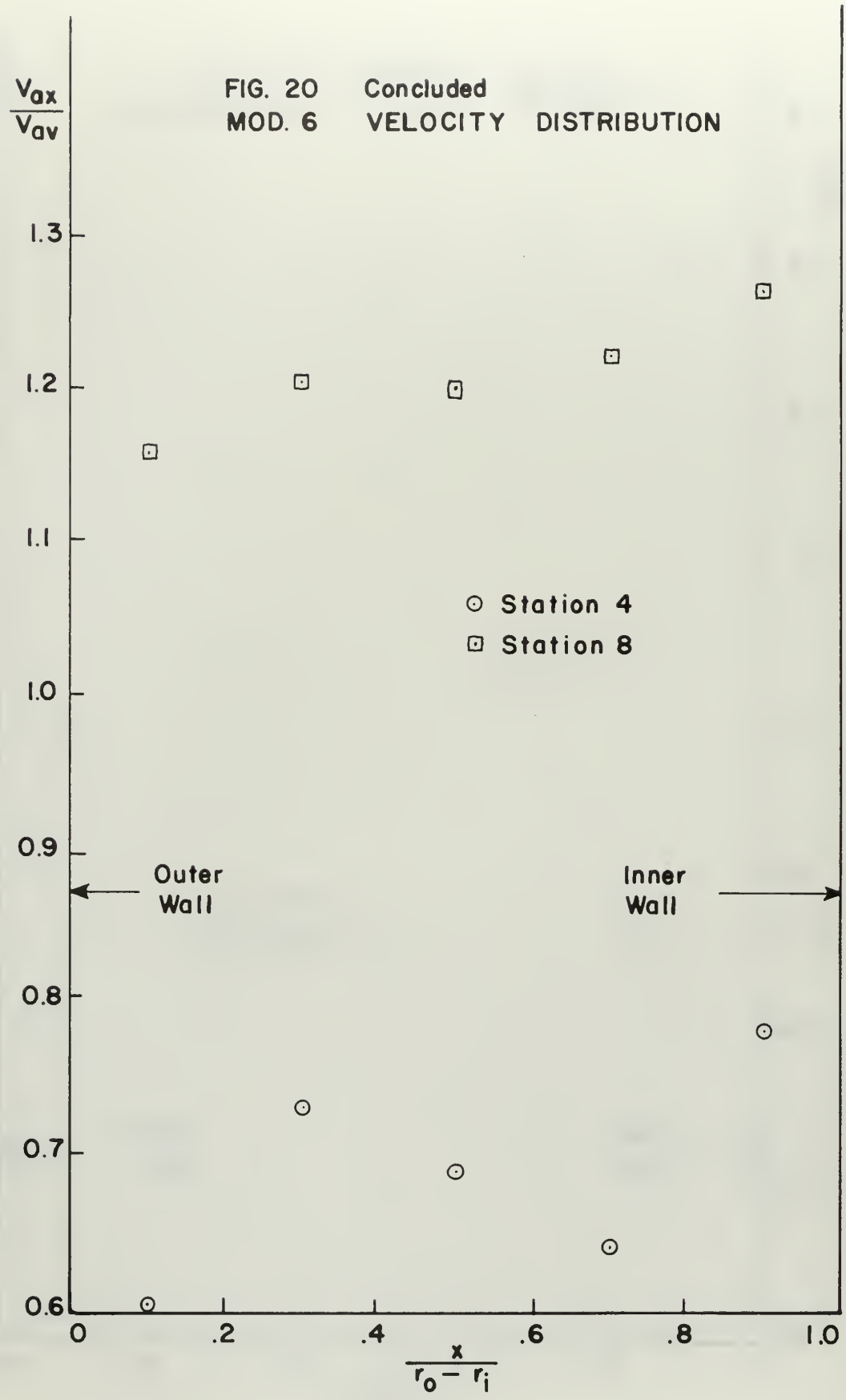
FIG. 20 Concluded
MOD. 6 VELOCITY DISTRIBUTION
$\frac{V_{ax}}{V_{av}}$
1.3
1.2
1.1
1.0
0.9
0.8
0.7
0.6
Station 4
Station 8
Outer Wall
Inner Wall
0
.2
.4
.6
.8
1.0
$\frac{x}{r_o - r_i}$

FIG. 21
MOD. 6 LOSS DISTRIBUTION

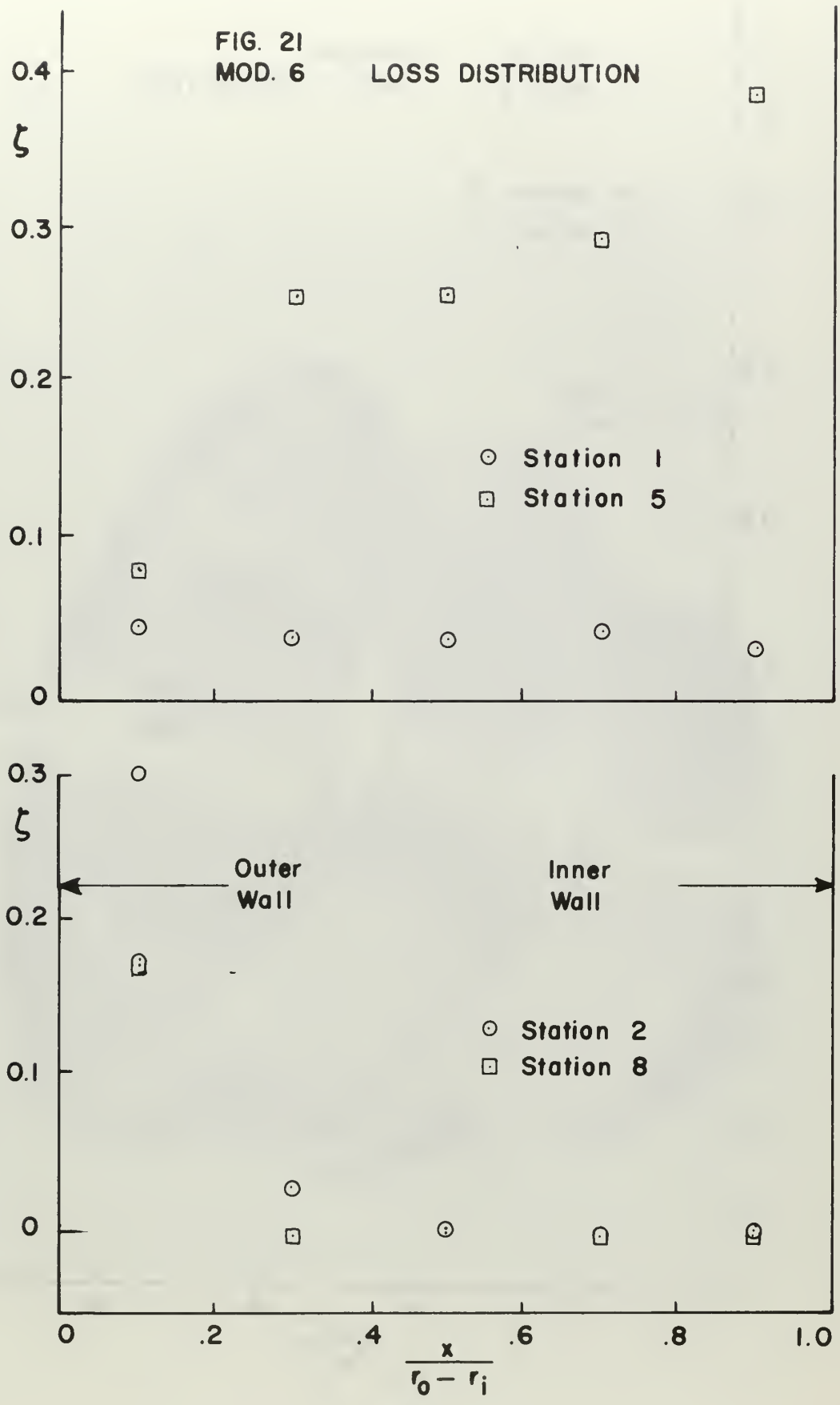

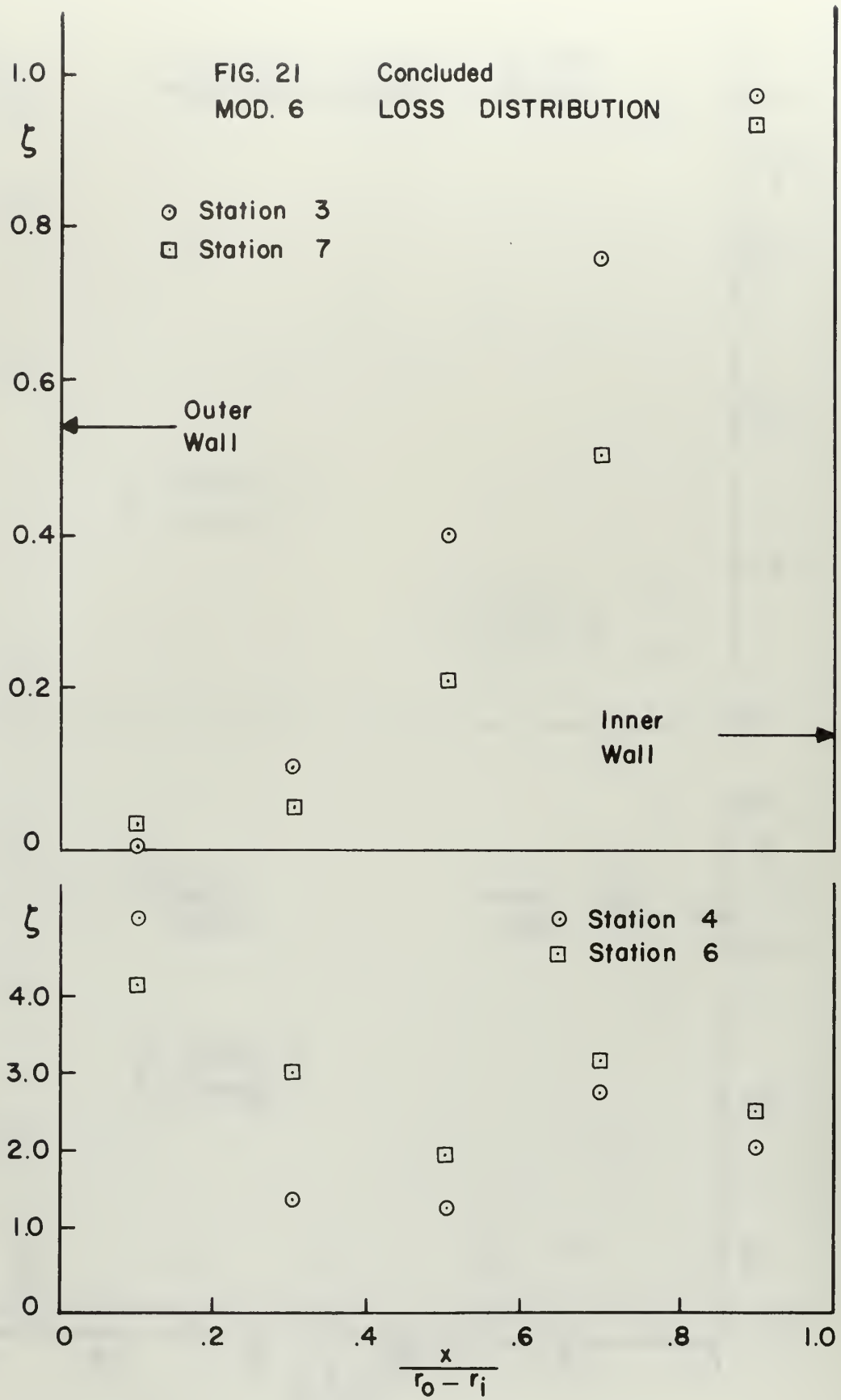
FIG. 21 Concluded
MOD. 6 LOSS DISTRIBUTION
ζ
Station 3
Station 7
Outer Wall
Inner Wall
Station 4
Station 6
1.0
0.8
0.6
0.4
0.2
0
4.0
3.0
2.0
1.0
0
.2
.4
.6
.8
1.0
x / r_o − r_i

Fig. 22

Modified Bellmouth

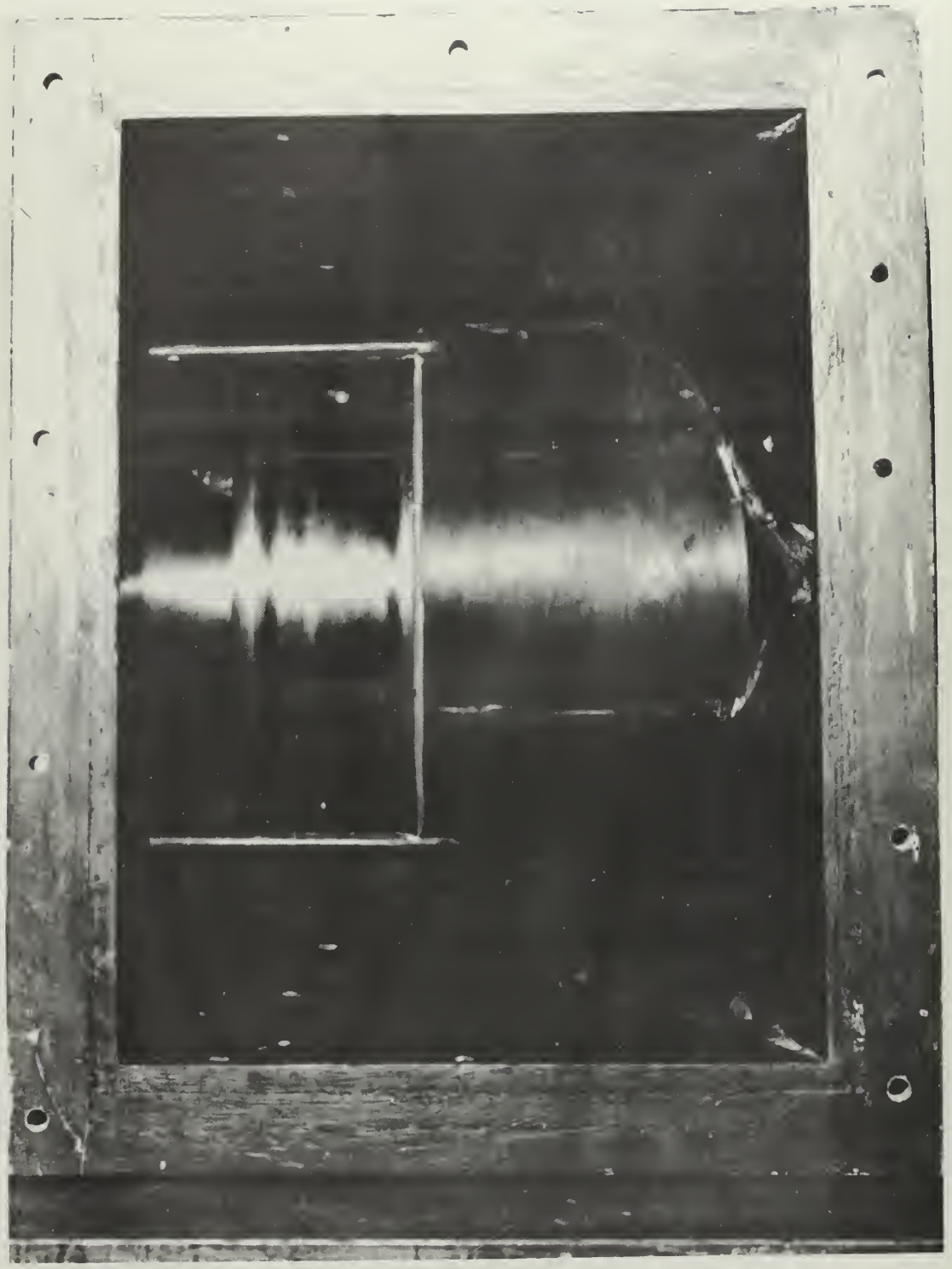

Fig. 23

Inlet Model - Mod. 7

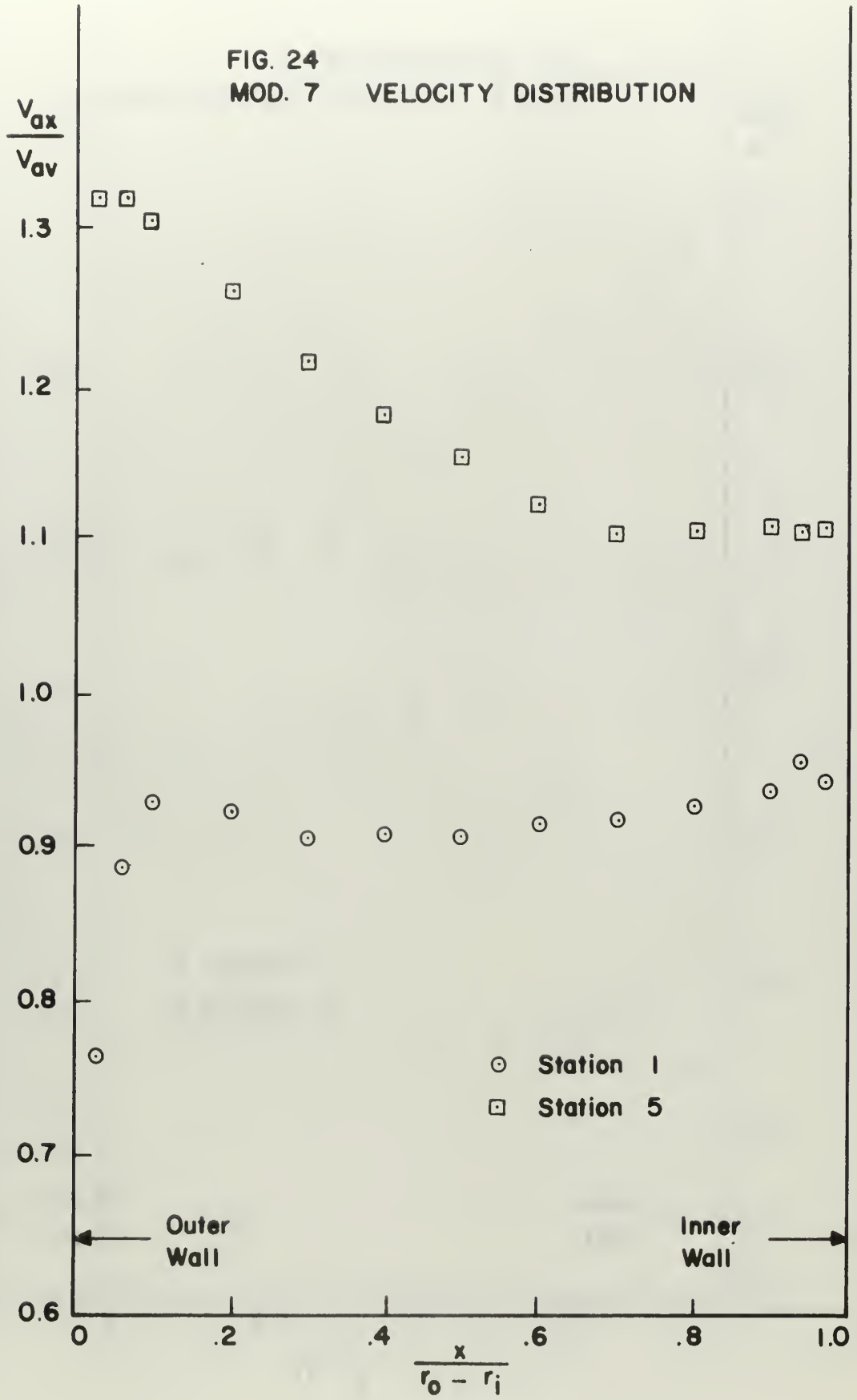
FIG. 24
MOD. 7 VELOCITY DISTRIBUTION
$\frac{V_{ax}}{V_{av}}$
1.3
1.2
1.1
1.0
0.9
0.8
0.7
0.6
Station 1
Station 5
Outer Wall
Inner Wall
0
.2
.4
.6
.8
1.0
$\frac{x}{r_o - r_i}$

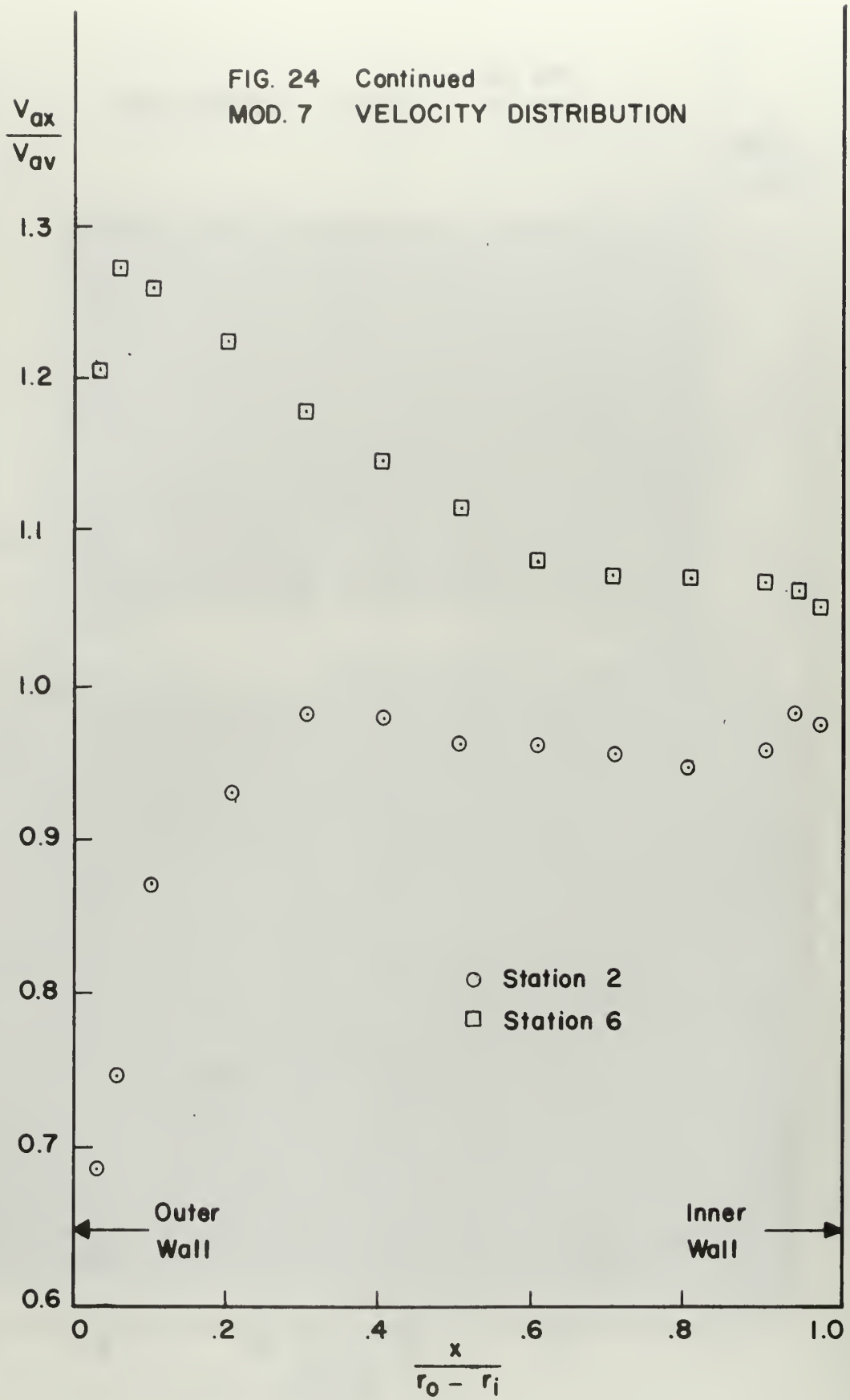
FIG. 24 Continued
MOD. 7 VELOCITY DISTRIBUTION
$\frac{V_{ax}}{V_{av}}$
1.3
1.2
1.1
1.0
0.9
0.8
0.7
0.6
Station 2
Station 6
Outer Wall
Inner Wall
0
.2
.4
.6
.8
1.0
$\frac{x}{r_o - r_i}$

FIG. 24 Continued
MOD. 7 VELOCITY DISTRIBUTION

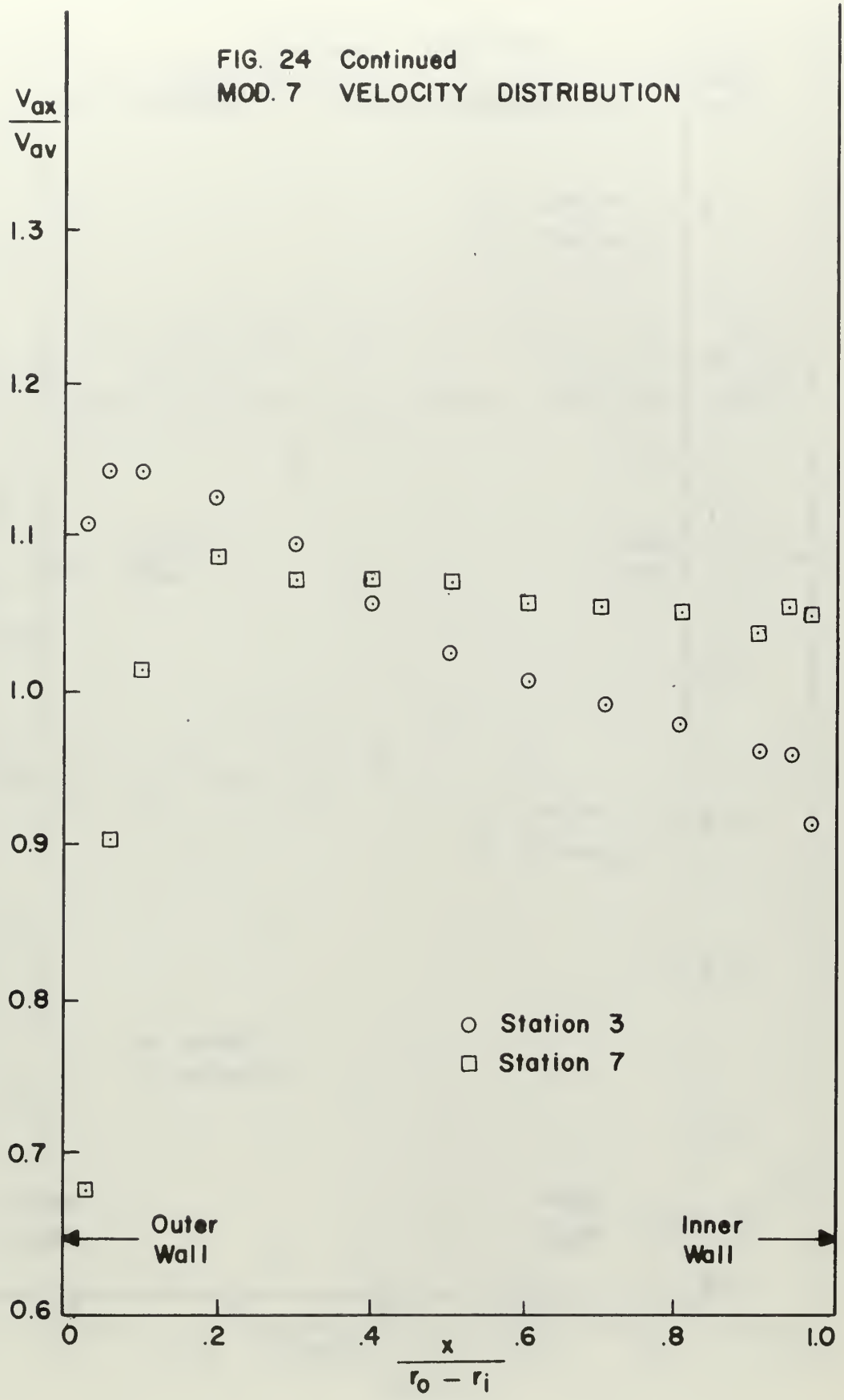

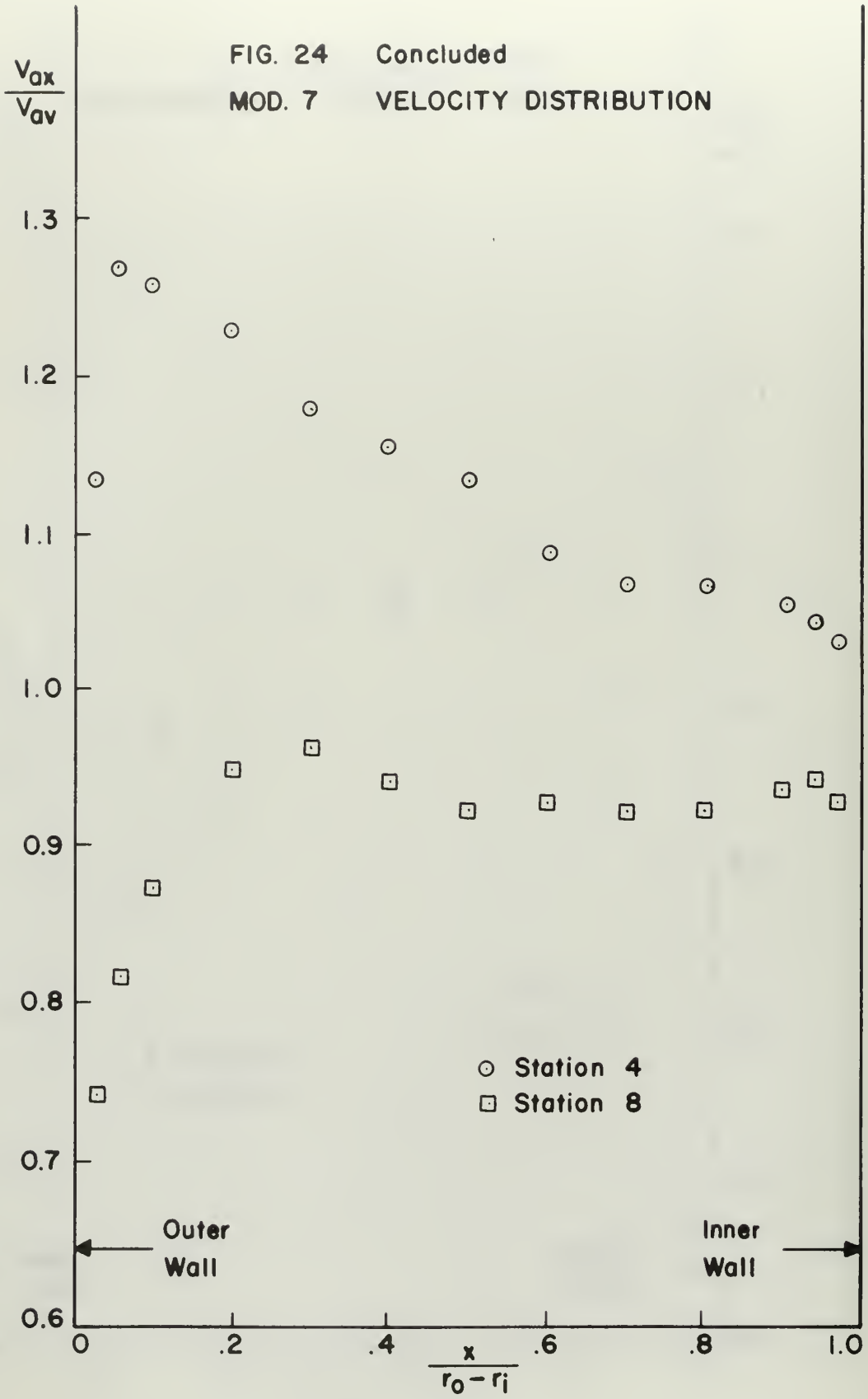
FIG. 24 Concluded
MOD. 7 VELOCITY DISTRIBUTION
$\frac{V_{ax}}{V_{av}}$
1.3
1.2
1.1
1.0
0.9
0.8
0.7
0.6
Station 4
Station 8
Outer Wall
Inner Wall
0
.2
.4
.6
.8
1.0
$\frac{x}{r_o - r_i}$

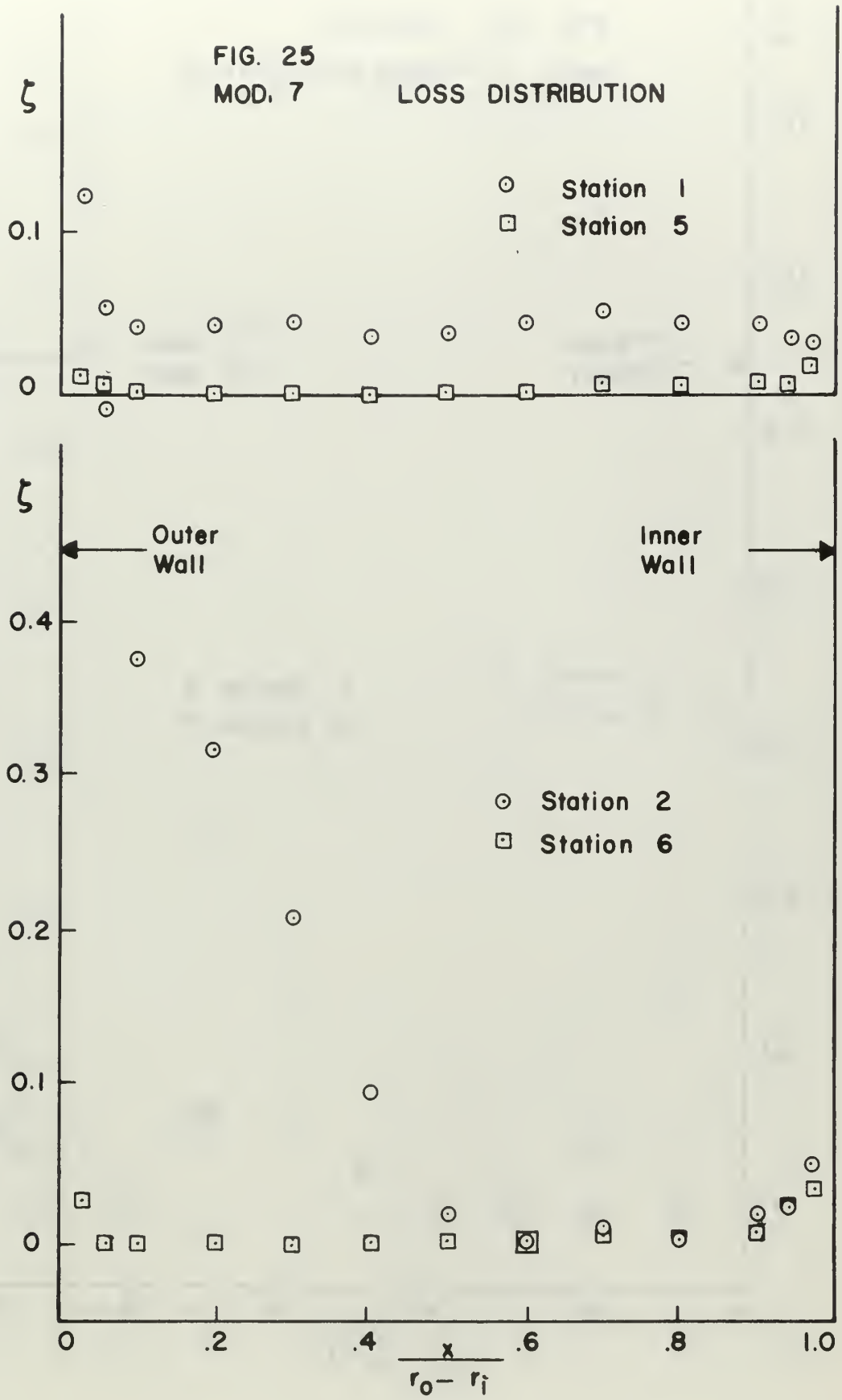
FIG. 25
MOD. 7 LOSS DISTRIBUTION
ζ
Station 1
Station 5
0.1
0
ζ
Outer Wall
Inner Wall
0.4
0.3
0.2
0.1
0
Station 2
Station 6
0
.2
.4
.6
.8
1.0
x / r_o − r_i

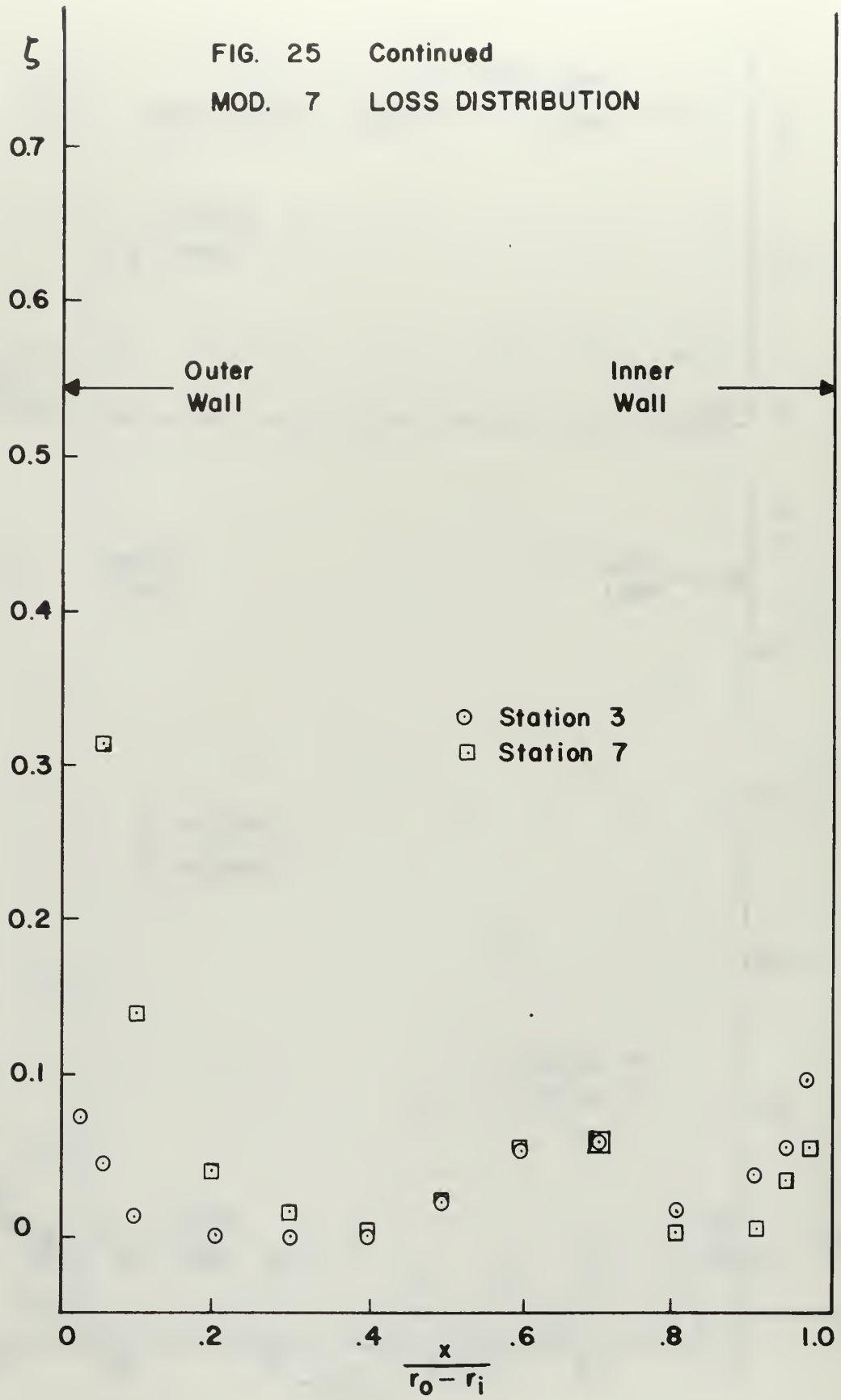
ζ
FIG. 25 Continued
MOD. 7 LOSS DISTRIBUTION
0.7
0.6
Outer Wall
Inner Wall
0.5
0.4
Station 3
Station 7
0.3
0.2
0.1
0
0
.2
.4
.6
.8
1.0
x / r_o − r_i

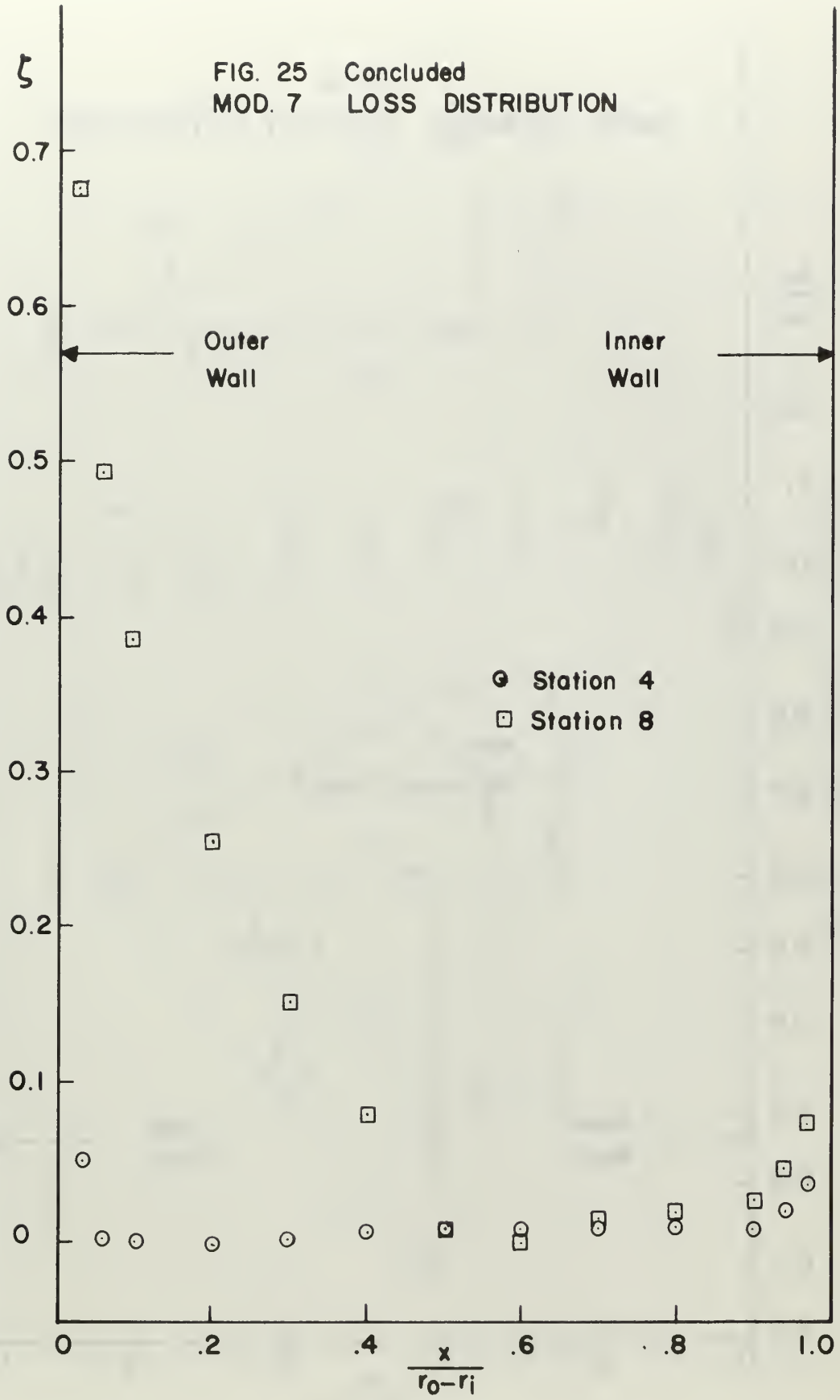
ζ
FIG. 25 Concluded
MOD. 7 LOSS DISTRIBUTION
0.7
0.6
0.5
0.4
0.3
0.2
0.1
0
Outer Wall
Inner Wall
Station 4
Station 8
0
.2
.4
.6
.8
1.0
x / r0−ri

FIG. 26

MODEL AVERAGED VELOCITY DISTRIBUTION

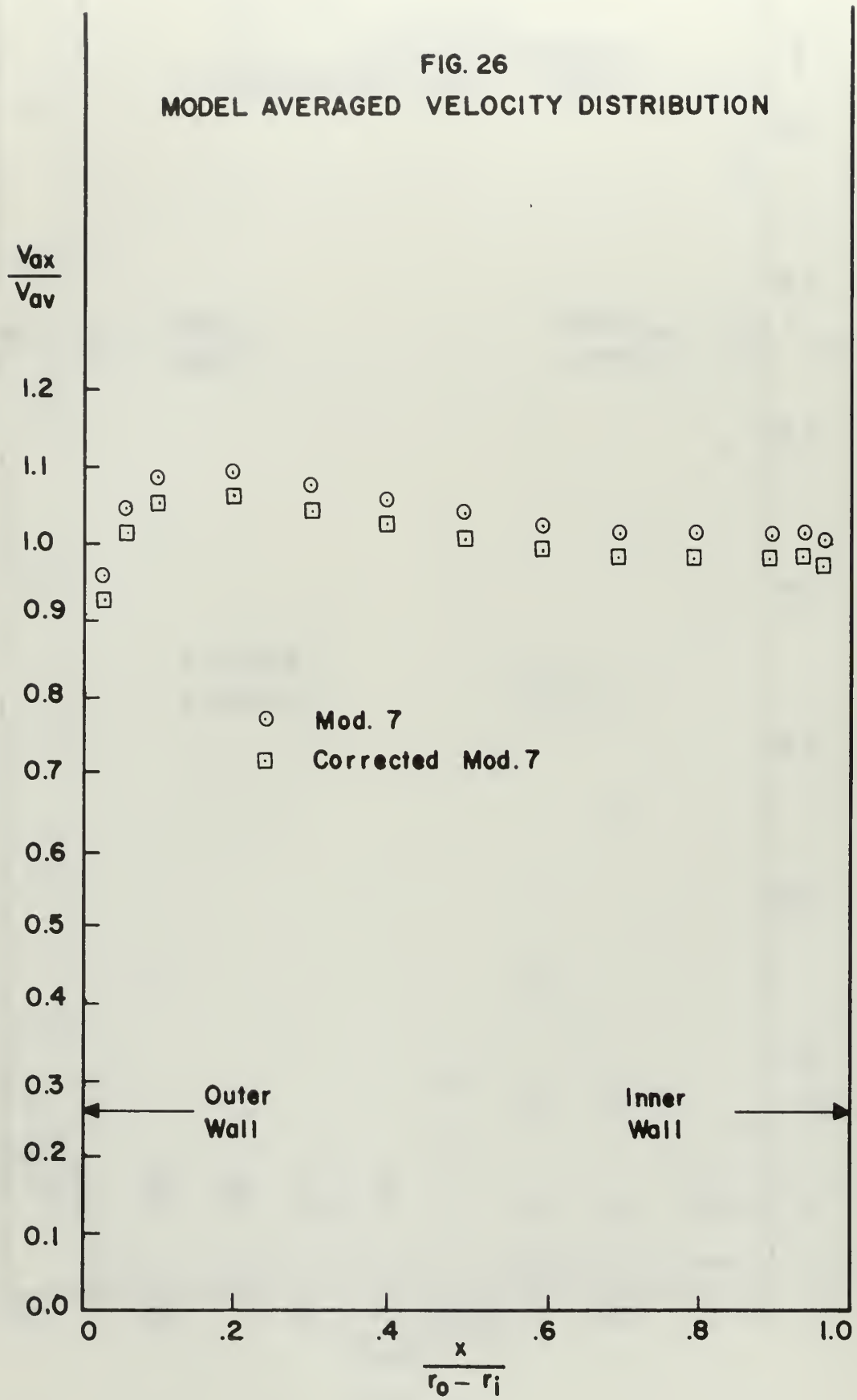

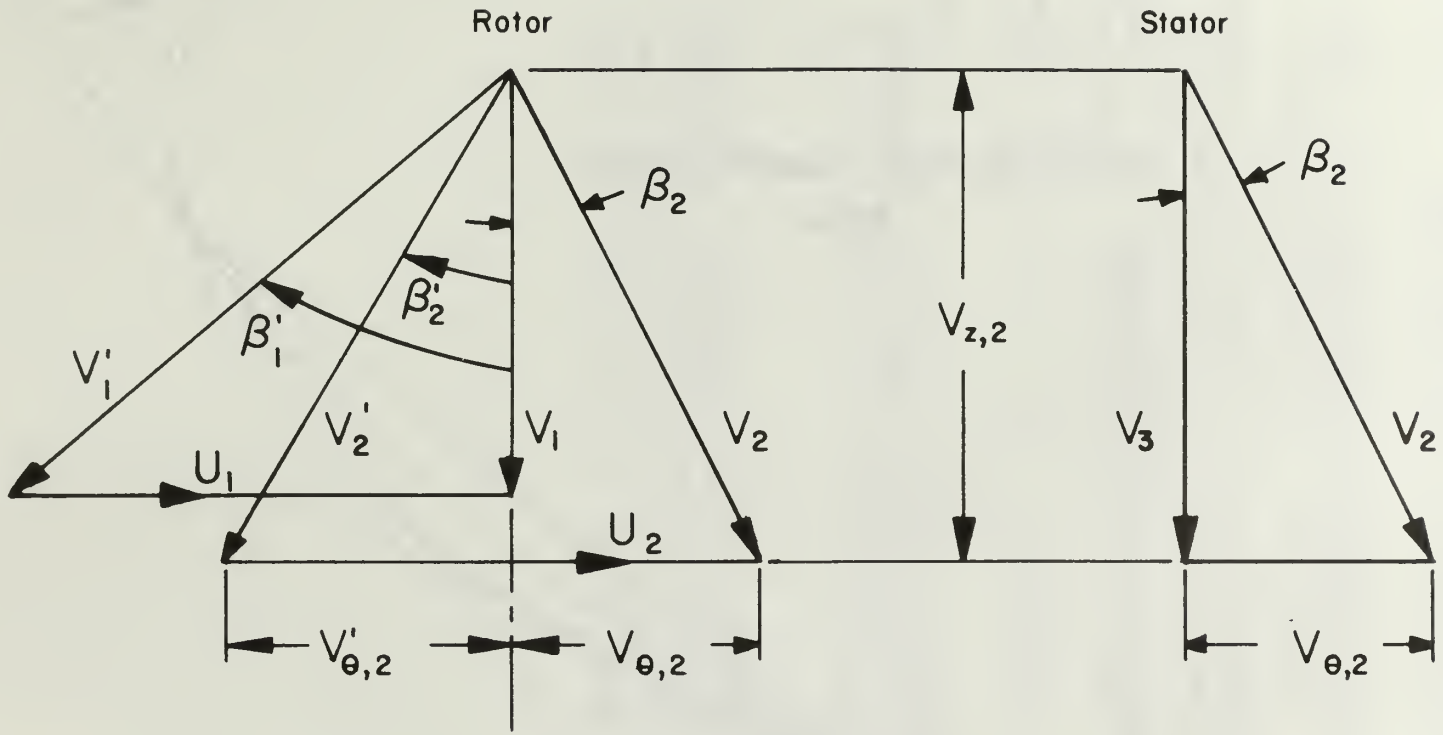

FIG. 27 FAN VELOCITY DIAGRAMS

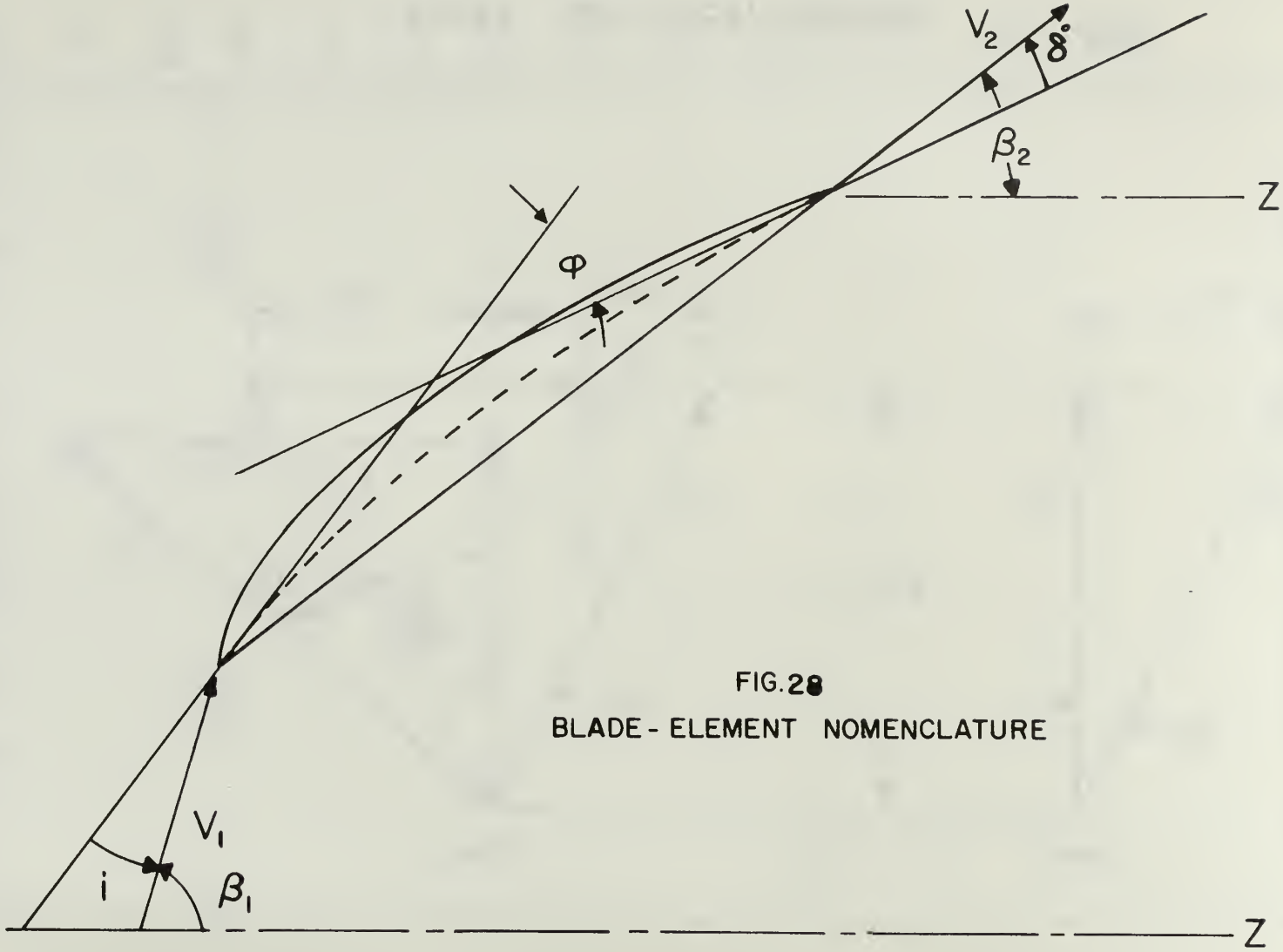

FIG. 28

BLADE - ELEMENT NOMENCLATURE

BIBLIOGRAPHY

1. Kelly, R. NPGS Department of Aeronautics TN-67T-1, Data for Flow Measurements in Addition of Building 230.

2. Vavra, M. H. von Karmon Institute, Course Note 54a, Part 1, Lecture Series on Problems of Fluid Mechanics in Radial Turbomachines, March 1965.

3. Johnsen, I. A., and R. O. Bullock (Editors), NASA SP-36, Aerodynamic Design of Axial-Flow Compressors, 1965.

4. Vavra, M. H. Aero-Thermodynamics and Flow in Turbomachines. John Wiley and Sons, 1960.

5. Keenan, J. M. and J. Kaye. Gas Tables. John Wiley and Sons, 1948.

6. Robbins, W. H. and F. W. Glaser. NACA Research Memorandum, RM E53D24, Investigation of an Axial-Flow-Compressor Rotor with Circular-Arc Blades Operating up to a Rotor-Inlet Relative Mach Number of 1.22, July 1953.

7. Robbins, W. H. and F. W. Glaser. NACA Research Memorandum, RM E57J17, Experimental Investigation of the Effect of Circumferential Inlet Flow Distortion on the Performance of a Five-Stage Axial-Flow Research Compressor With Transonic Rotors in all Stages, March 1958.

APPENDIX A

REDUCED DATA FOR MODEL TEST - MOD. 7

Model Test - Flow Rate

Station	Δp in Hg	p_u in H_2O	t_u ^oR	T_P ^oR	P_I cm H_2O	p_{atm} cm H_2O	p_{av} cm H_2O	w_n^* in^2	w_d^* in^2
1	34.398	58.0	559.3	560.9	15.18	1040.05	1042.08	4.115	4.689
2	34.378	58.0	558.0	552.4	15.16	1039.35	1038.35	4.115	4.703
3	34.398	58.0	558.5	560.2	15.30	1040.05	1037.22	4.109	4.704
4	34.398	58.0	558.3	560.5	15.26	1040.05	1034.72	4.112	4.719
5	34.398	58.0	559.3	560.4	15.25	1040.05	1033.74	4.112	4.723
6	34.378	58.0	557.0	558.7	15.23	1039.35	1034.22	4.111	4.717
7	34.398	58.0	559.0	561.4	15.19	1040.05	1036.81	4.109	4.706
8	34.388	58.0	559.0	561.0	15.20	1039.70	1039.58	4.117	4.701

Model Test - Station 1

x in.	P_1-P_{atm} cm H_2O	P_1-P_2 cm H_2O	P_4-P_5 cm H_2O	$\frac{P_4-P_5}{P_1-P_2}$	Θ deg	$\frac{P-p}{P_1-P_2}$	$P-p$ cm H_2O	Ψ deg	p cm H_2O	ζ	$\frac{q}{q_{av}}$	$\frac{V_{ax}}{V_{av}}$
.05	14.0	8.4	0.1	.012	6.8	1.087	9.13	-11.6	4.87	.129	.623	.768
.10	14.5	10.9	-0.1	-.009	5.0	1.089	11.87	- 7.2	2.63	.057	.811	.890
.17	14.6	11.8	- 0.1	-.008	5.0	1.089	12.85	- 1.7	1.75	.045	.876	.932
.34	14.6	11.9	0.3	.025	7.8	1.083	12.89	1.4	1.71	.045	.880	.929
.50	14.6	11.5	0.4	.035	8.5	1.083	12.45	2.2	2.15	.047	.850	.911
.67	14.7	11.3	- 0.1	-.009	5.0	1.089	12.31	2.7	2.39	.039	.841	.913
.84	14.7	11.2	- 0.7	-.063	1.8	1.093	12.24	2.7	2.46	.039	.836	.913
1.01	14.6	11.3	- 1.3	-.115	- 1.3	1.105	12.49	3.6	2.11	.046	.853	.921
1.18	14.5	11.2	- 2.0	-.179	- 4.0	1.127	12.62	4.8	1.88	.054	.862	.923
1.34	14.6	11.3	- 2.7	-.239	- 6.6	1.150	13.00	6.2	1.60	.045	.888	.931
1.51	14.6	11.5	- 2.9	-.252	- 7.5	1.158	13.32	5.8	1.28	.044	.910	.941
1.58	14.7	11.9	- 3.5	-.294	- 9.2	1.172	13.95	5.2	0.75	.034	.953	.960
1.63	14.7	11.7	- 4.3	-.368	-13.0	1.190	13.92	4.5	0.78	.034	.951	.947

Model Test - Station 2

x in.	$P_1 - P_{atm}$ cm H_2O	$P_1 - P_2$ cm H_2O	$P_4 - P_5$ cm H_2O	$\frac{P_4 - P_5}{P_1 - P_2}$	Θ deg	$\frac{P - p}{P_1 - P_2}$	$P - p$ cm H_2O	Ψ deg	p cm H_2O	ζ	$\frac{q}{q_{av}}$	$\frac{V_{ax}}{V_{av}}$
.05	7.3	6.4	- 6.3	-.984	---	---	---	20.4	---	---	---	---
.10	9.4	8.7	- 4.6	-.529	- 21.5	1.227	10.67	19.2	- 1.27	.540	.727	.749
.17	10.3	10.9	- 3.5	-.321	- 10.0	1.180	12.86	18.9	- 2.56	.378	.876	.872
.34	10.8	11.6	- 3.4	-.293	- 9.2	1.172	13.60	10.2	- 2.80	.321	.927	.935
.50	12.1	12.5	- 3.3	-.264	- 7.8	1.160	14.50	0.0	- 2.40	.211	.988	.985
.67	13.7	12.9	- 2.9	-.225	- 6.1	1.147	14.80	- 9.3	- 1.10	.099	1.008	.985
.84	14.9	13.3	- 2.6	-.196	- 4.8	1.133	15.07	-16.6	-0.17	.017	1.027	.968
1.01	15.2	13.8	- 2.4	-.174	- 3.6	1.123	15.50	-19.5	- 0.30	0.0	1.056	.966
1.18	15.0	13.7	- 1.9	-.139	- 2.5	1.113	15.25	-19.2	- 0.25	.010	1.039	.962
1.34	15.1	13.5	- 1.3	-.096	- 0.5	1.098	14.82	-18.6	0.28	.004	1.010	.952
1.51	14.9	13.6	- 1.3	-.096	- 0.5	1.098	14.93	-16.8	- 0.03	.017	1.017	.965
1.58	14.8	13.8	- 1.9	-.138	- 2.5	1.113	15.36	-14.7	- 0.56	.023	1.046	.988
1.63	14.4	13.2	- 3.1	-.225	- 6.6	1.150	15.18	-13.7	- 0.78	.050	1.034	.981

Model Test - Station 3

x in.	$P_1 - P_{atm}$ cm H_2O	$P_1 - P_2$ cm H_2O	$P_4 - P_5$ cm H_2O	$\frac{P_4 - P_5}{P_1 - P_2}$	θ deg	$\frac{P - p}{P_1 - P_2}$	P - p cm H_2O	ψ deg	p cm H_2O	ζ	$\frac{q}{q_{av}}$	$\frac{V_{ax}}{V_{av}}$
.05	13.8	16.6	- 5.4	- .325	- 10.5	1.180	19.59	- 11.4	- 5.79	.077	1.336	1.114
.10	14.4	18.0	- 2.7	- .150	- 2.9	1.118	20.12	- 11.6	- 5.72	.045	1.372	1.146
.17	15.0	18.7	- 0.8	- .043	3.0	1.092	20.42	- 13.0	- 5.42	.015	1.392	1.148
.34	15.5	18.5	0.1	.005	6.8	1.088	20.13	- 13.8	- 4.63	0	1.372	1.130
.50	15.4	17.6	0.5	.028	7.9	1.083	19.06	- 13.0	- 3.66	0	1.299	1.100
.67	15.3	16.7	0.7	.042	9.0	1.081	18.05	- 14.4	- 3.75	0	1.231	1.062
.84	14.9	15.8	0.7	.044	9.3	1.080	17.06	- 14.6	- 2.16	.023	1.163	1.030
1.01	14.4	14.9	0.1	.007	6.8	1.088	16.21	- 14.1	- 1.81	.056	1.105	1.012
1.18	14.4	14.4	- 0.3	- .021	4.5	1.091	15.71	- 14.7	- 1.31	.060	1.071	0.998
1.34	15.0	14.4	- 0.3	- .021	4.5	1.091	15.71	- 17.5	- 0.71	.019	1.071	0.984
1.51	14.7	14.4	0	0	6.2	1.078	15.52	-19.2	- 0.82	.039	1.058	0.966
1.58	14.4	14.2	0.3	.021	7.0	1.084	15.39	- 18.6	- 0.99	.058	1.049	0.963
1.63	13.9	13.0	1.6	.123	12.2	1.076	13.99	- 16.2	- 0.09	.100	0.954	0.917

Model Test - Station 4

x in.	$P_1 - P_{atm}$ cm H_2O	$P_1 - P_2$ cm H_2O	$P_4 - P_5$ cm H_2O	$\frac{P_4 - P_5}{P_1 - P_2}$	θ deg	$\frac{P - p}{P_1 - P_2}$	P - p cm H_2O	ψ deg	p cm H_2O	ζ	$\frac{q}{q_{av}}$	$\frac{V_{ax}}{V_{av}}$
.05	14.0	18.8	-11.0	- .585	- 23.6	1.240	23.31	- 9.6	- 9.31	.054	1.583	1.137
.10	15.2	21.7	- 4.1	- .189	- 4.7	1.131	24.54	- 8.5	- 9.34	.002	1.666	1.272
.17	15.3	22.0	- 0.8	- .036	3.4	1.092	24.02	- 8.2	- 8.72	0	1.631	1.262
.34	15.3	21.5	0.7	.033	8.3	1.083	23.28	- 8.1	- 7.98	0	1.581	1.232
.50	15.2	20.1	1.0	.050	9.5	1.080	21.71	- 8.5	- 6.51	.003	1.474	1.184
.67	15.1	19.3	1.0	.052	9.6	1.080	20.84	- 9.3	- 5.74	.008	1.415	1.158
.84	15.1	18.3	1.0	.055	9.7	1.081	19.78	- 9.8	- 4.68	.008	1.373	1.138
1.01	15.1	17.3	1.0	.058	9.8	1.081	18.70	- 10.6	- 3.60	.009	1.270	1.091
1.18	15.1	16.7	0.7	.042	9.0	1.081	18.05	- 11.5	- 2.95	.009	1.226	1.071
1.34	15.1	16.6	0.4	.024	7.8	1.083	17.98	- 12.6	- 2.88	.009	1.221	1.069
1.51	15.1	16.4	0.4	.024	7.8	1.083	17.76	- 13.6	- 2.66	.009	1.206	1.058
1.58	14.9	16.1	0.6	.037	8.6	1.082	17.42	- 13.2	- 2.52	.021	1.183	1.047
1.63	14.6	15.7	1.1	.070	10.3	1.080	16.96	- 11.7	- 2.36	.039	1.152	1.034

Model Test - Station 5

x in.	$P_1 - P_{atm}$ cm H_2O	$P_1 - P_2$ cm H_2O	$P_4 - P_5$ cm H_2O	$\frac{P_4 - P_5}{P_1 - P_2}$	θ deg	$\frac{P - p}{P_1 - P_2}$	$P - p$ cm H_2O	ψ deg	p cm H_2O	ζ	$\frac{q}{q_{av}}$	$\frac{V_{ax}}{V_{av}}$
.05	15.0	23.0	- 4.9	- .213	- 5.6	1.139	26.20	- 2.6	- 11.20	.010	1.778	1.326
.10	15.1	23.2	- 3.7	- .159	- 3.2	1.120	25.98	- 2.1	- 10.88	.006	1.763	1.325
.17	15.3	23.4	- 0.5	- .021	4.5	1.091	25.53	- 2.0	- 10.23	0	1.732	1.311
.34	15.3	22.5	1.1	.049	9.5	1.080	24.30	- 1.8	- 9.00	0	1.649	1.266
.50	15.2	20.9	1.2	.057	9.7	1.081	22.59	- 1.5	- 7.39	.002	1.533	1.220
.67	15.2	19.8	1.2	.061	10.0	1.079	21.36	- 1.7	- 6.16	.002	1.449	1.185
.84	15.2	18.8	1.0	.053	9.6	1.081	20.32	- 2.4	- 5.12	.002	1.379	1.157
1.01	15.2	17.9	0.9	.050	9.5	1.080	19.33	- 3.2	- 4.13	.003	1.312	1.128
1.18	15.1	17.3	0.8	.046	9.4	1.080	18.68	- 2.7	- 3.58	.008	1.268	1.110
1.34	15.1	17.1	0.5	.029	7.9	1.083	18.52	- 2.7	- 3.42	.008	1.257	1.110
1.51	15.1	17.2	0.5	.029	7.9	1.083	18.63	- 1.4	- 3.53	.008	1.264	1.113
1.58	15.1	17.3	0.9	.052	9.6	1.080	18.68	- 0.7	- 3.58	.008	1.268	1.110
1.63	14.9	17.4	1.1	.063	10.0	1.079	18.77	- 0.2	- 3.87	.019	1.274	1.112

Model Test - Station 6

x in.	$P_1 - P_{atm}$ cm H_2O	$P_1 - P_2$ cm H_2O	$P_4 - P_5$ cm H_2O	$\frac{P_4 - P_5}{P_1 - P_2}$	θ deg	$\frac{P - p}{P_1 - P_2}$	$P - p$ cm H_2O	ψ deg	p cm H_2O	ζ	$\frac{q}{q_{av}}$	$\frac{V_{ax}}{V_{av}}$
.05	14.5	19.8	- 8.9	- .449	- 18.3	1.212	24.00	2.2	- 9.50	.030	1.632	1.212
.10	15.2	21.8	- 2.7	- .124	- 1.8	1.107	24.13	3.3	- 8.93	.001	1.641	1.278
.17	15.2	21.8	- 0.5	- .023	4.5	1.091	23.78	3.4	- 8.58	.001	1.617	1.265
.34	15.2	21.1	0.7	.033	8.3	1.083	22.85	4.5	- 7.65	.001	1.554	1.230
.50	15.2	19.8	1.0	.050	9.5	1.080	21.38	5.1	- 6.18	.001	1.454	1.184
.67	15.2	18.7	1.0	.053	9.6	1.081	20.21	5.6	- 5.01	.001	1.374	1.150
.84	15.2	17.8	1.0	.056	9.7	1.081	19.24	6.3	- 4.04	.002	1.308	1.121
1.01	15.2	16.9	1.0	.059	9.8	1.081	18.27	7.3	- 3.07	.002	1.242	1.089
1.18	15.2	16.5	0.7	.042	9.0	1.081	17.84	8.3	- 2.64	.002	1.213	1.077
1.34	15.1	16.4	0.5	.031	8.1	1.083	17.76	8.7	- 2.66	.007	1.208	1.076
1.51	15.1	16.4	0.5	.031	8.1	1.083	17.76	9.1	- 2.66	.007	1.208	1.074
1.58	14.7	16.3	0.7	.043	9.1	1.081	17.62	9.2	- 2.92	.030	1.198	1.067
1.63	14.6	16.2	1.3	.080	10.8	1.078	17.46	9.0	- 2.86	.036	1.187	1.057

Model Test - Station 7

x in.	$P_1 - P_{atm}$ cm H_2O	$P_1 - P_2$ cm H_2O	$P_4 - P_5$ cm H_2O	$\frac{P_4 - P_5}{P_1 - P_2}$	θ deg	$\frac{P - p}{P_1 - P_2}$	$P - p$ cm H_2O	ψ deg	p cm H_2O	ζ	$\frac{q}{q_{av}}$	$\frac{V_{ax}}{V_{av}}$
.05	7.4	8.2	5.2	.634	31.5	1.145	9.39	- 5.6	- 1.99	.830	0.640	0.679
.10	11.0	12.1	2.4	.198	15.6	1.081	13.08	5.2	- 2.08	.320	0.891	0.906
.17	12.9	14.6	- 0.3	- .021	4.5	1.091	15.93	11.6	- 3.03	.144	1.086	1.018
.34	14.4	16.7	- 2.7	- .162	- 3.2	1.120	18.70	14.2	- 4.30	.042	1.274	1.093
.50	14.9	16.2	- 2.7	- .167	- 3.6	1.123	18.19	14.2	- 3.29	.016	1.240	1.077
.67	15.1	16.2	- 2.7	- .167	- 3.6	1.123	18.19	14.2	- 3.09	.005	1.240	1.077
.84	14.7	16.2	- 2.5	- .154	- 2.9	1.118	18.11	13.8	- 3.41	.027	1.234	1.077
1.01	14.1	15.8	- 1.9	- .120	- 1.7	1.106	17.47	12.6	- 3.37	.062	1.190	1.064
1.18	14.1	16.0	- 0.9	- .056	2.1	1.092	17.47	13.6	- 3.37	.062	1.190	1.060
1.34	15.1	16.6	- 0.4	- .024	4.5	1.091	18.11	17.4	- 3.01	.005	1.234	1.057
1.51	15.1	16.8	- 0.4	- .024	4.5	1.091	18.33	20.6	- 3.23	.005	1.249	1.043
1.58	14.5	16.9	- 1.1	- .065	1.5	1.094	18.49	19.2	- 3.99	.037	1.260	1.060
1.63	14.1	16.2	- 2.3	- .142	- 2.5	1.113	18.03	18.3	- 3.93	.060	1.229	1.052

Model Test - Station 8

x in.	$P_1 - P_{atm}$ cm H_2O	$P_1 - P_2$ cm H_2O	$P_4 - P_5$ cm H_2O	$\frac{P_4 - P_5}{P_1 - P_2}$	Θ deg	$\frac{P - p}{P_1 - P_2}$	$P - p$ cm H_2O	Ψ deg	p cm H_2O	β	$\frac{q}{q_{av}}$	$\frac{V_{ax}}{V_{av}}$
.05	9.5	7.2	- 1.9	- .264	- 7.8	1.160	8.35	2.2	1.15	.683	0.569	0.747
.10	10.2	9.0	- 1.3	- .144	- 2.5	1.113	10.02	- 5.4	0.18	.499	0.682	0.822
.17	10.7	10.2	- 1.9	- .186	- 4.7	1.131	11.54	- 5.8	- 0.84	.390	0.786	0.879
.34	11.7	11.7	- 2.9	- .248	- 7.1	1.156	13.53	1.0	- 1.83	.259	0.921	0.952
.50	13.0	12.3	- 2.9	- .236	- 6.6	1.150	14.15	8.0	- 1.15	.155	0.964	0.966
.67	14.0	12.6	- 2.8	- .222	- 6.1	1.147	14.45	16.6	- 0.45	.083	0.984	0.945
.84	15.1	13.2	- 2.7	- .205	- 5.0	1.134	14.97	22.7	0.13	.007	1.020	0.928
1.01	15.3	13.6	- 2.4	- .177	- 3.9	1.126	15.31	23.6	- 0.01	0	1.043	0.934
1.18	15.0	13.3	- 1.9	- .143	- 2.5	1.113	14.80	22.4	0.20	.014	1.008	0.927
1.34	14.9	13.2	- 1.5	- .114	- 1.3	1.105	14.59	21.2	0.31	.021	0.994	0.929
1.51	14.8	13.0	- 1.4	- .108	- 1.1	1.102	14.33	17.5	0.47	.028	0.976	0.942
1.58	14.5	12.8	- 2.2	- .172	- 3.6	1.123	14.37	16.4	0.13	.049	0.979	0.947
1.63	14.1	11.9	- 3.6	- .303	- 9.2	1.172	13.95	14.1	0.15	.079	0.950	0.933

INITIAL DISTRIBUTION LIST

		No. Copies
1.	Defense Documentation Center Cameron Station Alexandria, Virginia 22314	20
2.	Library Naval Postgraduate School Monterey, California	2
3.	Professor M. H. Vavra Department of Aeronautics Naval Postgraduate School Monterey, California	3
4.	LCDR Ronald W. Pyle, USN USS Saratoga (CVA-60) c/o Fleet Post Office New York, New York	1
5.	LT Milton W. York, USN USS Iwo Jima (LPH-2) c/o Fleet Post Office San Francisco, California	1
6.	Commander, Naval Air Systems Command Navy Department Washington, D. C. 20360	1
7.	Chairman, Department of Aeronautics Naval Postgraduate School Monterey, California	1

DOCUMENT CONTROL DATA - R&D

(Security classification of title, body of abstract and indexing annotation must be entered when the overall report is classified)

1. ORIGINATING ACTIVITY (Corporate author)
Naval Postgraduate School,
Monterey, California

2a. REPORT SECURITY CLASSIFICATION
Unclassified

2b. GROUP

3. REPORT TITLE
TRANSONIC FAN FOR AIRCRAFT AIR-CONDITIONING UNIT

4. DESCRIPTIVE NOTES (Type of report and inclusive dates)

5. AUTHOR(S) (Last name, first name, initial)
PYLE, Ronald W., LCDR, USN
YORK, Milton W., LT, USN

6. REPORT DATE June 1967

7a. TOTAL NO. OF PAGES
118

7b. NO. OF REFS
7

8a. CONTRACT OR GRANT NO.

b. PROJECT NO.

c.

d. Unlimited dist.

9a. ORIGINATOR'S REPORT NUMBER(S)

9b. OTHER REPORT NO(S) (Any other numbers that may be assigned this report)

10. AVAILABILITY/LIMITATION NOTICES
This document is subject to special export controls and each transmittal to foreign governments or foreign nationals may be made only with prior approval of the Naval Postgraduate School.

11. SUPPLEMENTARY NOTES

12. SPONSORING MILITARY ACTIVITY
Naval Postgraduate School,
Monterey, California

13. ABSTRACT

This study presents the results of the aerodynamic design of a transonic axial-flow fan for an aircraft air-conditioning unit. The design is based on fan design-point specifications and the experimental test results for a model of a proposed fan-inlet.

The fan-inlet model was tested under flow conditions that gave Reynolds number similarity to the design inlet conditions. Three-dimensional pressure probes were used to measure the model discharge flow conditions at eight stations. The flow was found to lack axial symmetry. Therefore, several internal modifications were made. Complete axial symmetry was not achieved for a reasonable loss in total pressure. It was necessary to circumferentially average the velocity distribution and mass-average the total-pressure loss in order to provide a basis for the fan design.

Concurrently another design based on uniform flow and model losses was made. The results were nearly identical.

DD FORM 1 JAN 64 1473

14 KEY WORDS	LINK A		LINK B		LINK C	
	ROLE	WT	ROLE	WT	ROLE	WT
Transonic Fan Aerodynamic Design Inlet Model Testing						

thesP985
Transonic fan for aircraft air-condition
3 2768 001 93069 6
DUDLEY KNOX LIBRARY